Exploration and Realization of Sub-Neuronal Carbon Fiber Electrodes for Recording and Stimulation in the Nervous System

by

Julianna M. Richie

A dissertation submitted in partial fulfillment
of the requirements for the degree of
Doctor of Philosophy
(Biomedical Engineering)
in the University of Michigan
2024

Doctoral Committee:

Professor Cynthia A. Chestek, Chair
Professor Scott F. Lempka
Professor Rebecca L. Peterson
Professor James D. Weiland

Julianna M. Richie

jmrichie@umich.edu

ORCID iD: 0000-0002-8920-6560

Dedication

This thesis is dedicated to many people – first and foremost myself. I entered this program in order to pursue my idea to optimize carbon fiber electrodes in a reliable manner. While I entered this program with trepidation and during a pandemic, I ultimately have gained the knowledge I set out to gain, friendships I did not think I would, and the confidence to go out into the world and continue to seek and spread knowledge.

Of course, I could not have done this without the support of my friends and colleagues. First and foremost, to the Reverend Daughter, Wami – If friends were bones, I'd pick you. To Riley – thank you for helping with my animals and being on the podcast every time you were forced to be on it. To Olivia – for constantly being confused and outraged at the graduate student struggle. To CJ – my child whom I found on the side of the road who has been nothing but a source of joy ever since. Theo, I didn't forget you – you're the only person I would jump in a suitcase for.

To my oldest friends: Meaghan, Julie, and Jacob. Thank you each for reminding me constantly that there's more to life than research. Meaghan, thank you for listening constantly. Thank you for giving me vet advice and for all the animal photos. Julie – thank you for ruining so much media for me and for all the clown sounds. Jacob – I'm still waiting for my spaghetti ballerina, but thank you for the once a year catch up sessions and the conspiracy about Alton. You three have been such wonderful influences on me and have changed my worldviews for the better. I would not be the person I am today without you.

To literally everyone in TNE – thank you so much. Thank you for laughing with me and inviting me to lunch. Thank you for all the party invites – even though I was too much of a grandma to show up to many of them. Thank you for all the feedback on my research, my presentation skills, my writing. Special thanks to Zainab, without whom I would never have made it through EECS 414. There is literally no way I would have made it through this without you. And while they're not in TNE, thank you, Christina for helping me keep on track with writing and grounded in the present.

To my music teacher, Catherine: thank you for reminding me that no matter what I was doing, at least it wasn't music theory. To Mohana – thank you for reminding me to always watch my six. And Eric – thanks for taking such good care of my car and making me muffins.

To all the women in my life who have helped me get through it all. Elissa, thank you for including me. Thank you for taking my call and calming me down. Thank you Elizabeth for always being ready to throw down. Thank you Elena for inviting me into your home and your family and teaching me SEM so, so many times. Thank you to the BI team – Elizabeth, Shelly, Frankie, Alanna, Laura – I became a better leader and strategist because of your guidance and I am so lucky to have you in my life.

To my family. Dad, you fostered in me a love of science from a young age. You taught me calculus in fifth grade and set up telescopes in the backyard to investigate the stars. You shared your love of amateur radio and taught me the science behind it. My love for science and problem solving comes from you. Mom, you taught me to never back down from what's right. You instilled in me a self-worth that made me speak up, talk back (though you weren't happy about that when I was a kid), and stand my ground. Those skills were necessary and needed for this PhD. Kate, you taught me how to fight without letting anyone know that we were fighting. I

learned to compromise and negotiate through our careful debates. And I learned how to cooperate and plan the best jokes and pranks on the family. Moose, you taught me the benefits of being Player 2- being able to take on a supporting role has been a big part of my program…as has talking about old video games. Thank you all.

To my best friend and spouse, Alexandra: Thank you for ordering so, so many pizzas. Thanks for taking me to bed when I fell asleep at my desk or on the couch…or on the floor curled up with the cat. Thanks for looking at spikes and images and figures and listening to practice talks. Thanks for buying scary games and playing them while I sat behind you with the dog for protection. I would not have made it through this PhD without your encouragement and support. My love for you is at least a meter wide (that's like 3 feet).

Xan, I would go to the moon for you.

Acknowledgements

My studies and research took place on the ancestral, traditional, and contemporary lands of the Anishinaabeg – The Three Fire Confederacy of the Ojibwe, Odawa, and Potawatomi nations as well as the Wyandot Nation. These lands were "gifted" to the University of Michigan in 1817 and their development allowed me to pursue and expand scientific knowledge. While the history and language surrounding the acquisition of this land are written by colonizing historians, it is my hope that paying respect and acknowledging this land's ancestry will pave way for more open conversations about de-colonizing the future and preserving and celebrating the lands' original culture.

The work presented here could not have been completed without the resources provided by the Lurie NanoFabrication Laboratory and the Michigan Material Characterization Center.

Thank you to the Neural Engineering Translational Program Fellowship for funding my PhD and allowing me so many opportunities to meet with people in my field to enrich my learning experience and better prepare me for work outside of the academic setting.

Of course, I must acknowledge my committee for their work to help me advance to this position. Cindy Chestek – thank you for seeing the potential in me in my first three months of working as a technician and welcoming me into your lab when I decided to pursue the PhD. Jim Weiland – thank you for being absolutely chaotic with me and also providing a space for me to vent and learn. Scott Lempka – thank you for believing in my coding and modeling skills. I'm still working on them, but it was nice to know someone believed in me to the point that I felt I

could put it in my thesis. Becky Peterson – thank you for agreeing to be on my committee even though we didn't really know each other that well. Your input and support were invaluable to me.

I would also like to acknowledge the team at RMIT, University of Melbourne, and Carbon Cybernetics for agreeing to meet with and then collaborate with me on carbon fiber neural devices. You are all absolute legends and I cannot express my gratitude for your welcome and the very unique education I gained with you.

And finally, the custodians and maintenance crew at the University of Michigan, specifically Daryl and Julie, who worked tirelessly to fight floods, trash, and sour moods. The maintenance crew at the UofM makes the research here possible as they clean up our careless messes and keep the university a safe and lovely place to work. Daryl and Julie – I wish you all the best and I cannot express my gratitude for your kindness over the years.

Table of Contents

List of Tables

List of Figures

Abstract

Carbon fiber (CF) electrodes have been used in neuroscience labs for years to study electrical signals in brains. While the carbon fiber electrode has been implemented in many forms, the tip of the electrode has been left unexplored. This is because optimizing the electrode geometry has long been a problem due to carbon fibers being small (7 μm in diameter) and challenging to handle. However, small surface area electrodes are desirable for specificity of stimulation and recording of cells, neurons, and axons. While carbon fibers have recorded action potentials in brain, tougher tissues like nerve and muscle cannot be accessed with traditional (scissor or laser cut) tip modification.

Thus, the work presented here is three-fold: (1) modifying the carbon fiber tip geometry for sub-cellular acute recordings that can penetrate tough tissues, (2) modeling nerve with carbon fiber electrodes to understand the benefits of a small, carbon electrode, and (3) creating documentation and distributing carbon fiber arrays to neuroscience labs.

Previous work showed that sharpened carbon fibers are capable of penetrating tough nerve tissue and recording electrophysiological signals. However, these electrodes had a large, variable surface area due to the sharpening method which minimized the chance of recording selectively within the nerve. To address the need for a small sharpened electrode, I applied a technique used in microscopy electrode fabrication, acid etching, and applied them to the carbon fiber electrodes. To my knowledge, this acid etching technique resulted in the smallest carbon fiber electrode tip (SPF) capable of recording *in vivo* across multiple animal and tissue models.

These small, pointed fibere electrode (SPFe) tips were compared with the previous large surface area sharpened electrodes resulting in less variability in the tip surface area and sharpness. In this work I show that carbon fiber electrodes can be modified to small, sharp geometries in a reliable manner.

Computational modeling was used to better understand the physics of a 3D carbon fiber electrode. Models consisted of a simplistic nerve and carbon fiber electrode, which was modified to represent three surfaces areas – a perfect point source, the SPFe, and the large electrode from previous work. This model predicted a large difference in performance between electrodes, with the SPFe predicted to record larger signals in nerve than the large surface area electrode. This model also predicted that the SPFe was able to perform almost as well as the point source electrode in almost all paradigms. This work indicates that a smaller electrode is indeed better for recording from nerve.

Finally, carbon fiber electrodes, while useful in neuroscience research, are difficult to acquire. In order to help distribute the science investigated in this thesis, a "how-to" guide was created and many of the carbon arrays used in the Chestek lab were made open-source to encourage labs to build their own neural arrays for their specific needs. This work explained all the steps necessary to build a carbon fiber and presented 3 previous tip optimizations (scissor, Nd:YAG laser cut, blowtorch) and a new UV laser optimization that could easily be implemented in a given lab. This work aimed to increase the accessibility of customizable arrays that could be fabricated without specialized training in a cleanroom.

In summary, this thesis focuses on the tip optimization of carbon fiber electrodes, which has many applications in neuroscience from basic science research to future clinical applications.

Chapter 1
Introduction

1.1 Human Needs

In a clinical setting, a patient talks with a doctor about options for their treatment plan regarding loss of limb function after a traumatic neural-related injury (i.e. stroke, paralysis, spinal cord injury (SCI)). Long ago, treatments may have been limited to either a medical accessory (e.g. a crutch or ill-fitted prosthetic) or a large dose of whisky before amputation by a barber-surgeon [1]. However, in the 21st century, researchers are investigating almost science-fiction levels of intervention in the form of a neural array – a device used to directly monitor or stimulate neural tissue – and brain computer interface (BCI) in their laboratories [2], [3], [4], [5].

When talking about traumatic neural injuries, we often think about spinal cord injury that results in paralysis. However, SCI can also result in chronic pain, organ dysregulation, and other comorbidities. Broadly speaking, SCI affects over 17,000 new patients per year in the United States alone [6]. Worldwide this incidence number is closer to 0.9 million per year with prevalent cases numbering over 20.6 million [7]. As the spinal cord carries signals from the brain down to the different parts of the body telling them how to function, the location of the injury determines which bodily functions are lost, from limb motor and sensory function to bladder control. SCI results not only in the loss of motor and sensory functions, but typically comes with co-morbidities such as depression [8] and pain [9]. Due to the wide range of symptoms and conditions resulting from SCI, medical research looks for ways to help treat and alleviate these co-morbidities.

BCI is used to directly access the affected tissues using a neural array to provide an electric intervention or therapy [3]. Neural arrays can be implanted in the spinal cord [10], brain [11], and nerves [12] to help patients regain lost functions and relieve their symptoms and regain control in their lives [2], [13]. A BCI system can monitor or manipulate the body's natural electrical signals sent from the brain to other areas of the body via the spinal cord. However, neural arrays tend to be an invasive intervention as surgery is required to get the device close to the target tissue so it is as effective as possible [14], [15]. This invasiveness is part of a trade-off to allow for better signal interfacing that can improve the efficacy of a neural array's application [15].

Neural arrays are not limited to spinal cord injury research – in fact, many of these arrays are used to study other disease models as well. Research using neural arrays is widespread among disease type, injury, and conditions. Retinal implants have been used to restore some sight to patients [16], [17], [18]. Epilepsy monitoring and prevention using neural arrays on the surface of the brain is an ongoing pursuit with promising results [19], [20], [21]. Chronic pain interventions focus on finding stimulation patterns to "block" or decrease pain signals [22], [23], [24]. Neurological conditions that are non-responsive to current medical treatment (e.g. extreme cases of depression and anxiety) are also using deep-brain stimulation (DBS) for both understanding and treatment of these conditions [2], [3]. While controversial in Deaf World [25], [26], [27], the cochlear implant is one of the most common neural implants [28], [29] and provides patients a sense of hearing. While primarily in laboratories and clinical settings, BMI applications are being translated from animal to human currently. Robotic arms are able to be controlled by users brain signals [30], [31] in amputee patients. Similarly, limb function may be able to be recovered for stroke and paralysis patients using functional electrical stimulation [31]

that uses the existing pathways in the body. They can also be used for monitoring brain waves and predicting a seizure for an epileptic patient [19], [20], [21]. Neural arrays in conjunction with BCI also open up a world of brain-machine interface (BMI) applications.

To demonstrate the power of a BMI, let us briefly consider Stephen Hawking. Stephen Hawking was a leading physicist in relativity who used a computer interface to communicate [32]. Stephen Hawking began losing his ability to communicate (via speech, writing, or sign language) when he was 21 and by 43 was deemed unable to communicate at all [32], [33]. Around that time a speaking program was developed by a researcher at Intel, who had also lost his voice [34], that tracked head and eye movement allowing Hawking to communicate through a speech synthesizer [35] allowing him to continue his research and contributions to society. Hawking's set up was not a true BMI and depended on his ability to move his eyes and head – an ability that not all communication disabled persons have. However, communication thought BCI continues to improve with users being able to use the interfaces faster, more accurately, and directly from brain signal decoding [36], [37]. This allows patients the freedom to speak naturally though a computerized voice as though it was their own and without the delay of typing or finding the word on a screen. BMIs open wide range of applications that may one day have be the standard in patient care. As exciting as these applications are, none of these potential advancements will be possible without a safe and robust neural array.

1.2 Neural Arrays and Electrodes

With such a wide range of potential uses, one might start to wonder, "What exactly is a neural array?" First, I must explain what an electrode is. An electrode is a conductor through which electricity travels either into or out of a given material or circuit – for the purposes of this thesis, an electrode is a conductor through which electricity travels to interface with biological

tissues primarily for recording and stimulation purposes. A neural array is a device with a given number of electrodes that interfaces with the nervous system in some capacity. The nervous system is comprised of the central nervous system (CNS) and the peripheral nervous system (PNS) [38]. The CNS is comprised of the brain and spinal cord. It is responsible for all of the sensory information that needs to be processed – sight, touch, smell, taste, and sound. These signals are comprised of chemical and electrical signals [38], [39], [40]. For the purposes of this thesis, we will focus solely on the electrical signals in the nervous system. The brain is comprised of cells called neurons which process information, makes a decision on how to respond, and then sends that signal to the appropriate body part through small cables called axons [38], [40]. Axons are the most interior part of and over all structure called the nerve. Axons are bundled together in a fascicle with thousands of other axons all carrying signal to and from the brain for the same parts of the body [15]. In turn, fascicles are also bundled within a nerve that signals headed to similar areas of the body around the body, branching off into smaller nerves when necessary. These branching nerves make up the PNS.

The PNS is comprised of two smaller nervous systems: the somatic and the autonomic, which can be further sub-sectioned into more specific tasks [38]. Overall, the PNS runs all the other functions that bodies need to survive: maintaining a heartbeat, breathing, digestion, movement, and proprioception. As these nervous systems ultimately run our lives, if one part of the system is damaged, missing, or has a maladaptive behavior, directly interfacing with it opens many doors for therapeutic intervention [2], [41] as opposed to applications with less specificity like pharmaceutical pain killers or large surface electrodes. Directly interfacing with the cells that control a behavior opens many doors for both understanding and controlling disease and injury [2], [3].

However, accessing the nervous system is no easy task. The neurons and nerves in the human CNS and PNS are very small with diameters ranging from 100 μm [42] down to 0.3 μm [43], though a majority of the smallest fibers, 84%, tend to be at least 2 μm in diameter [43], [44]. As such, the electrodes in these arrays must be ideal for their purpose.

Unfortunately, many clinical electrodes, like those used in DBS, use large electrodes that aren't very specific in their stimulation. These large electrodes will effectively stimulate our target; they will just also stimulate everything else in the area, which can have negative consequences. Conversely, if we wanted to record neurons or axons using a DBS-sized electrode, we would end up averaging all the signals around that large electrode into a waveform called a 'multi-unit' or if the waveform is too indistinct to claim neuron/axon level activity, a Local Field Potential. This is detrimental as our aim in this thesis is to target a specific cell or axon carrying a specific signal as the electrical potentials in the body are extremely small (μV scales) and thus it will be swallowed by the noise of the recording system and other cells in the area [45]. Thus, to record a small cell body in the nervous system carrying a very particular signal, we cannot use a large electrode, as the signal is too small to be perceived above all the other signals in the area. For the purposes of this document, I will focus on *recording* from those small-cell bodies and axons (< 10 μm in diameter) and the requirements therein of the electrodes for this explicit purpose. There are ideal parameters for the design of electrodes meant to isolate single cell and axon signals for processing.

To record from a small-cell, like neurons (< 20 μm diameter) or axon nodes of Ranvier (< 8 μm in diameter and width), an electrode should have certain qualities. The first being that it should be able to get near the target neuron or axon. The closer an electrode can get to a cell, the larger the recorded amplitude on the electrode will be [14], [15]. Additionally, the size of the

electrode is also highly important to recording good neural signals [14], [39], [46]. Recall, if an electrode is large, many cells will be recorded and averaged across the electrode. However, if an electrode is close to the size of its target, the recorded amplitude of interest should be larger as there is less averaging across the electrode's surface [14], [39].

However, small electrodes result in a high impedance - the effective resistance of an alternating current system. In a electrode-tissue interface there are three main sources of impedances to take into consideration: 1) biological properties of the tissue 2) electrode geomety and 3) electrode properties. A high impedance caused by the biological tissue itself though immune responses can dampen the signal's recorded amplitude making it more difficult to detect the signals of interest [47]. While the immune response can be lowered, the tissue impedance is expected to be high and unchangeable. The electrode geometry is important to consider as well, as surface area and impedance are inversely related. Additionally, the shape (flat disc, cone, cylinder) and surface area of an electrode can also affect the impedance of an electrode. [] The smaller an electrode, the higher its impedance will be. This causes issues for recording and stimulating selectively within a tissue.

For stimulation, the goal is to apply a current to the electrode that will excite nearby cells and cause them to fire off a signal. This current amplitude is typically limited to a safe range that will prevent damaging the surrounding tissue through hydrolysis (creating bubbles) or electrocuting cells (cell death). A high impedance electrode requires that more voltage is needed to overcome the impedance, which pushes the stimulation parameters out of safe compliance levels. Additionally, a higher voltage is not ideal for the electrode itself long-term as it can lead to corrosion and electrolysis on the electrode [48] causing it to degrade over time. Essentially, with a high impedance it becomes harder for current pass through the electrode-tissue interface

making it difficult to stimulate or record a signal from the targeted neuron or axon. There is mixed opinion about the importance of a low impedance in recording electrodes, especially as much of the noise caused by a high impedance can be mitigated though amplifiers [49]. However, impedance can be used chronically to monitor the state of the electrode over time.

The ideal small-site electrode has to have a low surface area and a low impedance to isolate the signal and increase the signal-to-noise ratio resulting in easy-to-define waveforms in the data [48]. Currently, the best way to lower the impedance for small surface area electrodes is to increase the *chemical surface area* of the electrode. Up to this point, we have considered only the *geometric surface area* of the electrode, which is defined as the total area that the surfaces that make up an exposed site take up. The *chemical surface area* is a more microscopic concept. This is the available area on the electrode that can interact chemically. Think of the difference between sanding a table with a smooth piece of paper and a piece of sandpaper of equal size. The papers have the same *geometric surface area,* however the "chemical" surface area here is larger on the sandpaper due to the rough surface allowing it to interact with the table more.

We can thus do a similar "roughening" of the recording site to lower the impedance. [50]. This can be achieved through electrochemical interventions like electroplating a conductive material like PEDOT:pTS/PSS [51], [52], [53] or platinum iridium [53], [54] onto the recording site. These conductive coatings allow researchers to tune the type of reaction (capacitive, faradaic) occurring at the surface of the electrode-electrolyte interface for easier current exchange with the surrounding tissue [39]. Mechanical interventions such as plasma ashing [55] or low pressure chemical vapor deposition [56] also help to reduce the impedance as they physically roughen the surface of the electrode adding additional chemical surface area.

However, the exposed electrode site is not the only consideration that must be taken into account when implanting devices. Electrodes are implanted with other materials to support and protect them within the body. Thus, a multitude of materials have been investigated and implemented in an attempt to create an electrode that does minimal damage and produces good signal quality [53], [57], [58]. Thus, these neural arrays must carefully consider every part that is implanted into tissue: from the electrode to the cables connecting it to a computer interface.

1.3 Challenges of Neural Arrays

While it is easy to get onto someone's nerves, it is much more difficult to get into them. The brain is one of the softest organs in the body [59] and thus it is relatively easy to implant electrodes once the skull is out of the way. Chronic arrays in brain have the benefit of the skull to anchor electrode arrays to which provides a stable point to hold the array connector in place [60], [61]. Take the Utah array as an example: the array sits directly on the brain and the signals are carried away from it through a flexible cable that attaches to a connector that is fixed to the skull [62]. This set up allows for a stable connection point for porting signals to a computer interface , thus making chronic signals achievable.

While this configuration works in brain, it becomes much more difficult in nerve. To begin with, nerves do not have a fixed bone surrounding them to allow for stable connection. The bones near nerve are typically buried in muscle and other tissues that make them infeasible as a stable connector point due to the amount of damage that would ensue getting down to the bone. Additionally, while the brain moves, it moves considerably less than nerve which not only moves in plane with joints and muscle, but stretch and contract [63], and even shrink and swell as part of an action potential [64]. Adding to this difficulty, the physiology of nerves creates more challenges for selective recordings. Nerves are split into fascicles [15] which have bundles of

thousands of axons all sending signals, both efferent and afferent, side by side. Additionally, these signals have low amplitudes on the microvolt scale. The largest signals recorded from nerve have amplitudes of around 100- 180 μV [65], [66] and is it difficult to parse out if those signals are from a single axon or multiple axons firing together due to the crowded nature of a nerve fascicle or if those spikes are anomalies associated grounding issues. So not only are we trying to penetrate the thick protective layer around a nerve, but trying to target the fascicles of interest, record, and finally trying to analyze the signals that were recorded. Many attempts to get into nerve have been made over the years, however, there has yet to be an array with both high selectivity (only recording from the axons or fascicles of interest) and low invasiveness (little damage to the nerve).

1.4 Neural Array Materials

When placing a neural device into the body, many factors come into consideration early on in the design process. In addition to the electrode size and placement, the materials supporting the electrode(s) must also be appropriate for use in a body. Biocompatibility, invasiveness (how much damage is done upon insertion due to modulus mismatch, geometric size, etc), selectivity, and ease of production are just a few of these concerns for all materials used in a neural array.

1.4.1 Common Materials

When discussing neural array materials, the properties of that material are vitally important to ensure it can record signal or stimulate safely and is biocompatible enough for practical use. Most electrodes are coated in a metal (gold [67], platinum [54], [68], etc.) or a conductive polymer (i.e. PEDOT:PSS/pTS [51], [52]) to ensure that a low impedance is

achieved. However, the supporting substrate material - on which electrodes are placed - also have mechanical properties that must be carefully considered.

A popular material to use in neural arrays is silicon [57]. Silicon allows for the easy production of batches of electrodes through lithographic techniques [57], [69], [70], [71]. These techniques allow for neural arrays to be "printed" in a fairly dense way. Not only can a large number of electrodes be "printed" in a small area, but multiple electrodes can be printed on the same silicon disk allowing for batch production [57], [72], [73]. Additionally, the electrodes can vary in size and density on the same device. Lithography makes for an extremely reproducible fabrication in a clean room. As it is the only device approved for long-term use in humans, the Utah Array [62], [74] is a silicon 'bed of nails' design that records signals. However, the Utah array is not the only device to utilize the advantages of silicon. Other commercial devices like Neuropixel [72], NeuroNexus [75], and Cambridge Neurotech [76] use silicon as a substrate for electrodes.

However, silicon also has its disadvantages as a material for neural arrays. From a biological standpoint, silicon causes tissue damage despite small array geometries [77], [78], [79]. Silicon is shown to cause scarring responses for up to 6-8 weeks [78] after insertion which makes recording or stimulating too unreliable during that time. Continuous inflammation around the silicon implant sites has been noted to last from less than 2 years to over 7 years [80] and explanted electrodes have had active macrophages attached to the shanks of the electrode [60] indicating a large separation between the electrodes and the targeted neurons/axons. Finally, cell death is prevalent around silicon electrodes. Utah arrays have been documented to have an average of 63% less cell density than control tissue around implant sites [77] and to be encapsulated by scar tissue [77], [81]. Silicon at large has been shown to decrease the neural

density around the target site either through death [80] or pushing neurons and axons away [79]. There have been attempts to reduce the initial scarring through different insertion techniques such as using pneumatic (fast) insertion [82], slow insertion [83], and the addition of a soft material or lubrication [84] on the silicon. Pharmaceutical interventions like combination antibacterial/anti-inflammatory coatings [84], [85], [86] have been employed to deter biofilm, inflammation, and protect neurons with promising histology results. However, these interventions have not been enough to mitigate all the damage done by the silicon array.

Mechanical properties of silicon often lead to failures either immediately or slowly over time [57], [81]. Silicon is known as a "hard" material as its mechanical properties are mismatched to the tissues in which they are implanted. "Hard" materials are denoted as having a large Young's Modulus (a measure of how much pressure is needed to deform a material), with materials like silicon, bone, and teeth having Young's moduli over 10^{10} Pa [57], [84]. Nervous system tissues on the other hand are "soft" and typically have a Young's Modulus of $10^2 – 10^4$ Pa [57], [84]. This mismatch of ability to deform means that the nervous system tissue will deform under the silicon leading to death of cells [77] and axons [74], [87]. Silicon also faces stresses that can cause bed-of-needle and planar shank designs to fail in similar ways. Electrode tips breaking account for up to 22% of failures on bed-of-needle designs [77] and electrode cracking on planar shanks [88]. As silicon devices typically have an additional layer of insulation, this adds another method of failure. Parylene C is a common insulator, however, has many failure models [89] such as delamination and degradation over time. Additionally, as silicon devices use metal electrodes, those metals often degrade *in vivo* and can corrode [57], [88].

One way to address the damage of silicon in tissue is to change the silicon out for a softer material. Softer materials have been investigated to help reduce the damage caused in insertion and allow for electrodes to move in tissue rather than act as a knife like silicon. There are many groups [90], [91], [92] that use Parylene C as a substrate and insulator for easy to prototype electrodes. These electrodes have been inserted into brain with the assistance of a shuttle causing less damage than seen in silicon counter parts. Additionally, these materials are ideal for cuff electrodes in nerve [91], [93]. However, because they are cuff electrodes, we cannot have a highly selective electrode as the cuff electrode sits on the outside of the nerve and thus is not close enough to axons to isolate a signal. Another soft material that has been investigated in nerve is polyimide. Polyimide has been used to insert into the nerve [94], [95], [96] however, while softer than silicon, this is still an invasive procedure and that often slices axons. Additionally, the soft polymer is much easier for the body to degrade overtime leading to a shortened chronic lifespan [95], [97]. Another approach uses SU-8 and other photoresists to create a very thin, more flexible substrate [98], [99]. These arrays are stiffened using PEG and then inserted into brain using a specialized shuttle. They cause very minimal damage on insertion and chronically. However, the photoresist, like other polymers, does degrade in the body over time leading to shorted electrodes, noisy signals, and eventual device failure.

Thus the search for neural electrode materials that are strong enough to penetrate tough tissue, cause low biological immune responses, have a high selectivity and low invasiveness is on-going. One material that shows great promise is carbon.

1.4.2 Carbon: Yarns and Fibers

When introducing a material into the body, the immune response to the material is most likely because that material is not native to the body [100]. One way to help address these issues

it to introduce a material reflective of the environment the implant will reside [100], [101]. As carbon fibers are a “soft material”, flexible, and made of carbon (a native material) [102] we should expect to see less of an immune response from the carbon fiber electrodes. Carbon fiber materials often show such little immune response in chronic (6 weeks) studies that identifying were the carbon fiber electrode is in the brain tissue is a challenge [103], [104], [105]. This low immune response could also be due to carbon fibers having such a small diameter (< 10 μm diameter with insulation [106]) that cells can simply ignore the intrusion, however, even large carbon yarn electrodes (18 - 28 μm diameter with insulation [105]) show minimal immune response and cell death around the exposed carbon recording after being inserted chronically [105]. This indicates that the carbon fibers are more bio-compatible than traditional materials and the body should be less likely to encapsulate the arrays in scar tissue and glial cells as is seen in silicon probes. This allows carbon fibers to be inserted near the cells of interest with low damage to the area and a low chance of cell death, thus increasing the chances of recording from the target area.

Carbon fibers are naturally sub-cellular in size meaning they will pick up less noise and better isolate the cell of interest. Due to their sub-cellular size and ability to insert into tissue, this has led to some labs using carbon fibers for intracellular recording [107]. While in the past carbon fibers have been difficult to insert into tough tissues like nerve, muscle, and retina, our lab and others have used blowtorching techniques to sharpen the carbon fibers to increase their ability to insert into brain [108] and insert into nerve at all [109]. Unfortunately, blowtorching is difficult to reproduce reliably with sharpened tips ranging from 100 μm to 500 μm [105], [108], [109] thereby eliminating the selectivity that is afforded to these electrodes due to their small size.

1.5 Summary of Thesis

In this thesis, I examine carbon fiber electrode neural arrays. Specifically, I attempt to optimize the tip geometry of a carbon fiber for recording in multiple tissue models including brain, retina, and nerve: meaning that the electrode needs to be sharpened to be able to penetrate the tougher tissues while remaining small (< 10 um) to increase the selectivity of the electrode. The SPFe is implemented across multiple animal models (octopus, sea slug, etc) and in multiple tissue types (brain, retina, etc) to test the modularity of this tip optimization. This tip optimization may provide better insight into small cells in upper layers of the brain, small retinal ganglia cells, and unmyelinated axons that have previously been difficult to isolate and study.

In Chapter 2, I discuss optimization of carbon fiber electrode tips to sub-neuronal scale (< 10μm in length) and acute recordings of the electrodes in rat motor cortex, octopus axial nerve cord, and stimulation in *aplysia* ganglia.

In Chapter 3, three carbon electrodes (SPFe from chapter 2, Welle [109], and Carbon Yarn [105]) were modeled inside of a simplistic single axon nerve to predict how different the signal amplitudes would change due to recording site size. The SPFe arrays were tested *in vivo* to help gauge the predictions of the model.

As the Neural Engineering Training Program, which has a major goal translational research education and activities, in part supported my training, I describe in Chapter 4 my efforts to create open-source carbon fiber neural arrays into other labs with open-source PCB designs, step-by-step fabrication instructions, and supplemental information for two additional arrays.

In summary: this thesis will examine potential avenues for integrating carbon fiber electrodes into common use in both neuroscience research and patient therapeutics.

Chapter 2
Fabrication and Validation of Sub-Cellular Carbon Fiber Electrodes

Julianna Richie, Joseph G. Letner, Autumn McLane-Svoboda, Yu Huan, Dorsa Haji Ghaffari,
Elena della Valle, Paras R Patel, Hillel J. Chiel,
Galit Pelled, James D. Weiland, Cynthia A. Chestek

A version of this chapter was accepted for publication in IEEE TSNRE.

2.1 Abstract

Multielectrode arrays for interfacing with neurons are of great interest for a wide range of medical applications. However, current electrodes cause damage over time. Ultra small carbon fibers help to address issues but controlling the electrode site geometry is difficult. Here we propose a methodology to create small, pointed fiber electrodes (SPFe). We compare the SPFe to previously made blowtorched fibers in characterization. The SPFe result in small site sizes (105.4 ± 20.8 μm2) with consistently sharp points (20.8 ± 7.64°). Additionally, these electrodes were able to record and/or stimulate neurons multiple animal models including rat cortex, mouse retina, Aplysia ganglia and octopus axial cord. In rat cortex, these electrodes recorded significantly higher peak amplitudes than the traditional blowtorched fibers. These SPFe may be applicable to a wide range of applications requiring a highly specific interface with individual neurons.

2.2 Introduction

A wide range of medical and clinical therapies rely on stimulating or recording neural tissue using implantable electrodes. For example, deep brain stimulation (DBS) has been used in over 160,000 people to treat Parkinson's related tremor and gait irregularity [110]. Recording with implantable electrodes is less common in clinical applications. However, there are emerging applications, including those that use recorded neural signals as biomarkers to modulate stimulation. For example, the RNS system (Neuropace, Mountain View, CA) detects pre-ictal activity to trigger neural stimulation to treat epilepsy [21].

The electrodes used to record and stimulate in those clinical applications interact with populations of neurons instead of individual neurons due to their large surface area. These particular therapies can provide benefit to patients despite their lack of neuron specificity. However, large electrodes cannot be used for therapies where targeting small groups of cells is a requirement. For example, in retina stimulation to provide vision for the blind, stimulating retinal ganglion cells (RGC) with a small electrode is required to activate only a small number of cells for the highest visual acuity [111]. Similarly, as a recording application, brain machine interfaces involve recording from specific neurons and interpreting their activity to provide commands for assistive technology [112]. Neuron level resolution enables differentiation between the activity representing different fingers, intended velocity, and amount of force translated from brain to arm[15], [39]. To fully isolate a single unit, an electrode needs to be similarly sized (100 μm^2) and close to the neuron [14]. Low impedance is likely required to have sufficiently low noise but this is challenging to achieve on small electrodes as surface area and impedance are inversely related.

Most electrode arrays designed to interface with individual neurons have been designed with small electrode sites on stiff substrates. Due to its widespread use in electronics, silicon devices are easiest to manufacture and many electrodes can be densely packed on a single wafer[62], [74]. Notably, the Utah Electrode Array (UEA) has been used for many years in humans and nonhuman primates with multi-year recordings[81], [113], [114], [115]. Planar shank-based designs (e.g., Neuropixel [72], Cambridge [116], NeuroNexus [73]) allow for simultaneous recording from multiple cortical layers, whereas the UEA places all electrode sites at one depth. But high-resolution planar shank-based electrode arrays are not routinely used as chronic electrodes in humans or NHP due to the planar geometry. The most recent silicon electrodes have substantially increased the number of channels from 100 on to close to 1000 [72]. However, silicon substrate arrays may fundamentally cause tissue damage [78], [80], continuous inflammation around the device sites, and counterproductively, a decrease in the neuron density around the recording site [60], [77], [80], [87], [100]. These issues motivate the investigation of other materials to preserve the tissue while maintaining the ability to record selectively from neurons.

Ideally, electrodes should cause very little foreign body response (FBR), and several strategies have been attempted to achieve this. For example using materials with lower Young's modulus (softer) may lead to a lower FBR [47], [57], [100], [117]. Reducing electrode substrate size to cellular sizes also leads to lower FBR, even when using stiffer materials [118], [119]. Additionally, the geometry can reduce the force needed to implant into brain that can cause initial damage. However, it is difficult to make robust probes from silicon alone at these small sizes. Therefore, cellular scale probes have been fabricated primarily using other materials. The Net10/50 probes [98], [120] and amorphous silicon carbide "ultramicroelectrodes" [121], both

utilize thin, flexible shanks that cause little insertion damage while still recording high quality signals. Specifically, the Net10 probes use SU-8 and lithography techniques to create a 10 μm x 1.5 μm cross-section. However, soft devices often require specialized insertion techniques, such as an insertion shuttle or a stiffening agent [57], [122], [123]. While many soft probes boast small cross-sectional areas, in practice wider devices are used more often than the smallest form factors due to durability.

Another limitation of putting lots of contacts along a shank is their confinement to a column of neurons. Many applications require recording capabilities across a larger brain area. For these applications, microwire arrays are a popular design as they are both commercially available and can also be fabricated by individual labs. These arrays have diameters down to 30-50 μm, and even down to 5 μm in research settings [124]. However, metal microwires tend to deform upon insertion [125], which causes unwanted tissue damage. More importantly, the deformation removes confidence in the placement of the electrodes until after the tissue can be imaged. As these microwires deform easily at these scales [126], [127], stiffeners [57] can be used to achieve more reliable placement. For example, the CHIME array [128] utilizes glass insulation to create a multi-electrode array that can hold its shape. While glass is sufficiently stiff ,it is brittle and breaks easily under stress preventing it from being a reliable chronic implant [5]. Additionally, microwires are known to corrode *in vivo* causing cracks to form in the insulation and at the electrode degrading the array's performance [129].

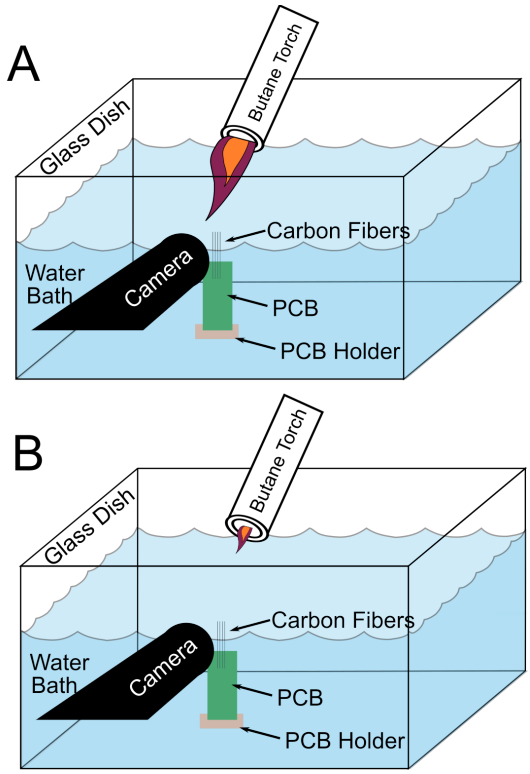

Figure 1: Large-blowtorch (A) vs small-blowtorch (B methods). The water bath is set up the same way, but the small-blowtorch flame is much smaller than the flame in A. The smaller flame allows for a smaller tip to be exposed (< 100 µm).

Carbon arrays have become a viable option[108], [109], [130], [131], [132], [133] due to carbon's inherent strength and conductivity. Carbon arrays have been implemented in a number of form factors. Carbon yarn [105], [134], [135] has been shown to record in nerve, and can be assembled in the lab with 10-30 µm diameters [105], [134]. To enable deep penetration into brain 64 fibers (7 µm diameter) were combined into a 200 µm diameter electrode [108]. However, these approaches do not allow for distributed array recordings across a large area. Our group has worked towards multi-channel arrays where carbon fibers are distributed over a larger substrate, where each fiber acts as an independent recording or stimulation channel [106], [136]. In previous work, we have demonstrated a carbon fiber array insertion into brain with individuated fibers for single unit recordings at up to 80 um pitch. We have also investigated modifying the fibers for insertion into tougher tissues like nerve and deeper unassisted insertion

into cortex. These applications require a sharpened fiber [65], [109], but the sharpening process left the fibers with relatively large recording sites that cannot readily isolate single units.

In this paper, we describe a fabrication process for "small, pointed fiber electrodes" (SPFe) that provide both small electrode surface area for single unit recording and sharpened tips for better penetration into tissue. We use chemical etching of carbon fibers to give the SPFe a repeatable ~100 μm^2 electrode area without loss of electrode functionality. The approach is based on that used for fabricating carbon fiber microscopy tips used in imaging [137], [138], [139]. Here, we evaluate the electrochemical and physical properties of SPFe and deposit conductive coatings to reduce impedance and enable microstimulation despite this small size. Finally, we demonstrate SPFe in multiple biological preparations to demonstrate feasibility. We show here that chemical etching is an appropriate and robust method for optimizing the carbon fiber electrode tip to sub-cellular size capable of recording and stimulating across multiple tissue types and animal models.

2.3 Methods

Probe Fabrication

Carbon fiber arrays were fabricated following similar methodologies as previously reported [106], [136]. Briefly, a printed circuit board with exposed gold traces was coated with silver conductive epoxy (H20E, Epoxy Technology, Billerica, MA) and carbon fibers were inserted into the silver epoxy. The epoxy was cured then insulated using a non-conductive epoxy ((NOA61;NorlandProducts,Inc., Cranbury,NJ).Arrays were coated with Parylene C (Parylene C Deposition System 2035, Specialty Coatings Systems, Indianapolis, IN) to a thickness of ~ 800 nm. The carbon fibers were then blowtorched [109] (Figure 1) to remove Parylene C from the tips and re-expose a small portion of the carbon fiber. One set of fibers (n = 69) was exposed

with a larger flame (Figure 1 A) exposing ~140 μm of carbon. This group was further processed using chemical etching (SPFe). Another group (n = 47) used a small blowtorch flame (Figure 1 B) to expose < 100 μm of the carbon fiber from Parylene C. For clarity, the groups will be referred to as large-blowtorch (~140 μm exposure, using historical data [109] n = 574), SPFe (chemical etch), and small-blowtorch (< 100 μm exposure). HDCF arrays were prepared for implant following previous literature [107] for ease of surgeon use. For HDCFs in this study, every other fiber was SPFe or large-blowtorch for easy comparison of the two electrode preparations.

To lower impedance of the electrodes a coating of PEDOT:pTS or Platinum Iridium (PtIr) was applied to the electrode following the methods in previous literature [54], [106], [140]. Simply, recording electrodes were coated with a solution of 0.1M:0.01M PEDOT:pTS by applying 600 pA current to each electrode for 10 minutes. PtIr was applied using a solution of 0.2 g/L Na3IrCl6H2O and 0.186 g/L Na2PtCl6H2O in 0.1 M nitric acid and applying a CV sweep from -0.1 to 0.1 V at 200 mV/s for 250-300 cycles depending on the size of the exposed carbon fiber.

Chemical Etching

A solution of 0.5 mM $K_2Cr_2O_7$|5 M H_2SO_4 was prepared to etch the tips of the carbon fibers [138], [139]. Following previous literature [139], the SPFe were lowered into the solution along with a reference and counter electrode (described in *Electrical Characterization*) (Figure 2 A). A constant 3.5 V_{rms} was applied in one-second increments for no more than a cumulative 4 seconds. The probes were triple rinsed in DI water and allowed to rest for a minute after each 1 second etch to help disperse the built-up surface charge on the electrode before measuring 1 kHz impedance in PBS solution. Scanning electron microscopy (SEM) confirmed a small, pointed tip

was reliably attained once an impedance increase of at least 1 MΩ (at 1 kHz) after etching was measured. This relative impedance increase of 1 MΩ from the un-etched impedance occurred between 2-4 seconds of etching for all fibers in the study.

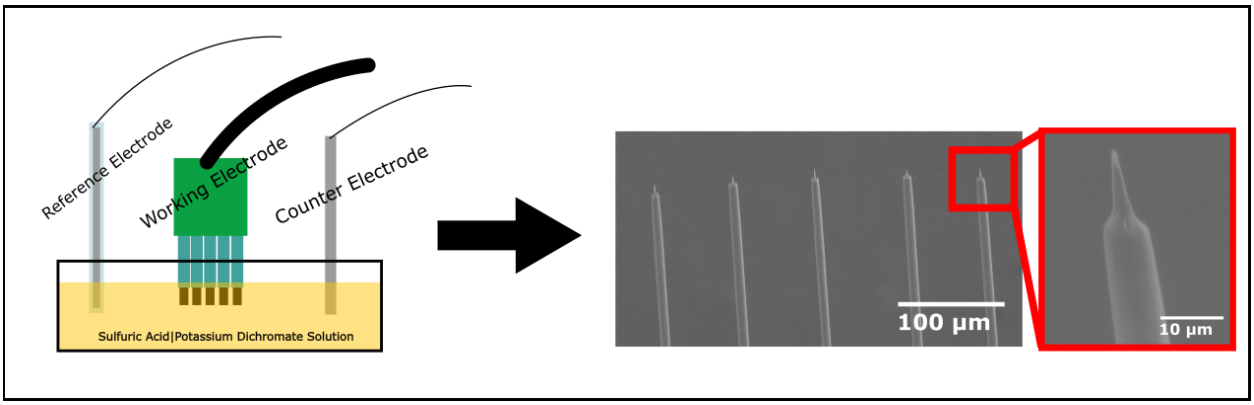

Figure 2: Schematic showing the etching set up (left) and resulting sharpened tips (right). Set up for etching is simple with a reference and counter electrode submerged in solution with the exposed tips of the carbon fiber array. A voltage pulse is applied for several seconds and then the fiber tips are imaged to check geometry. The tips are sharpened and sub-cellular in size as seen in the far right image.

Physical Characterization

Tip length and sharpness were quantified using scanning electron microscopy (SEM) imaging (Tescan Rise, Tescan Orsay Holding, Brno—Kohoutovice, Czech Republic). SEM imaging was performed under low vacuum mode (LVSTD, low vacuum secondary electron Tescan detector) to preserve electrode functionality. An excitation voltage between 5 and 20 kV was used. Tip length was defined as the distance between the tip of the exposed carbon to the lowest edge of the Parylene C transition. Sharpness was measured using the built in angle tool in the SEM software. The surface area of a cone was calculated using the measured height, h, and r = 3.5 µm:

$$SA = \pi \cdot r * \sqrt{h^2 + r^2} \qquad \text{Eq. 1}$$

Insertion Testing

Insertion tests were performed following previous methodologies [106] in perfused rat brain. In short, a rodent brain perfused with 1x PBS was exposed and dura and pia were removed. A set of SFPe (0.5 mm – 5 mm, 0.5 mm increments) were lowered using a stereotaxic manipulator. Fibers were recorded as successful if they were able to penetrate into the brain and continue insertion along their full length. Unsuccessful insertion was determined by a continuous buckling of the fiber that never penetrated. Results were analyzed using a Wilson Binomial Confidence Interval Test to determine the 95% confidence intervals around each data point. Data was compared to historical data [106] using a Pearson's Chi-Squared Test to determine significance.

Electrical Characterization

All electrodes were subjected to cyclic voltammetry (CV) and electrochemical impedance spectroscopy (EIS) during different stages of the fabrication process. Impedances of the bare fibers were taken at several points during fabrication to ensure electrical connection and verify exposed area: after flame exposure, throughout the chemical etch process, and to ensure good coating of any added conductors. Following previous methods [106], a 1 kHz impedance scan was conducted in 1x PBS (BP3994, Fisher, Waltham, MA) with an Ag|AgCl reference electrode (RE-5B, BASi, West Lafayette, MA) and a 2 mm diameter, 3 cm long, hollow stainless-steel rod as the counter electrode. A PGSTAT12 Autolab potentiostat (EcoChemie, Utrecht, Netherlands) using NOVA software provided by the vendor was used to run the EIS and CV measurements. Results were analyzed using custom MATLAB scripts (MathWorks, Natick, MA) and reported as 'mean ± standard deviation'.

Full-spectrum EIS was performed in a frequency range from 31 kHz to 10 Hz applying a 10 mV_{rms} sine wave following previous methods [106]. All EIS were performed in 1x PBS

solution in the three-electrode configuration following the 1 kHz measurements above.. Cyclic voltammetry was taken only at the end of the tip preparation and before and after coating. This was done to monitor and characterize any redox reactions and to ensure a safe water window for each group of probes for use *ex vivo*. CV scans were obtained by sweeping three times between −0.6 and 0.8 V versus Ag|AgCl at a scan rate of 1 V/s. Charge storage capacitance (CSC_C, [39]) was estimated from the CV data using the custom Matlab script.

In-Vivo and In-Vitro Validation

All animal procedures were approved by the Institutional Animal Care and Use Committees at the University of Michigan or Michigan State University. Several animal models were used to investigate the modularity of the SPFe tips in different tissue types: rat motor cortex (softer tissue), mice RGCs (small cell), octopus axial nerve cord (ANC) (tough tissue), and A*plysia* ganglia (large cell).

Rat Motor Cortex *In vivo* validation of SPFe tip recording capacity in rat cortex closely followed our previously reported terminal procedures performed to acutely measure electrophysiology [109], [140], [141]. We implanted high-density carbon fiber (HDCF) electrode arrays [104] with SPFe tips into adult male Long-Evans rats (n=2) weighing 330 & 370 g. Each rat was implanted with two electrode arrays, where the first was removed prior to implanting the second. In one rat, the electrode arrays had alternating large-blowtorch [109] and SPFe tips for direct comparisons of single unit amplitudes *in vivo*. Rats were briefly anaesthetized with isoflurane (5% v/v) to facilitate intraperitoneal injection of ketamine/xylazine (90/10 mg/kg) for anesthesia induction, which was maintained with periodic update injections of ketamine (30 mg/kg). Carprofen (5 mg/kg) was administered subcutaneously as an analgesic. Breath rate and temperature were monitored throughout the procedure. After an incision along the head's

midline, clearing the periosteum, and cleaning the skull, a stainless steel bone screw (cat. # 1ZY93, Grainger, Lake Forest, IL) was screwed through the skull, posterior to lambda, to touch the brain as an electrical reference. A craniotomy was drilled into the right hemisphere 1-3.5 or 1-2 mm mediolaterally (M/L) and 1-3.5 or 1-3 mm anteroposteriorly (A/P) relative to bregma targeting motor cortex. The first array was lowered via a stereotaxic arm to the dura surface to zero the probe coordinates on the dorsoventral axis followed by a durotomy and connecting a reference wire on the probe to the bone screw. Each probe was inserted to multiple depths spanning layers I – V of the motor cortex (0-1600 μm, [142], [143]) and electrophysiology was recorded at each depth.for 3 minutes using a ZC16 headstage, RA16PA pre-amplifier, and RX7 Pentusa base station (Tucker-Davis Technologies, Alachua, FL) in a faraday cage with a sampling frequency of 24414.1 Hz. Rats were euthanized at the end of the procedure.

Mouse Retina Intraretinal stimulation was performed using SPFe in *ex vivo* retina obtained from (C57BL/6) mice. The eyes were previously injected with rAAV2-CAG-GCaMP6f-WPRE-bGH to express calcium indicator GCaMP6f in retinal ganglion cells (RGC) [144], [145]. Three to four weeks after intraocular injection of the AAV vector, animals were euthanized with ketamine (100 mg kg^{-1}) and xylazine (10 mg kg^{-1}). Retinas were isolated, mounted on a transparent chamber, and superfused with bicarbonate-buffered Ame's Medium to ensure cell health throughout the experiment. Carbon fiber electrodes were inserted from the photoreceptor side of the retina and calcium imaging was performed from the RGC side. The electrode tip was positioned at 20 μm distance from the RGC layer vertically using a micromanipulator, using the baseline fluorescence of the RGCs to locate the RGC layer. Electrical stimulation was delivered by the PlexStim electrical stimulator (Plexon Inc., Dallas, TX) and the voltage transient across the electrodes was recorded by an oscilloscope connected to the voltage transient (VT) output of the

PlexStim. Cathodic-first biphasic pulses with 100 μs duration per phase were delivered at 120 Hz and various current amplitudes (5 – 15 μA).

Aplysia Ganglia. The SPFe was tested in *Aplysia* neurons for its intracellular recording ability, following the method in Huan et al., 2021 [107]. Briefly, the buccal ganglia were isolated from the animal and were pinned to the Sylgard base of a dish. One buccal ganglion was carefully desheathed to expose individual neurons. To obtain an intracellular action potential, a SPFe fiber was inserted into a neuron until it penetrated the cell membrane. A glass microelectrode was inserted into the same neuron after the SPFe insertion to compare the recordings. To provide a direct comparison, both electrodes were connected to a DC-coupled intracellular amplifier (A-M Systems Model 1600, Everett, WA) and the signals were recorded in AxoGraph X (AxoGraph Scientific, Foster City, CA) at a sampling rate of 5000 Hz. The impedance of the glass microelectrode was 3.4 MΩ.

Octopus Axial Nerve Cord (ANC). Adult specimens of *Octopus bimaculoides* collected from the California coast were used to validate the insertion and recording capabilities of the electrodes [146]. The left front arm was amputated from the octopus body and placed in a dissection tray perfused with filtered saltwater from the housing tank for longevity. Dissection of the arm to isolate the ANC, a structure similar to that of the spinal cord, ensured that recordings would be only of neuronal activity. The SPFe was inserted directly into the ANC tissue at the base of the octopus arm for recording. To elicit activity, mechanical stimulation at the distal portion of the arm was performed. Recordings were taken through Spike2 (Cambridge Electronic Design Limited, Cambridge, England) software sampling at 30 kHz.

Motor Cortex Spike Analysis

The recordings of the SPFe tips in rat cortex were analyzed using our previously described protocol [103], [140]. Briefly, electrophysiology was first common average referenced [147] in MATLAB 2022a (MathWorks, Natick, MA). Signals were then loaded into Plexon Offline Sorter (version 3.3.5) (Plexon Inc., Dallas, TX) and high-pass filtered (250 Hz cutoff, 4^{th} order Butterworth filter). A trained operator estimated the RMS baseline noise (V_{rms}) for each channel by manually identifying five segments per channel that were 100 ms in length with low neural activity and low artifact noise. Thresholds were set at -3.5× V_{rms}. To remove noise waveforms, cross-channel artifacts were invalidated, prospective clusters were manually selected in principal component analysis (PCA) space, waveforms assigned with K-Means clustering, and clusters containing clear noise clusters were invalidated. The remaining waveforms were clustered using Plexon Offline Sorter's Standard Expectation-Maximization Scan function [140], after which oversorting and undersorting were corrected manually, and clusters were cleaned of remaining noise. Sorted waveforms were exported back to MATLAB for analysis using custom scripts.

Retina Stimulation Data Analysis

Carbon fibers were inserted into the mouse retina as described above. A stimulation pulse train was delivered for 5 seconds. The recorded images of the calcium transient were then analyzed in MATLAB. Baseline fluorescence images were subtracted from images recorded during stimulation to obtain RGC spatial activity. This result was further normalized relative to baseline to account for the noise in the fluorescence signal.

Aplysia Ganglia Spike Analysis

Recorded intracellular spike trains were loaded into MATLAB. The same action potentials recorded by the glass electrode and the SPFe were analyzed. To visualize the relative size of the spikes recorded by the two electrodes, the action potentials were superimposed on one

other. To compare the sizes, the average amplitude of the spikes was calculated. Because the insertion of the electrode could disturb the cell membrane and trigger a train of action potentials, only action potentials after the train were used for the amplitude calculation. Only the last few action potentials within the train were used to determine the stabilized amplitude after insertion. Spike amplitudes are shown as 'mean ± standard deviation.'

Octopus ANC Spike Analysis

As Spike2 does not allow for the same spike sorting protocols used in Plexon, potential units were identified in MATLAB after waveform sorting in Spike2. A bandpass filter (0.1 to 3 kHz, 2nd order Butterworth) was run on each channel and spikes were detected using a -4 × Std threshold. Spikes were automatically sorted into templates based on shape and clustered utilizing principal component analysis. Identified waveforms were exported to MATLAB. The spikes were color-coded and plotted to indicate 3 potential units using thresholds arbitrarily set at -40, -20, and 0 μV (Figure 3).

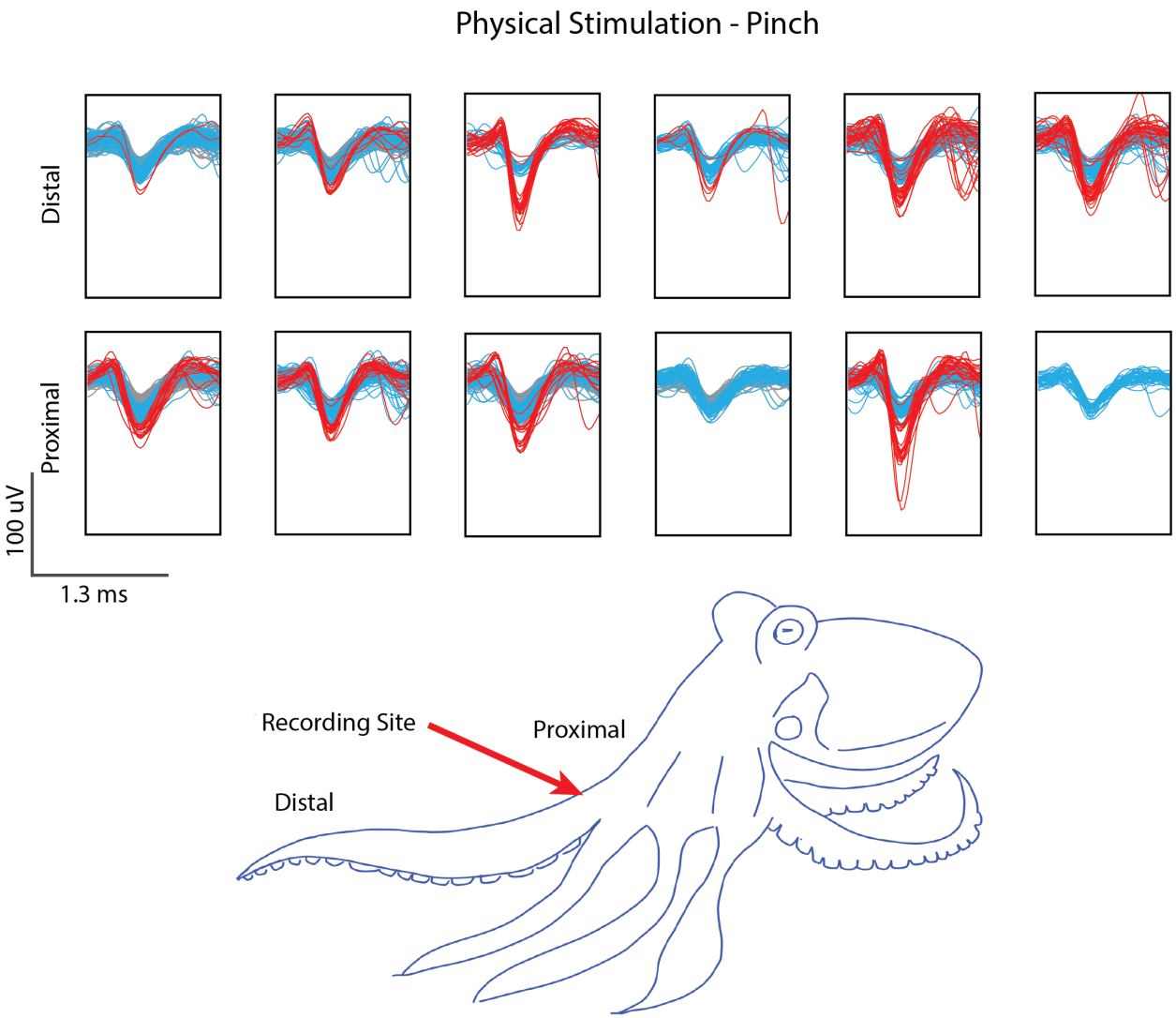

Figure 3: Spike panels from octopus arm. Arms were stimulated at the proximal and distal locations and the electrode array recorded at the proximal location. The gray lines represent waveforms with thresholds of < -20 µV, blue -20 to -40 µV, and red > 40 µV. Red arrow indicates the recording site.

2.4 Results

Physical Characterization

To fabricate electrode tips that are sharp and small, we evaluated a chemical etching technique used in imaging literature [53], [54]. We compared SPFe to two blowtorch sharpened carbon fibers (large-blowtorch and small- blowtorch)[45], [65]. Figure 4 shows representative tips from these groups and characteristics reported as 'mean ± SD.' SPFe tips were generally sharp and consistent in size. To quantify the surface area exposed, SEM images were obtained

(Figure 4). SPFe had an average surface area of 105.4 ± 20.8 μm2 (n = 35). Compared to the large-blowtorch (2734.5 ± 402.5 μm2, n=32 [56]) and the small-blowtorch (477.1 ± 57.4 μm2, n=6) the SPFe are much closer to cellular sizes. Additionally, the angle of sharpening was 20.8 ± 7.64° (n = 30) for SPFe, 58.2 ± 14.59° (n = 4) for small-blowtorch, and 72.3 ± 33.5° (n = 32) [45] for large-blowtorch suggesting that chemical etching generates a sharper point.

To determine if blowtorching alone could achieve the small surface area of SPFe without chemical etching, a small-flame blowtorch was used to sharpen the carbon fiber tips (Figure 1 B). While the small-blowtorch was able to produce smaller tip geometries than large-blowtorch, the resulting tips were not sub-cellular in size; the smallest recorded height was 30 μm. Moreover, the yield was low, often requiring an hour of effort per array. In contrast, chemical etch provided consistent sharpening after 1-4 seconds.

Electrical Characterization

Given the smaller electrode site sizes, we wanted to determine whether the impedance remains at a level comparable to other cellular scale neural probes. First, 1 kHz impedance measurements were taken before both tip treatments to establish a baseline prior to any tip coatings that may increase the effective surface area. Predictably, large-blowtorched fibers had the lowest 1 kHz impedance (~300 kΩ) followed by small-blowtorch fibers (~1MΩ), and SPFe fibers had the largest (> 4 MΩ) (see Figure 4for specific values). We then applied a conductive coating to all geometries to lower the impedance and improve recording and stimulation performance.

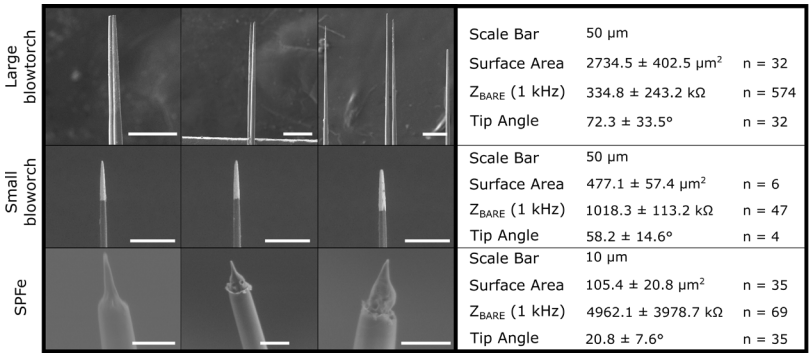

	Bare Fiber Impedance (kΩ)	PEDOT:pTS Impedance (kΩ)
Large Blowtorch	334.8 ±243.2 n = 574	32.3 ±55.7 n = 565
Small Blowtorch	1018.3 ± 113.2 n = 47	15.6 ± 6.4 n = 47
SPFe	4962.1 ± 3978.7 n = 69	30.8 ±12.5 n = 32

SPFe Impedance and CSC_c

	PEDOT:pTS	PtIr
Impedance (kΩ)	30.8 ± 12.5 n = 32	1341.4 ± 517.8 n = 21
CSC_c (uC/cm²)	7164.6 ± 2135.8 n = 48	2401.8 ± 857.1 n = 16

Figure 4: Example images from each type of sharpening method (left) with accompanying physical characteristics. Tables on the right show the 1 kHz impedance characterization across electrode tip geometry (top) as well as impedance and charge storage capacity across coating type (bottom).

Specifically for recording, we applied PEDOT:pTS, which has a complex topography that impedance does not necessarily scale directly with area [52]. Applying this to the electrodes lowered the impedances to similar values in the 10s of kiloOhms despite their differences in surface area (Figure 4). These values are in an appropriate range for effective single-unit

recordings.

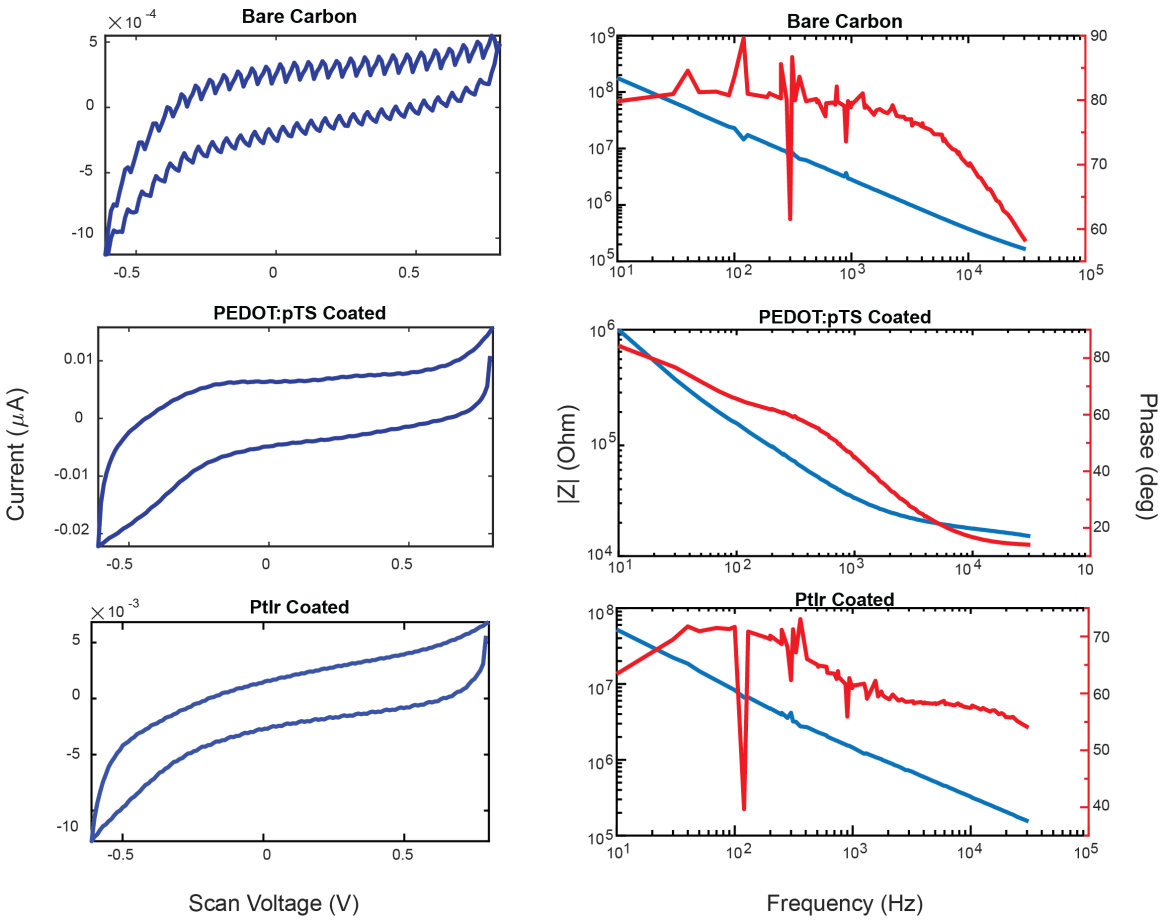

Figure 5: Cyclic voltammetry (left) and bode magnitude and phase (right) for a non-coated, PEDOT:pTS coated, and PtIr coated SPFe . Notice the change in scale along the Y-axis for both sets of plots.

To determine the viability of the SPFe as a stimulation electrode, a different set of electrodes were coated with PtIr, which is more stable for stimulation than PEDOT:pTS [107]. Cyclic voltammetry, EIS, and voltage transient of a PtIr functionalized electrode were analyzed. SPFe cyclic voltammograms (Figure 5) showed very small deflections in their redox peak. The calculated cathodic charge-storage capacity (CSC_C) for these SPFe when coated in either PEDOT:pTS or PtIr are reported in Figure 4. Briefly, CSC_C resulted in ~7000 μC/cm^2 after PEDOT:pTS coating and ~2000 μC/cm^2 after PtIr coating. Impedance for these PtIr functionalized SPFe at 1 kHz was 1341.4 ± 517.8 kΩ (n=21), which does scale appropriately to

its associated surface area when compared to large-blowtorch electrodes (344 ± 16.9 kΩ, n = 70) as noted in previous literature [148]. While there is a large variability in the capacitance and impedance for these electrodes before coating, the plating step tends to act as a cleaning step [149] which helps to lower the variability post-coating in both PEDOT:pTS and PtIr cases. Also, the SPFe shape has variablility, which is reflected in the impedance data.

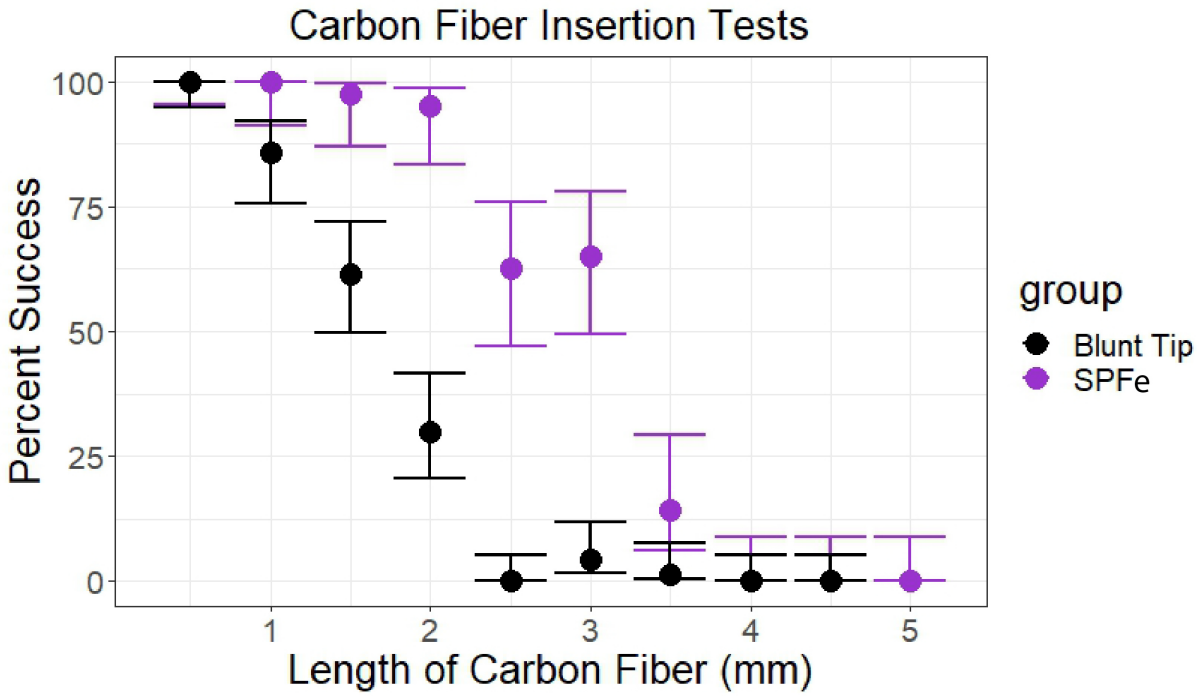

Figure 6: Successful insertion of the carbon fiber into rat brain. Sharpened fibers not only penetrate deeper into the cortex than blunt fibers, but also change the insertion profile of the carbon fiber as a chi square test shows a p <2e-6 significant difference for the confidence intervals at each point in the comparison. For lengths 0.5-5 mm blunt n= 80, for SPFe n = 40, except at lengths 3.5 mm and 0.5 mm, which were n = 35 and n = 80 respectively.

Insertion Trials

To evaluate SPFe insertion capabilities, SPFe fibers were inserted into rodent brain acutely following techniques from previous literature [50]. We compared the insertion profile of SPFe to historical data collected from blunt tipped carbon fibers [50]. Blunt carbon fiber electrodes could insert into brain without aid of a shuttle or surgical intervention with a 100% success rate at a length of 500 µm. The SPFe tips extend that 'self-insertion' length to 1.5 mm (p

< 2e-6). Overall, the SPFe tips were usually able to insert into the brain at < 2 mm lengths (Figure 6). A Wilson Binomial Confidence Interval Test was used to compare blunt (n = 70) and SPFe tips (n at least 35). A Pearson's Chi-Squared Test was used to determine significant differences between the groups. A p-value of p < 2e-6 indicated that sharpening the fiber changes the insertion profile at all lengths. Sharpening the tips therefore allows fibers to insert more easily to cortical depths deeper than Layer 3 without need of a shuttle.

As the SPFe tips are much thinner than the rest of the fiber (1-2 µm at the tip vs 8 µm along the insulated fiber), inserted electrodes (n = 8) were inspected to ensure that the tips had been robust enough to survive surgical insertion. The arrays were explanted, cleaned, and imaged using SEM. Figure 7 shows three representative functionalized fibers explanted from rat cortex. The tips maintained not only their pointed geometry but the PEDOT:pTS coating as well. This suggests the SPFe tips can survive implantation and maintain the small, sharpened tip that is desirable for recording electrodes.

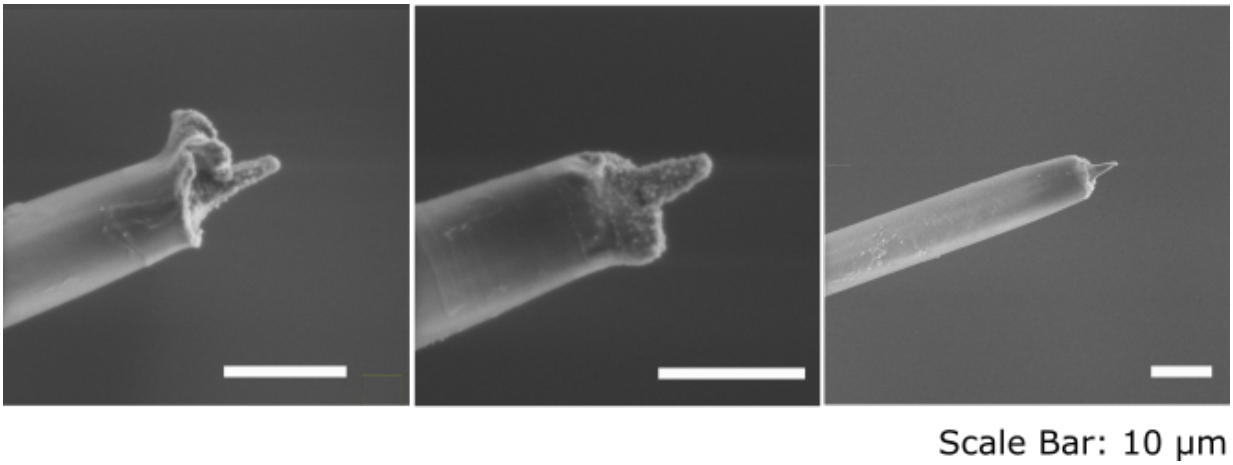

Figure 7: Example SEM images of explanted SPFe after being inserted to depths of 1.5mm in rat cortex. Note the geometry of the tip is still present and the PEDOT:pTS can be observed (rough texture on the tips).

In-Vivo Viability

Recordings were obtained from an array with both large-blowtorch and SPFe tips (n = 8 each) for direct comparison in performance. The array was inserted into rat motor cortex from

400 – 1600 µm in 200 µm steps. Yield for both electrode type is reported with the average amplitude across the electrodes that were able to record at a given depth. Yield is reported as electrodes with spikes larger than 50 µV/number of working electrodes. Representative waveforms from 600 µm and 1.2 mm depths can be seen in Figure 8 as proof-of-concept from 2 arrays. Overall, SPFe tips had higher yield and higher average peak-to-peak waveform values at both 600 µm (158.13 ± 38.03 µV, yield = 8/8) and 1.2 mm (249.5 ± 123.90 µV, yield = 15/16) than the large-blowtorch probes at the same depths (99.4 ± 25.24 µV, yield= 5/8; 158.13 ± 38.03 µV yield = 2/16). The p-value for a one-tailed T-test at 600 µm was $p < 0.005$, and for 1.2 mm $p < 0.05$. This indicates a significant increase in amplitudes recorded from the SPFe compared to the large-blowtorch fiber, which is expected due to averaging across less of the electric field from each neuron.

Aplysia neurons are relatively large and easier to access, so they were used for testing the intracellular recording ability of SPFe. Intracellular action potentials on the SPFe were reliably recorded from several *Aplysia* motor neurons and ranged in amplitude from 15 – 27 mV. In one case, the SPFe was also compared to a traditional glass microelectrode to test its intracellular recording ability. Figure 9 shows a representative spike from a glass electrode and SPFe inside of the same neuron. The average amplitude recorded by the SPFe was 18.2 ± 1.4 mV (n = 36). The average amplitude recorded by the glass microelectrode was 41.4 ± 2.7 mV (n = 36). Although the goal was a direct comparison, multiple penetrations of the cell membrane could damage the integrity of the cell and decrease the recorded membrane potential. When stimulating as the only electrode in the neuron, the SPFe action potentials were observed at 25.4 ± 1.0 mV (n = 15). The addition of a glass microelectrode into the same neuron reduced the stabilized SPFe amplitude to 18.2 ± 0.8 mV (n = 15). The same action potentials recorded by the glass microelectrode

stabilized at 40.2 ± 0.8 mV (n = 15). Overall, the action potential amplitude recorded by SPFe was smaller than that recorded by a traditional glass microelectrode, but was still sufficient to clearly discriminate intracellular spikes.

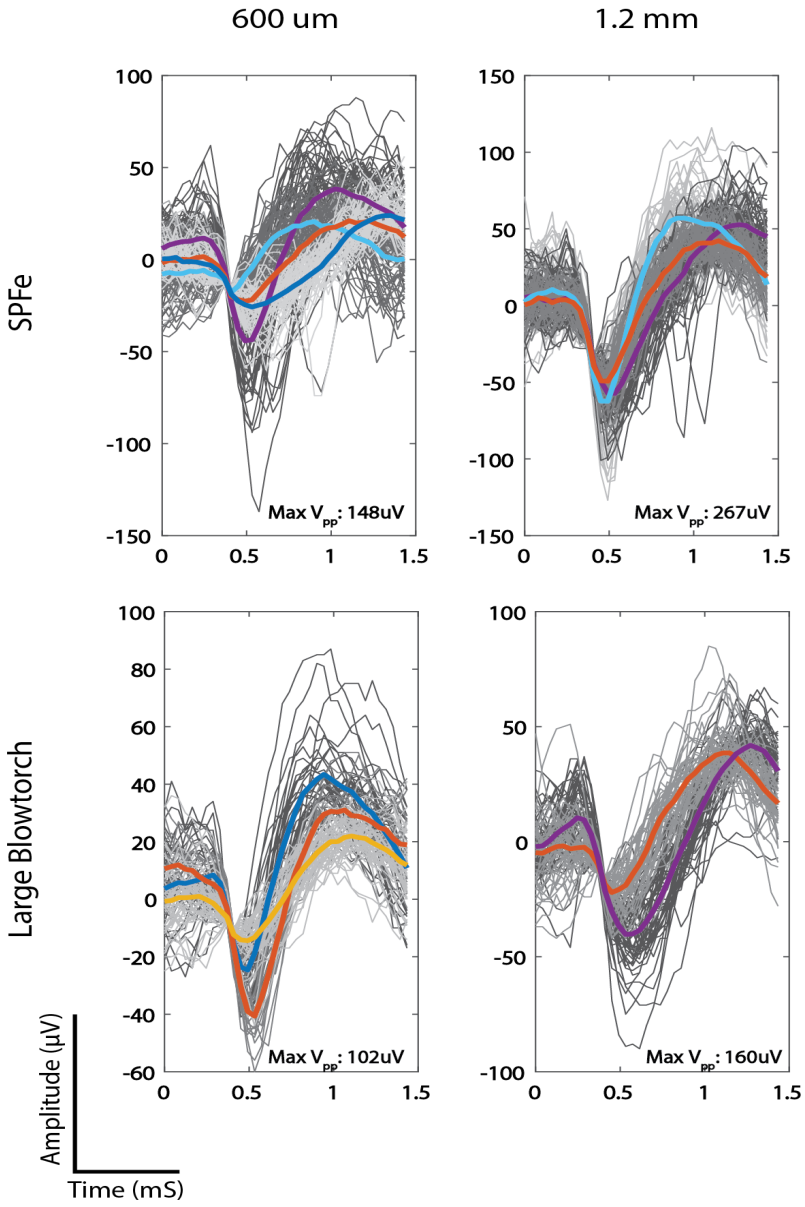

Figure 8: Rat motor cortex spikes from simultaneously inserted large blowtorch and SPFe tips at 600 μm and 1.2 mm. The maximum peak-to-peak voltage for the representative electrode shown is listed in the bottom right corner of the plots. The SPFe has significantly larger units at both locations.

Peripheral recordings are another difficult recording challenge since the tissue that binds and protects nerve fibers is tough to penetrate [45], [70]. SPFe arrays coated in PEDOT:pTS

were implanted into octopus ANC to test SPFe penetration and recording in this model. The octopus arm was removed from the body and the ANC was exposed before inserting an array of SPFe. The arm was stimulated physically and the recorded response was analyzed using Spike2 and MATLAB. Spike panels from the analysis (Figure 3REU) show several representative spikes from each stimulation recording paradigm. The largest recorded spike had a peak-to-peak amplitude of 111.4 µV. Previous attempts recording from octopus using the large-blowtorch method resulted in noisy signals and no detectable waveforms. By reducing the size of the electrode, units could be identified. This indicates that the SPFe can be used in vivo and record reliably in nerve-like structures.

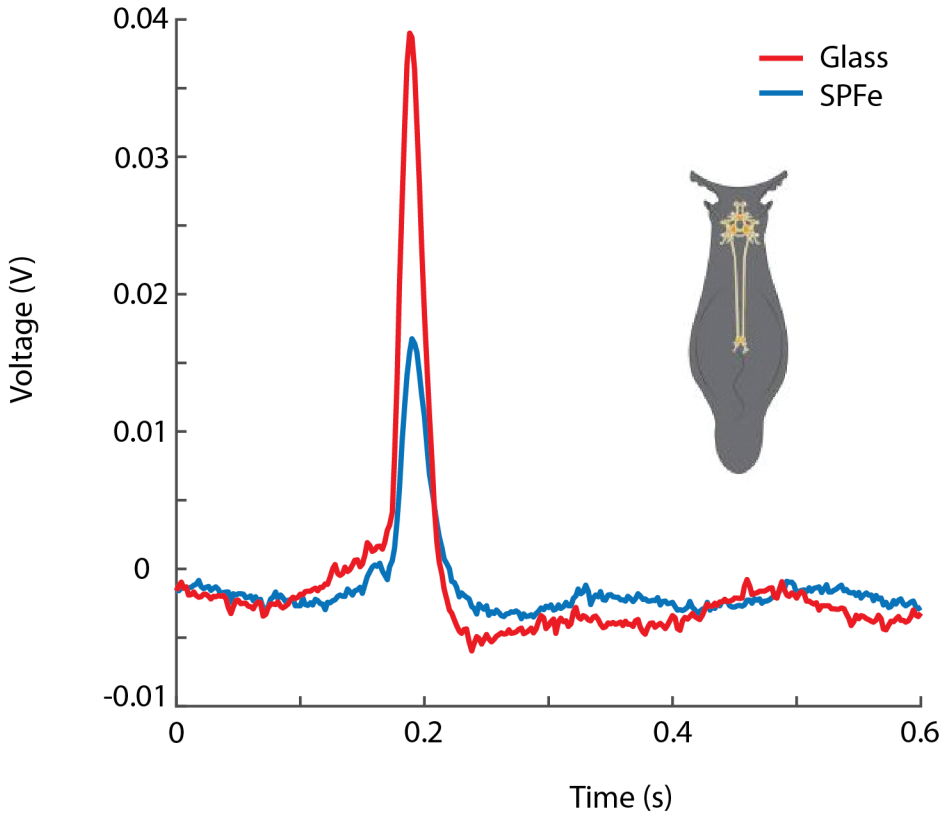

Figure 9: Spikes recorded after stimulating an Aplysia neurons. The spike amplitude of the SPFe (blue) was smaller than but comparable to that of the glass microelectrode (red).

Intraretinal Stimulation

Retinal stimulation was explored with SPFe. Wild-type mice retina were extracted and perfused on a transparent chamber. Carbon fibers were inserted such that the tips were 20 µm from the RGC from the photoreceptor side. A train of pulses were applied to the retina and RGCs, and the resulting fluorescence images were recorded with an EMCCD camera. Figure 10(left panel) shows change in fluorescence evoked by stimulation pulses of 5, 10, and 15 µA amplitude. Single RGC resolution was achieved with the SPFe, indicating an extremely selective stimulation electrode. Voltage transients (VT) were recorded (Figure 10, right panel), for PtIr coated SPFe, when stimulating the retina at different current levels of 5, 7, 10, and 15 µA. The shape of the VT is typical for stimulation electrodes [57] and the lack of a distorted waveform is an indicator that no significant hydrolysis occurred when applying these pulses to the SPFe.

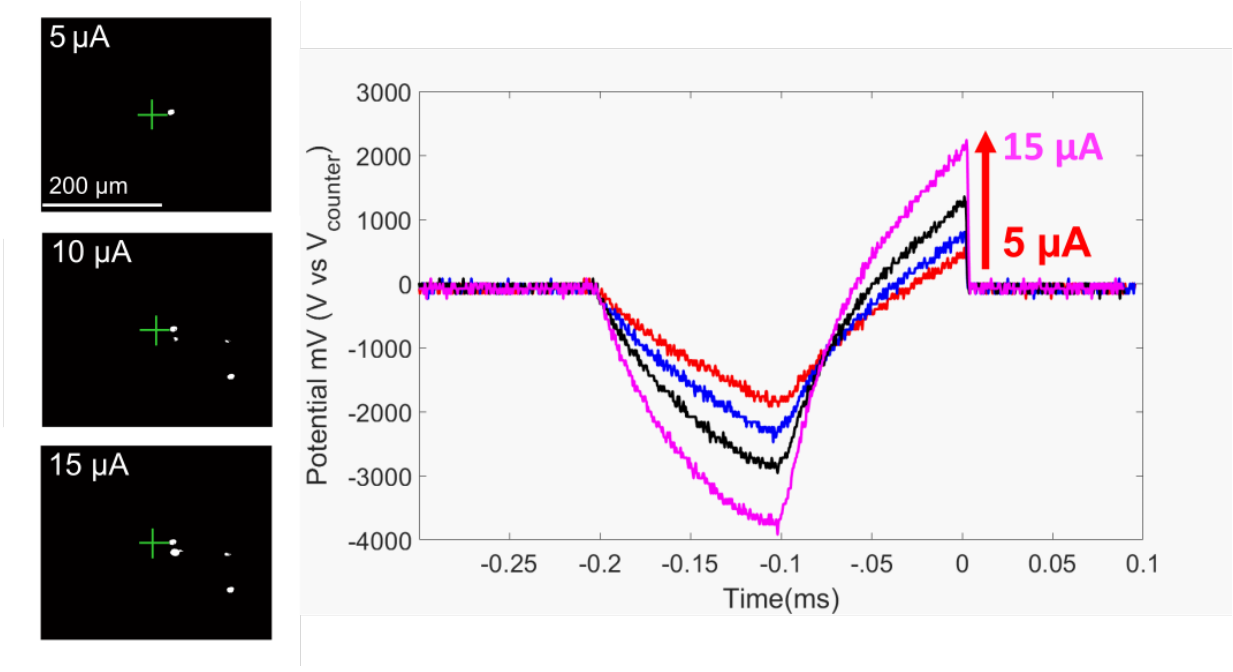

Figure 10: Resolution of the stimulation from SPFe can be seen (left). The green cross hair denotes the tip of the carbon fiber. The white indicates RGC activation in response to stimulation. Single cell resolution can be achieved at low stimulation amplitudes. Recorded voltage transients are shown on the right side when applying a current of 5, 7, 10, and 15 µA

The VT traces reported in Figure 10**Error! Reference source not found.** represent how increasing the current amplitude increases the voltage across the electrode interface. VTs were

monitored during the stimulation process to ensure no loss of coating occurred. Finally, EIS before and after each stimulation confirmed electrode stability (data not shown).

2.5 Discussion

We demonstrate fabrication and validation of the novel SPFe version of the carbon fiber electrode. Our prior work included carbon fibers with small electrode area but blunt tips and separately carbon fibers with sharpened tips, but larger electrode area. The former enabled precise unit recording while the latter improved penetration into neural tissue. SPFe incorporates those two desirable features into a single device. These SPFe showed the capability to record in vivo from small structures (Figures 4, 8, 9). This expands the experimental applications of carbon fibers to smaller neural structures that have been difficult to record from previously. One such example is insect nervous systems. Honeybee [71], [72]and dragonfly [73] researchers trying to decode different insect behaviors struggle with finding electrodes small enough to insert without damaging the fragile insect body. Carbon fibers would be an excellent option for these systems, and adding the SPFe tips would allow for selective recording in these already very tiny systems.

While the SPFe opens the door to new non-mammalian models, it can improve upon existing neural interfaces used in mammalian models as well. Targeting specific cells with retinal prostheses has been a challenge. Distance between the electrodes and target cells, large electrode size, and unintended stimulation of axons can lead to off-target RGC activation and a lower image resolution [62], [74]–[76]. Multiple studies have investigated intraretinal electrodes to increase stimulation precision with retinal implants. One study placed a glass pipette in the retina to evoke RGC responses [77]. While this gave information on the magnitude of stimulation needed for intraretinal electrodes, glass pipettes are impractical for prostheses and placement was

not well controlled. Another study showed biocompatibility and functional testing of 10μm pillar electrodes with 55 μm and 40 μm pitch on a subretinal implant. Migration of retinal tissue into the space between pillars was noted [78] and stimulus threshold was decreased [79]. Pillar height of 10μm limited the amount of penetration into the retina, but reduced proximity to the target cells and threshold by 78%. Our prior work using blowtorched carbon fibers also show decreased threshold [63]. The NR600 is an experimental retinal prosthesis with an array of penetrating electrodes. This intraretinal prosthesis was implanted in 9 patients [80]. The intraretinal array includes 25 μm diameter fibers spaced at 100 μm. The perceptual thresholds averaged 1.3 nC, which is significantly lower than epiretinal implants. Carbon fibers allow for stimulation [57] and their strength at small diameter allows penetration into the retina. With respect to the NR600 form factor, using carbon fibers would reduce the cross section of the penetrating electrode shanks to 13% of the existing size. The SPFe's small surface area and charge storage capacity shown in this paper may allow for selective stimulation down to single cell resolution while the small diameter of the carbon fibers will minimize damage to the retina. The small electrode surface area creates challenges for electrochemical measurements. Cyclic voltammagrams were acquired at higher scan rates than is typical, to increase the signal (vs. noise, see Figure 5 for noise on bare carbon fiber). Voltage transients did not show clear demarcations to allow Emc measurements [5]. Thus, comparisons of SPF stimulation performance via accepted figures of merit will require further experimentation. Nevertheless, we demonstrated electrically elicited retinal responses using SPF coated with PtIr. This opens the possibility for high-density retinal implants that are necessary to achieve improved visual acuity. While carbon fiber arrays are difficult to build, especially in high density configurations, many groups are working on automated placement [81], [82] to make these arrays more viable as commercial products.

Similarly, Layers 1-3 of cortex present some of the same challenges as retina. While much of epilepsy work relies on surface stimulation and recording, having a penetrating electrode might allow for better resolution in pre-ictal detection and response [83], [84]. However, cortical layers 1-3 contain small neurons from which it is difficult to record. SPFe could provide the ability to penetrate into brain and record from neurons with small cell bodies. While the arrays in this paper were linearly placed, alternative backend connectorization for carbon fibers [40], [85] has been explored previously and combining these approaches would be straightforward.

More difficulties lie in recording from tougher tissues like nerve that are also usually embedded in actively moving muscles. Previous work from our lab [45], [51], [86] has shown that carbon fibers can become more robust when adding a thin layer of silicone rubber to the base of the carbon fibers as it reduces the shear forces at the interface of the fiber and the board. Welle et al., show that these fibers are capable of recording from feline DRG [45]. As was seen in the octopus data, having a smaller surface area probe allowed for units to be recorded. As octopus axon cords have no myelination [87], recordings from mammalian nerves with myelination may also be improved due to the small surface area of the SPFe.

While this study has a plethora of preliminary data in a number of animal models, there is still optimization to be done. The PEDOT:pTS deposition technique follows previous methodology [56] that was optimized for a larger site electrode. While we did not see significant geometrical changes of the tip under SEM, this process could be further optimized for smaller site deposition. While we found PEDOT:pTS to be unstable in stimulation and switched to PtIr, other groups have found success with PEDOT:pTS for stimulation [88], [89]. The lack of

stability for PEDOT:pTS may lie in the deposition method presented here and will be further examined in future work.

2.6 Acknowledgement

Additionally, we would like to thank the Lurie Nanofabrication Facility and Michigan Characterization Center at the University of Michigan for use of their equipment. Finally, we acknowledge the contribution of Dr. Chris Andrews for his consultation on statistical analysis.

Chapter 3
Computational Model Predictions for Nerve Recordings Using Carbon Fiber Electrodes

Julianna Richie, Kathleen Kish

3.1 Introduction

Nerve signals are difficult to obtain, however are of interest for numerous applications. Dorsal root ganglia has been used in conjunction with electrodes to monitor and stimulate bladder activity [150]. The vagus nerve innervates the stomach, heart, lungs, intestines, liver, pancreas, and many more systems in the body [64] – thus making it a key target for many studies of diseases related to those systems. However, these studies are limited due to the types of electrodes available to them.

Most commonly used nerve electrodes tend to be a "cuff" design [93], [151], [152], [153]– a flat surface with recording electrodes that wrap around the nerve and are secured in place with a suture or other mechanism. These electrodes allow for electrical signals in the nerve to be recorded similar to ECoG arrays in the brain – at a surface level. Because the cuffs do not insert into the nerve, these electrodes lack the specificity needed to isolate signals within the nerve fascicles [15], [154].

The Utah Slant Array [155] is able to insert and get into the fascicles and can record signals. The slant array is a modified version of the Utah array commonly used in brain studies and was modified to be better suited to nerve recordings. However, the modification of the array was geometrical only and did not take into account the bio-response previously seen to the Utah

array in brain. Inserting this slanted silicon electrode into nerve resulted in histology indicating the axons in the nerve were pushed away from the electrode or killed upon insertion [79]. Additionally, the electrode recording sites are 25 – 50 μm in height which while small are still quite large compared to the axon nodes from which we wish to record [44], [64].

Recently, sharpened carbon fibers were used to penetrate and record units from the vagus nerve in rats [65] and the DRG in cat [109]. Carbon fiber electrodes offer many benefits to nerve recording as they are small and can have a low impedance [109], [140]. However, the fibers used had a large electrode site and were only able to achieve multi-unit activity [109]. Nerves carry signals through axons – small diameter (< 10 μm) structures. Axons are made up of sections of insulation along its length, however, the insulation is not perfect and there are tiny (~ 1 μm), uninsulated gaps between this insulation where signal escapes and can be recorded. These are called 'nodes of Ranvier,' or 'nodes.' Additionally, axons are densely packed within the nerve. Taking this into account, large electrodes inserted into the nerve pass through low voltage areas that average out along the length of the electrode and thus make it very difficult to identify individual axon signals. However, a small electrode recording site closer in size to the node's size would provide a more selective recording as the electrode would enter less node electrical fields. Figure 11 shows the electrical field of a 5.7 μm diameter axon compared to two carbon fiber electrodes to demonstrate this point.

In order to investigate the optimal geometry for a peripheral nerve recording electrode, the small pointed fiber electrode from the previous chapter was used as inspiration to determine the effects of tip optimization on recording potential. The goal was to improve the recording potential seen in previous carbon fiber work to be closer to that of an ideal electrode (infinitesimally small point source electrode). However, no carbon fiber recording or stimulation

model in the nerve existed at the time of this work, and as such, needed to be constructed. To do so, several pieces of literature were combined.

Moffitt and McIntyre produced a model in 2005 [14] to determine the effect of geometric size on recorded signal amplitude using a planar electrode next to a large neuron. This paper predicted that a surface area of 100 μm2 was similar to recording from a point source while larger electrodes recorded smaller amplitudes. However, this model was done entirely in brain which has many differences to the physiology of nerve. To begin with, in brain, the soma (the bottom of the neuron cell body) is the point of interest as it has the largest spiking amplitude. In nerve, the point of interest are nodes of Ranvier which have much smaller action potentials than what is seen in somas [156]. The amplitude of the signal that is seen at a node of Ranvier depends on the amount of current provided by the upstream cell body, the distance from that cell body, and the diameter of the axon [157].

Importantly, this paper introduced the use of "Reciprocity" to predict the recorded signal amplitude. The 'theorem of reciprocity' states that the voltage generated at a given point in a circuit is equivalent to the voltage that would be detected by a recording electrode in response to a unit current at that same point [14]. This simple theorem took away a large amount of simulation work that was previously required. Now, modelers could create a model of the electrode and tissue. They could assign impedances and conductances of these parts and then apply a 1A current to the tip of the electrode to generate an electric field. This allowed for an ohmic transform to be calculated for every point (or a select points determined by the modeler) within the model. Using a different modeling software that could produce the transmembrane currents, NEURON, allowed for every current to be calculated throughout the course of an action potential for a given cell model. Combining the two models the theorem of reciprocity allows for

modelers to then transform the two data sets and calculate the waveform that would be sensed at the tip of the electrode.

While a model of the carbon fiber electrode was unavailable, there was an axon model available for use in calculating the action potentials in this model. McIntryre, Richardson, and Grill (MRG) axon model [158] to act as a generic, mammalian axon in a nerve model. This model is extremely useful as it has parameters for calculating the action potentials of multiple diameters of axons. Primarily, this model creates a transition between the myelinated sections and the node that are more representative of physiology. This model also was validated *in vivo* when it was introduced and has become a staple for modeling nerves [158].

In this aim, we will combine these aforementioned models to create a simplistic nerve and carbon fiber electrode to predict the effects of size on recording potential. First, several carbon fiber models will be built with blunt tips to compare the effects of surface area on a 3D carbon fiber electrode. We will then examine the effects of sharpening, seen previously in SPFe and Welle methodologies, on the electrode recording potential compared to the blunt tips.

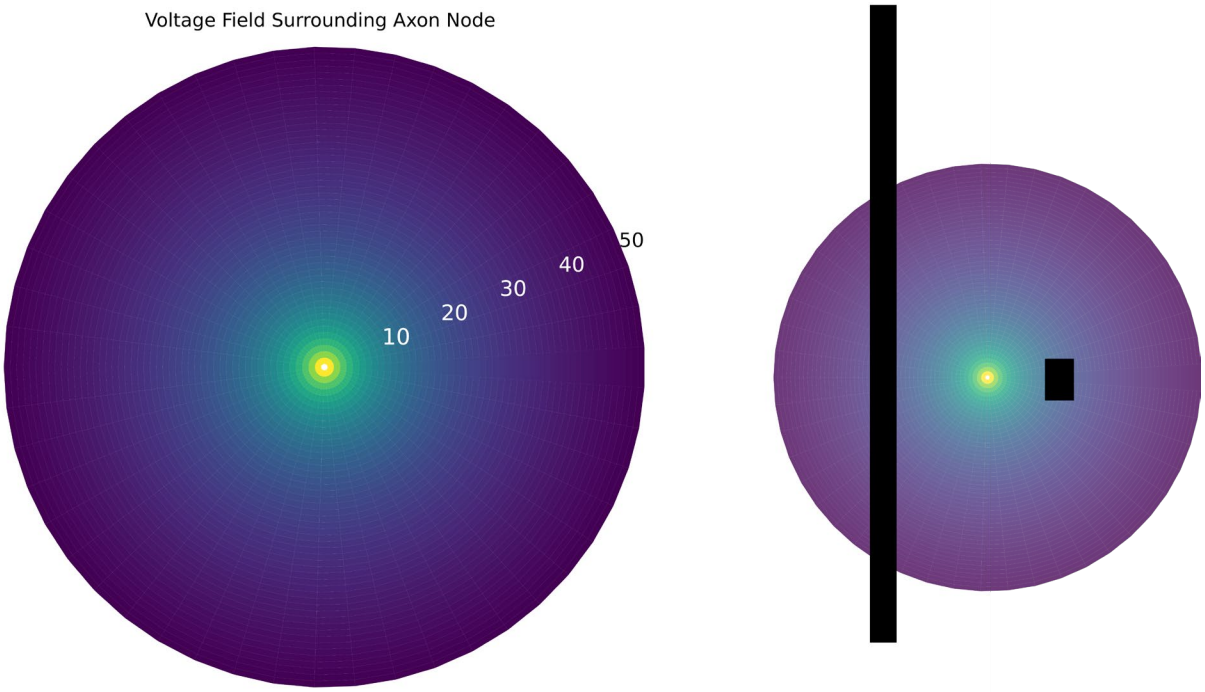

Figure 11: (Left) The voltage field surrounding a 50 µm radius around a 5.7 µm axon node. Yellow indicates a high voltage with darkening colors indicating lowering colors. (Right) Two black bars represent the size of an electrode as it passes through the axon voltage field. Note that the large (150 µm) electrode passes through the voltage field hotspot as well as the surrounding areas that approach zero amplitude. The small (10 µm) sits more firmly within the hotspot and does not exist in the zero space to the extent that the large electrode does.

3.2 Methods

A volume conductor model of a simplified nerve with a 3D carbon fiber recording electrode inserted perpendicularly was built in COMSOL Multiphysics v 5.5 to mimic surgical use [109]. The nerve model consisted of nested cylinders representing a large saline bath (6 mm diameter, 50 mm length), epineurium (200 µm diameter, 24 mm length), and the nerve fascicle (150 µm diameter, 24 mm length). The carbon fiber electrode was modeled as a carbon fiber cylinder core (3.4 µm radius, 600 µm length) with an insulation layer (3 µm thickness) encapsulating all but the exposed tip in the nerve fascicle. Conductivities for the components were taken from literature for vagus nerve and manufacturer data sheets [159], [160], [161]. The model was used to generate data for a large "Welle" electrode (149 µm carbon exposed), a small "SPF" electrode (10 µm), and an idealized point source electrode (IS). The Welle was generated

at 149 µm as at 150 µm COMSOL ran into boundary issues where the end of the fiber intersected with epineurium/nerve interface- the exposed carbon was reduced to allow the fiber to remain entirely inside the nerve section as opposed to extending the fiber into the epineurium. A 1 ampere current was applied to the tip of the electrode and a quasi-static solver was used to calculate the electric potential distribution.

Additionally, two sharpened carbon fiber models were generated – a true SPFe and Welle with sharpened points at the average tip angles respective to each. Due to the constraints of COMSOL's modeling functionality, both tips were modeled in SolidWorks and imported. As the sizes were very small, the solidworks models approximated the geometries as best as could be done. The fibers were modeled in three sections: a base, a frustrum of appropriate tip angle, and a rounded tip represented as a half-sphere. Because carbon electrodes are organic, their sharpening profile is variable. As such, these dimensions were chosen to allow the software to create the desired tip angles and overall shape of the electrodes. The final drawings of the models are shown in Figure 12. The Welle was created with a 145 µm cylinder lofted to reduce its radius from 3.4 µm at the base to 1.7 µm at the joint with the 4 µm tall cylinder was reduced in radius to gain a semi angle of 72 degrees. A 0.17 µm diameter semi-sphere was added to the tip to give a rounded point to the overall structure. The SPFe was created with an 8 µm cylinder that reduced its radius from 3.4 µm to obtain at 20 degree tip angle and was topped with a semi-sphere to round the tip.

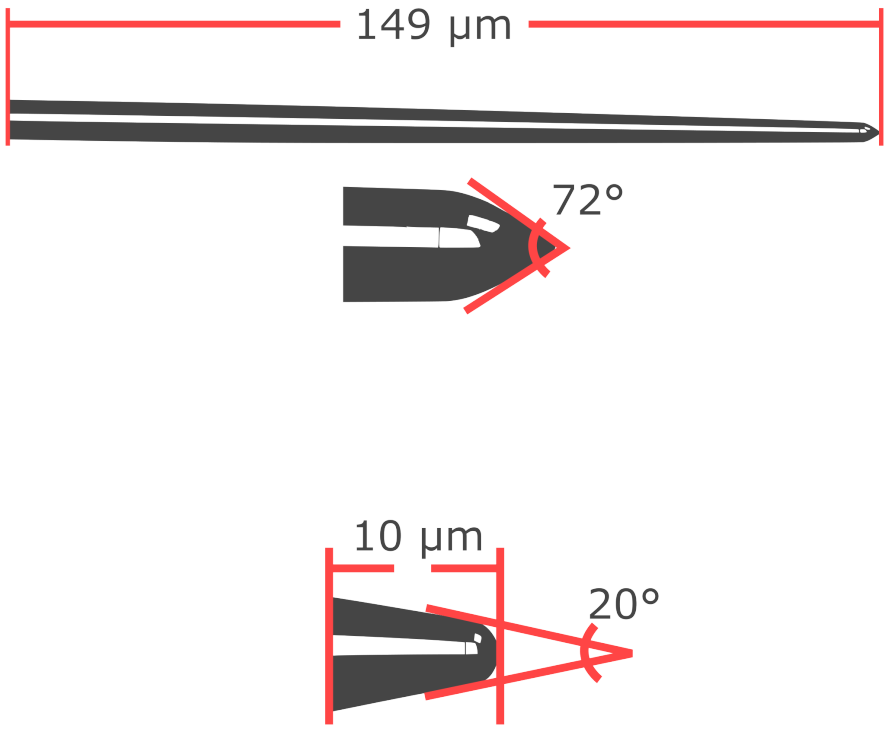

Figure 12: Computational models produced in SolidWorks to create two sharpened fibers (top: Welle, bottom: SPFe).

Using Python and NEURON, a multi-compartment cable model of a myelinated axon was generated using equations from the McIntyre, Richardson, and Grill (MRG) axon model [158]. The axon diameter was set to 5.7 µm, the smallest set of parameters available in the MRG, to more closely mimic small axons in physiological models [44]. This model was paired with the COMSOL model to place this axon in space around the blunt electrode tip. The central axon node was centered under each blunt of electrode and placed 5, 10, 25, 50, and 100 µm from the tip of the electrode vertically and horizontally. Additionally, the node was shifted so the electrode was offset over myelination to look at the insulation effects on recording from the node when not perfectly centered.

Sharpened fibers were compared in amplitudes to their respective counter blunt tipped electrodes to determine the effect of the sharpening on the recording potential for the carbon

fiber recording electrodes. COMSOL voltage plots were generated for all carbon fiber models to illustrate the “hot spots” for recording between the different geometries. The electrodes were compared only in the axon shifting upward paradigm.

3.3 Results

Figure 13 shows the predicted amplitudes for the electrodes in arbitrary units next to a graphic illustrating the movement of the axon in space with respect to the fiber electrode. Changes in the vertical distance to the probe showed similar recording amplitudes at 100 µm distances for all three electrodes. However, as the distance decreases, the difference between the small electrodes and the Welle electrode are obvious. At the closest distance, the IS out performed the SPFe by 53.9% and the Welle by 91.1%. The SPFe outperformed the Welle electrode by 80.7% at the 5 µm distance and 55.7% at 100 µm.

For horizontal shifts away from the electrode tip at a fixed distance of 50 µm and a horizontal shift of 5 µm, the IS recorded amplitudes 13% and 68% higher than SPFe and Welle, respectively. The SPFe recorded 63.1% higher than the Welle at the same point. At the furthest distances, again we see the IS and SPFe record 48.2% and 46.2% higher amplitudes than the Welle electrode.

When keeping the axon 50 µm away from the electrode tip and shifting the axon so that the electrode tip is over myelination, we see similar trends with the IS and SPFe performing similarly with only a 12.9% difference in amplitude when the node was centered. However, the Welle probe recorded amplitudes 68.1% and 63.3% lower than the IS and SPFe, respectively. At the furthest distance from the node the Welle still performs 48.8% and 46.8% lower than the IS and SPFe.

While the surface area of the probe did change the recorded amplitude as we see in planar and metal electrodes, the shape of the probe is also altered in SPFe and Welle electrode fabrication from a blunt tip to a sharpened point. Two tips were modeled in SolidWorks and imported into COMSOL and compared to their blunt counterpoints for the upward shifted axon. When comparing the two types of tips, the sharpened points were not predicted to record as high of amplitudes than their blunt counterparts (Figure 14). The smaller electrodes with heights of 10 µm were more similar in their differences than the larger 150 µm electrodes.

For sharpened SPFe, the recording potential was 11.4% less than the blunt tip electrode at when the axon was 5 µm away. The two electrodes perform similarly at all other distance points with differences of less than 8%. The sharpened SPFe performed similarly to the blunt SPFe electrode when compared to the IS recording amplitudes, though with less recording potential at each distance point. The same held true for the sharpened Welle electrodes with the sharpened electrodes recording 21.2% less amplitude than the blunt tips at 5 µm away from the axon. Predictably, then compared to the IS, the sharpened electrodes followed the same trend as the blunt tipped electrode, however, with less recorded amplitude (93.0% - 61.5% less than IS).

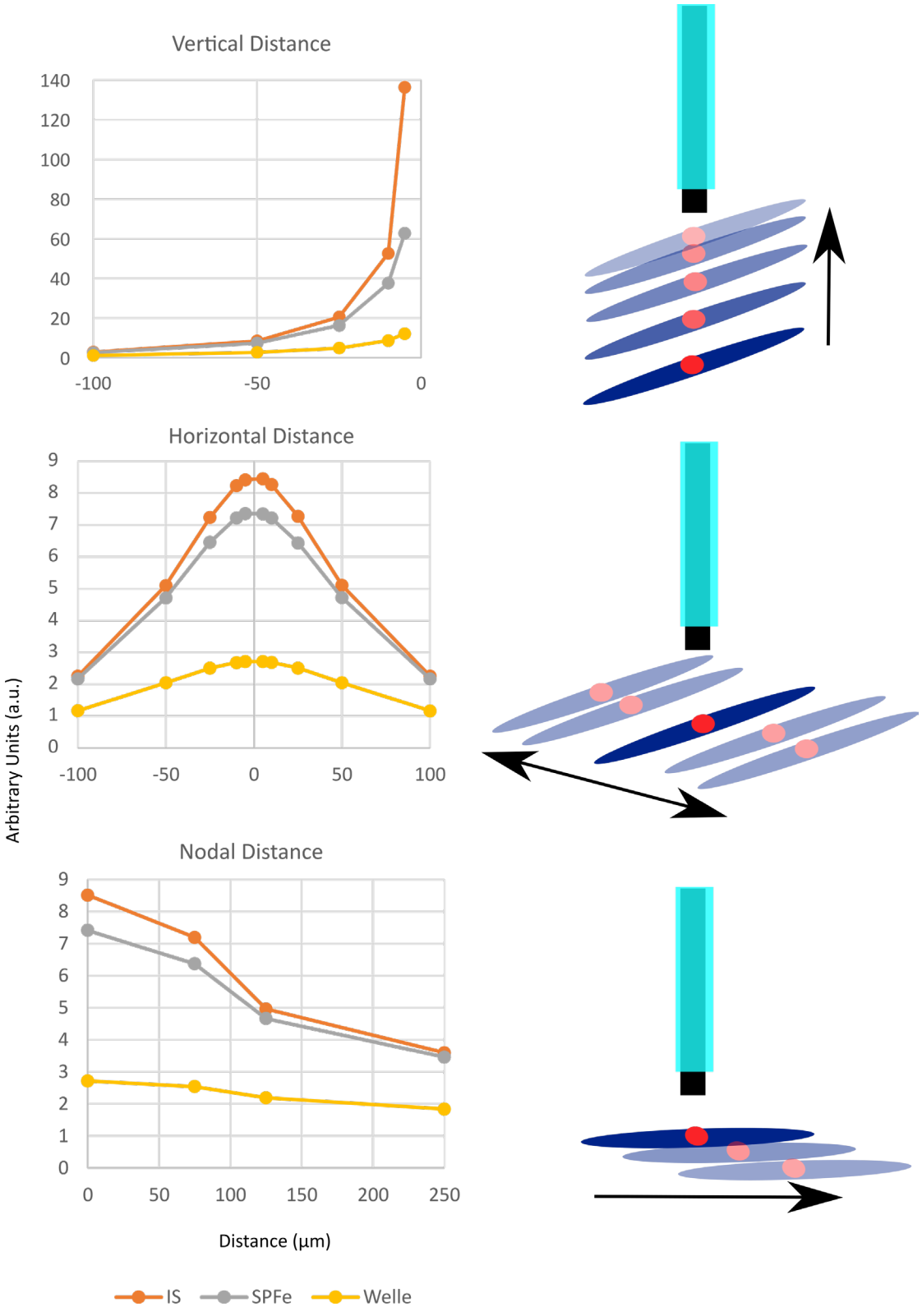

Figure 13: Predicted recorded amplitudes of an action potential through the nerve. Plots on the left show the amplitude changes with distance to the electrode. Images on the right show the movement in space that is occurring.

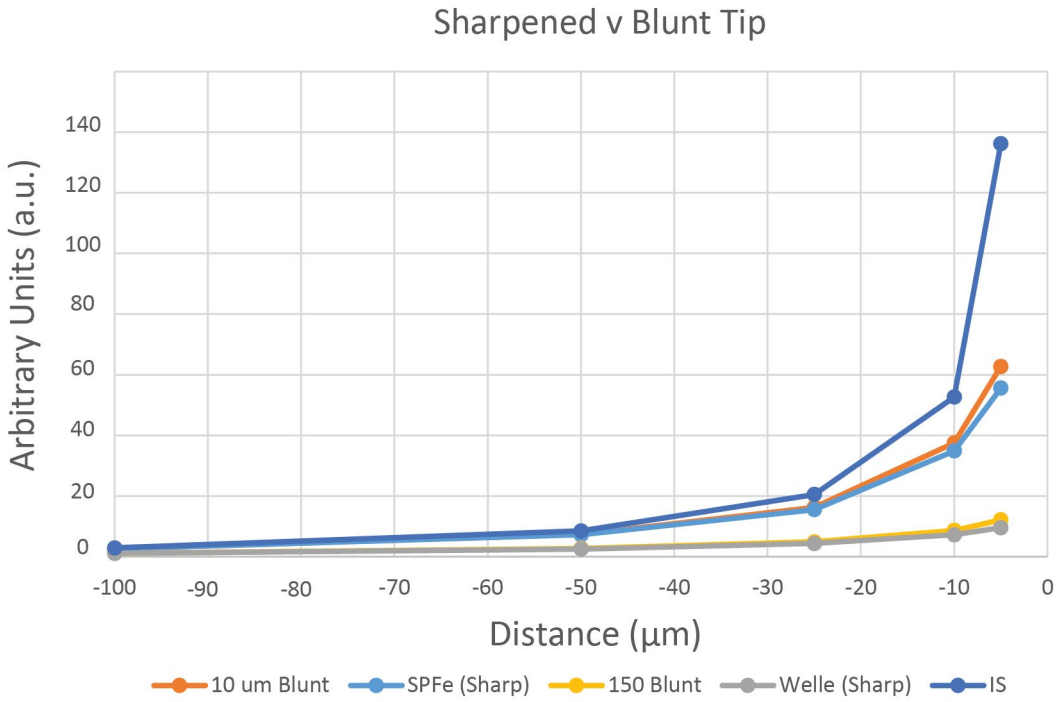

Figure 14: Sharpened models were compared in the vertical movement paradigm to their blunt tip counter parts. They were additionally compared to the insulated point source. The sharpened probes preform worse than their blunt counterparts.

3.4 Discussion

While this model does not perfectly imitate the geometries of the electrodes used in sharpened carbon fiber electrode nerve recordings, the surface areas of the model are similar enough to be used as a guideline for optimizing carbon fiber electrode tips. The smaller an electrode tip, the higher the expected recording can be. This makes sense physically as the number of possible signals being recorded at once is much smaller on a small electrode leading to less averaging across the electrode. Meanwhile, a large electrode can record many more signals simultaneously leading to more averaging across the electrode, thus reducing the recorded amplitude. Thus, the model agrees with previously understood biophysics.

However, when we take into account the drop in recorded amplitudes with a sharpened tip, this notion of ‘agreed biophysics’ appears to falter. The sharpened tips will have a smaller

surface area and thus should result in higher amplitudes, however what is seen is a lowering in amplitude. This is because surface area, while a key factor, is not the only factor shaping the physics at play. We expect points and places of curvature to gather more electrons and thus have a greater electric field. However, the carbon fiber pointed tips did push the limits of both modeling softwares used. Both SolidWorks and COMSOL had difficulty generating the models. SolidWorks struggled to get micron level resolution graphically, and erred out several times during the iterative process to make the tips as close to what is seen in real carbon fiber sharpened tips. COMSOL, while it was able to import the SolidWorks model, does notoriously have issues with generating meshes at such small resolutions. This could have led to some estimations on the backend of the software running that led to the discrepancies seen here.

This is extremely important for applications that want to record from nerve like octopus arm recording and human nerve intervention where axon nodes can be extremely small compared to the biological noise in the nerve. Additionally, the small SPFe electrode behaving so closely to the IS electrode is indicative fabrication of an even smaller electrode may be able to mimic an IS electrode which could be extremely beneficial in singling out electrophysiological signals. There are several limitations in this model that could be addressed in future work. Modeling multiple axons in the fascicle and adding biological “pink” noise [162] could be useful to study the selectivity of recording electrodes. Additionally, this model could be used to study the reverse recruitment of small nerve fibers in stimulation and the effects of electrode surface area and selectivity on this phenomenon.

Chapter 4

Open-source Toolkit: Benchtop Carbon Fiber Microelectrode Array for Nerve Recording

Julianna M. Richie, Paras R. Patel, Elissa J. Welle, Tianshu Dong, Lei Chen, Albert J. Shih, Cynthia A. Chestek

A version of this chapter was accepted for publication in JoVE.

4.1 Abstract

Conventional peripheral nerve probes are primarily fabricated in a cleanroom, requiring the use of multiple expensive and highly specialized tools. This paper presents a cleanroom "light" fabrication process of carbon fiber neural electrode arrays that can be learned quickly by an inexperienced cleanroom user. This carbon fiber electrode array fabrication process requires just one cleanroom tool, a Parylene C deposition machine, that can be learned quickly or outsourced to a commercial processing facility at marginal cost. This fabrication process also includes hand-populating printed circuit boards, insulation, and tip optimization.

The three different tip optimizations explored here (Nd:YAG laser, blowtorch, and UV laser) result in a range of tip geometries and 1 kHz impedances, with blowtorched fibers resulting in the lowest impedance. While previous experiments have proven laser and blowtorch electrode efficacy, this paper also shows that UV laser cut fibers can record neural signals in vivo. Existing carbon fiber arrays either do not have individuated electrodes in favor of bundles or require cleanroom fabricated guides for population and insulation. The proposed arrays use only tools that can be used at a benchtop for fiber population. This carbon fiber electrode array

fabrication process allows for quick customization of bulk array fabrication at a reduced price compared to commercially available probes.

4.2 Introduction

Much of neuroscience research relies upon recording neural signals using electrophysiology (ePhys). These neural signals are crucial to understanding functions of neural networks and novel medical treatments such as brain machine and peripheral nerve interfaces [151], [163], [164], [165], [166], [167]. Research surrounding peripheral nerves requires custom-made or commercially available neural recording electrodes. Neural recording electrodes—unique tools with micron-scale dimensions and fragile materials—require a specialized set of skills and equipment to fabricate. A variety of specialized probes have been developed for specific end uses; however, this implies that experiments must either be designed around currently available commercial probes, or a laboratory must invest in the development of a specialized probe, which is a lengthy process. Due to the wide variety of neural research in peripheral nerve, there is high demand for a versatile ePhys probe [65], [109], [166]. An ideal ePhys probe would feature a small recording site, low impedance [14], and a financially realistic price point for implementation in a system [165].

Current commercial electrodes tend to either be extraneural, or cuff, electrodes (Neural Cuff [168], MicroProbes Nerve Cuff Electrode [169]), which sit outside of the nerve, or intrafascicular, which penetrate the nerve and sit within the fascicle of interest. However, as cuff electrodes sit further away from the fibers, they pick up more noise from nearby muscles and other fascicles that may not be the target. These probes also tend to constrict the nerve, which can lead to biofouling—a build-up of glial cells and scar tissue—at the electrode interface while the tissue heals. Intrafascicular electrodes (such as LIFE [170], TIME [94], and Utah Arrays

[171]) add the benefit of fascicle selectivity and have good signal-to-noise ratios, which is important in discriminating signals for machine interfacing. However, these probes do have issues with biocompatibility, with nerves becoming deformed over time [15], [87], [165]. When bought commercially, both these probes have static designs with no option for experiment-specific customization and are costly for newer laboratories.

In response to the high cost and biocompatibility issues presented by other probes, carbon fiber electrodes may offer an avenue for neuroscience laboratories to build their own probes without the need for specialized equipment. Carbon fibers are an alternative recording material with a small form factor that allows for low damage insertion. Carbon fibers provide better biocompatibility and considerably lower scar response than silicon [103], [172], [173] without the intensive cleanroom processing [94], [151], [171]. Carbon fibers are flexible, durable, easily integrated with other biomaterials[173], and can penetrate and record from nerve [65], [174]. Despite the many advantages of carbon fibers, many laboratories find manual fabrication of these arrays to be arduous. Some groups [108] combine carbon fibers into bundles that collectively result in a larger (~200 μm) diameter; however, to our knowledge, these bundles have not been verified in nerve. Others have fabricated individuated carbon fiber electrode arrays, although their methods require cleanroom-fabricated carbon fiber guides [104], [175], [176] and equipment to populate their arrays [103], [175], [176]. To address this, we propose a method of fabricating a carbon fiber array that can be performed at the laboratory benchtop that allows for impromptu modifications. The resulting array maintains individuated electrode tips without specialized fiber populating tools. Additionally, multiple geometries are presented to match the needs of the research experiment. Building from previous work [103], [104], [109], [140], this

paper provides detailed methodologies to build and modify several styles of arrays manually with minimal cleanroom training time needed.

4.3 Protocol

4.3.1 Carbon Fiber Array Assembly

Carbon fiber arrays are composed of three parts: a custom printed circuit board (PCB), a backend connector, and an inexpensive sample of 6.8 μm carbon fibers (T-650/35 3K, Cytec Thornel, Woodland Park, NJ). All design files associated with de-signs presented below are available for download, including three different PCBs: “Flex Array”, “Wide Board”, and “ZIF” (Figure 15) on the MINT website (https://mint.engin.umich.edu/technology-platforms/carbon-fiber-electrodes/). The population and functionalization of a 16-channel Flex Array build is described in detail (build video in supplemental) in this chapter with additional instructions for the other boards provided in **Error! Reference source not found.**. Several tip optimization techniques to improve electrophysiological recording will also be discussed. A complete materials list including cost is shown in Table 1, with processing steps explained below.

Materials	Part Number	Distributor	Qty	Unit Cost (USD)
3 prong clams	05-769-6Q	Fisher	2	20
3,4-ethylenedioxythiophene (25g) (PEDOT)	96618	Sigma-Aldrich	1	102
353ND-T Epoxy (8oz)++ (ZIF and Wide Board Only)	353ND-T/8OZ	Epoxy Technology	1	48
Ag/AgCl (3M NaCl) Reference Electrode (pack of 3)	50-854-570	Fisher	1	100
Autolab	PGSTAT12	Metrohm		
Blowtorch	1WG61	Grainger	1	36
Carbon Fibers	T-650/35 3K	Cytec Thornel	1	n/a
Carbon tape	NC1784521	Fisher	1	27
Cotton Tipped Applicator	WOD1002	MediChoice	1	0.57
Delayed Set Epoxy++	1FBG8	Grainger	1	3
DI Water	n/a	n/a	n/a	n/a
Dumont Tweezers #5	50-822-409	Fisher	1	73
Flex Array**	n/a	MicroConnex	1	68
Flux	SMD291ST8CC	DigiKey	1	13
Glass Capillaries (pack of 350)	50-821-986	Fisher	1	60
Glass Dish	n/a	n/a	1	n/a
Hirose Connector (ZIF Only)	H3859CT-ND	DigiKey	2	2
Light Resistant Glass Bottle	n/a	Fisher	1	n/a
Micropipette Heating Filiment	FB315B	Sutter Instrument Co	1	n/a
Micropipette Puller	P-97	Sutter Instrument Co	1	n/a
Nitrile Gloves (pack of 200)	19-041-171C	Fisher	1	47
Offline Sorter software	n/a	Plexon	1	n/a
Omnetics Connector* (Flex Array Only)	A79025-001	Omnetics Inc	1	35
Omnetics Connector* (Flex Array Only)	A79024-001	Omnetics Inc	1	35
Omnetics to ZIF connector	ZCA-OMN16	Tucker-Davis Technologies	1	n/a
Pin Terminal Connector (Wide Board Only)	ED11523-ND	DigiKey	16	10
Probe storage box	G2085	Melmat	1	2
Razor Blade	4A807	Grainger	1	2
SEM post	16327	Inf	1	3
Silver Epoxy (1oz)++	H20E/1OZ	Epoxy Technology	1	125
Silver GND REF wires	50-822-122	Fisher	1	423.2
Sodium p-toulenesulphonate(pTS)- 100g	152536	Sigma-Aldrich	1	59
Solder	24-6337-9703	DigiKey	1	60
Soldering Iron Tip	T0054449899N-ND	Digikey	1	13
Soldering Station	WD1002N-ND	Digikey	1	374
SpotCure-B UV LED Cure System	n/a	FusionNet LLC	1	895
Stainless steel rod	n/a	n/a	1	n/a
Stir Plate	n/a	Fisher	1	n/a
Surgical Scissors	08-953-1B	Fisher	1	100
TDT Shroud (ZIF Only)	Z3_ZC16SHRD_RSN	TDT	1	3.5
Teflon Tweezers	50-380-043	Fisher	1	47
UV & Visible Light Safety Glassees	92522	Loctite	1	45
UV Epoxy (8oz)++ (Flex Array Only)	OG142-87/8OZ	Epoxy Technology	1	83
UV Laser	n/a	WER	1	30
Weigh boat (pack of 500)	08-732-112	Fisher	1	58
Wide Board+	n/a	Advanced Circuits	1	3
ZIF Active Headstage	ZC16	Tucker-Davis Technologies	1	925
ZIF Passive Headstage	ZC16-P	Tucker-Davis Technologies	1	625
ZIF*	n/a	Coast to Coast Circuits	1	9

Table 1: Estimated prices for one board based on 2020 prices. These prices are based on publicly available price listing and do not take into account academic pricing. *Assumes an order of 100, **Assumes an order of 50 with initial $800 NRE charge, +Assumes an order of 200, ++Price is for initial purchase, but can be used for multiple builds.

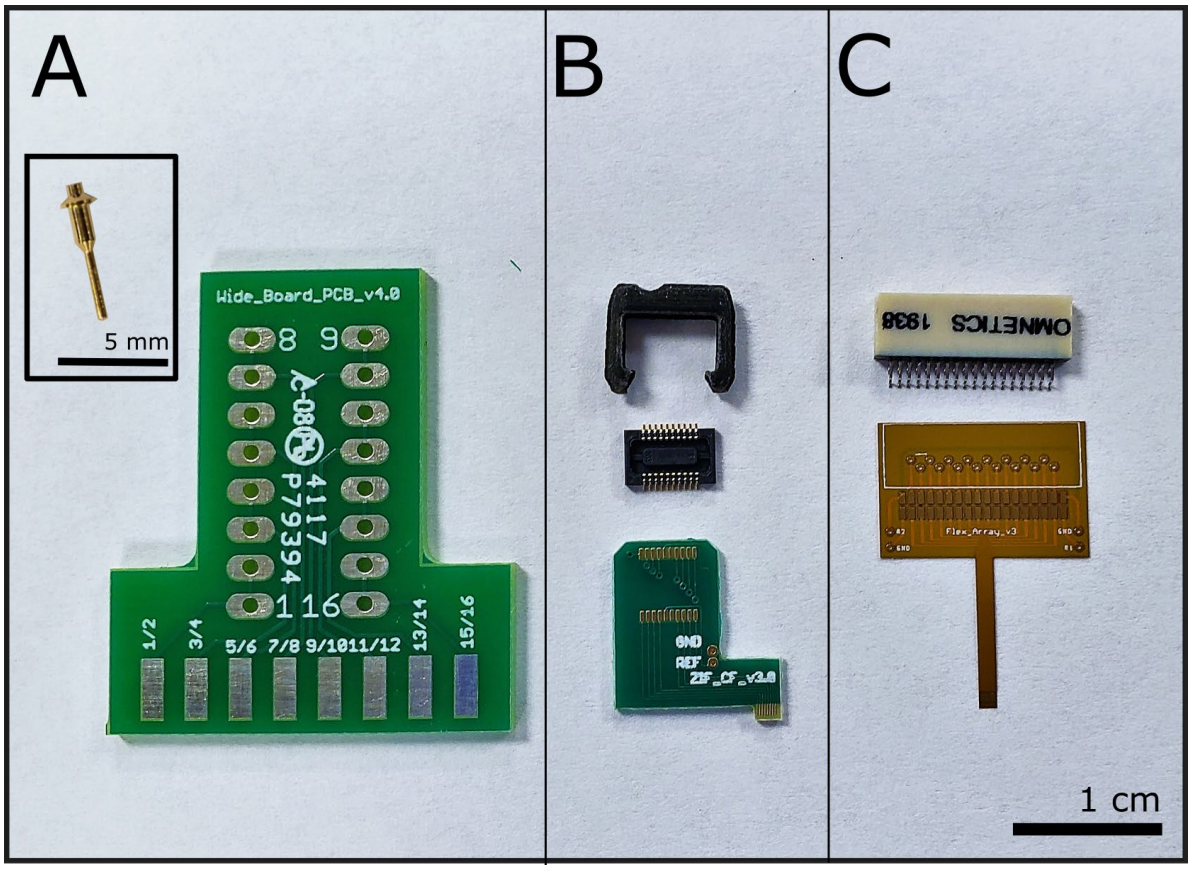

Figure 15: Connectors and associated printed circuit boards. (A) Wide Board with one of sixteen necessary connectors in inset (inset scale bar = 5 mm). (B) ZIF and one of two connectors and one shroud. (C) Flex Array with a 36-pin connector;scale bar = 1 cm.

4.3.2 Printed Circuit Boards

Wide Board, a ZIF based PCB (referred to as 'ZIF' here onwards), and Flex Array PCBs were designed in Eagle CAD (Autodesk, San Rafael, CA). Wide Board and ZIF designs were commercially manufactured (Advanced Circuits, Aurora, CO) and are compatible with Tucker-Davis Technologies (TDT) headstages (Figure 15 A and B respectively). Flex Arrays were fabricated at a commercial facility (MicroConnex, Snoqualmie, WA) (Figure 15 C). Soldering pad and trace sizing vary between each design (Table 3). Wide Boards are the easiest to fabricate. They have a pitch of 3 mm, ex-posed trace size of 1.5 mm x 4 mm, and are useful for applications where interelectrode distance doesn't matter, for example, soak testing or testing

coating viability. The 16-channel ZIFs have a pitch of 150 µm and an exposed trace size of 0.75 mm x 0.07 mm, which is sufficiently small for insertion testing or acute or chronic ePhys recordings. The smallest of these three designs is the 16-channel Flex Array, with an electrode pitch of 132 µm. Due to the small pitch, two traces are used per fiber to help align the fibers and create a well for the silver epoxy. One fiber per trace is possible (66 µm pitch, for 32-channels) with smaller particle epoxy, but requires a skilled hand to place the epoxy and fiber without shorting the electrodes.

PCB NAME	CONNECTOR	SOLDERING PAD SIZE (mm)	EXPOSED TRACE SIZE (mm)	TRACE PITCH (µm)	CHANNELS
Wide Board	Mill-Max 9976-0-00-15-00-00-03-0	3.25 x 1.6	1.5 x 4.0	3000	8
ZIF	Hirose DF30FC-20DS-0.4V,	0.23 x 0.7	0.75 x 0.07	152.4	16
Flex Array	Omnetics A79024-001	0.4 x 0.8	0.6 x 0.033	132	16

Table 2: Each PCB has a different connector and pitch associated with it. Abbreviation: PCB = printed circuit board.

4.3.3 Soldering Omnetics

The first step in building any of these devices is soldering the connector. This requires the use of a stereoscope (SMZ445, Nikon Instruments Inc, Melville, NY) and a soldering iron with a fine tip (0.1-0.2mm). For a lab without soldering equipment, this step can be outsourced to any PCB assembly house. Due to the melting temperature of the polyimide board, a soldering iron temperature of 315oC (600oF) was used to reduce the chance of pads separating from the board. Flux was applied to all contacts before a small amount of solder was placed on the back row of pads. Solder mounds had flat tops so the Omnetics pins were able to sit evenly across them (Figure 16 A). The two outer-most pins were pushed into the solder with the tip of the iron to secure the connector in place. The remaining pins were secured by pushing the tip of the iron be-

tween the front pins and pushing them down (Figure 16 B). The front pins were soldered to their respective pads. The remaining flux was cleaned off with 100% isopropyl alcohol (IPA) rinses and a brush (855-5, MG Chemicals, Canada) with bristles cut down to ~5 mm.

To prevent the Omnetics connector from deforming and pulling away from the Flex Array, the connections were insulated using a two-part epoxy (Sy-SS, Super Glue Corporation, Ontario, CA). Epoxy was mixed in a dish, pulled into a 1 mL syringe, ex-cess epoxy was wiped from the tip, and a 23 G needle attached. Epoxy was applied bevel side down against the top of the pins to encase the pins and minimizing air bubbles (Figure 16 C). A small amount of epoxy was applied to each side of the Omnetics connector on the board to secure the two during future handling steps (Figure 16 D). Boards were left to cure overnight at room temperature.

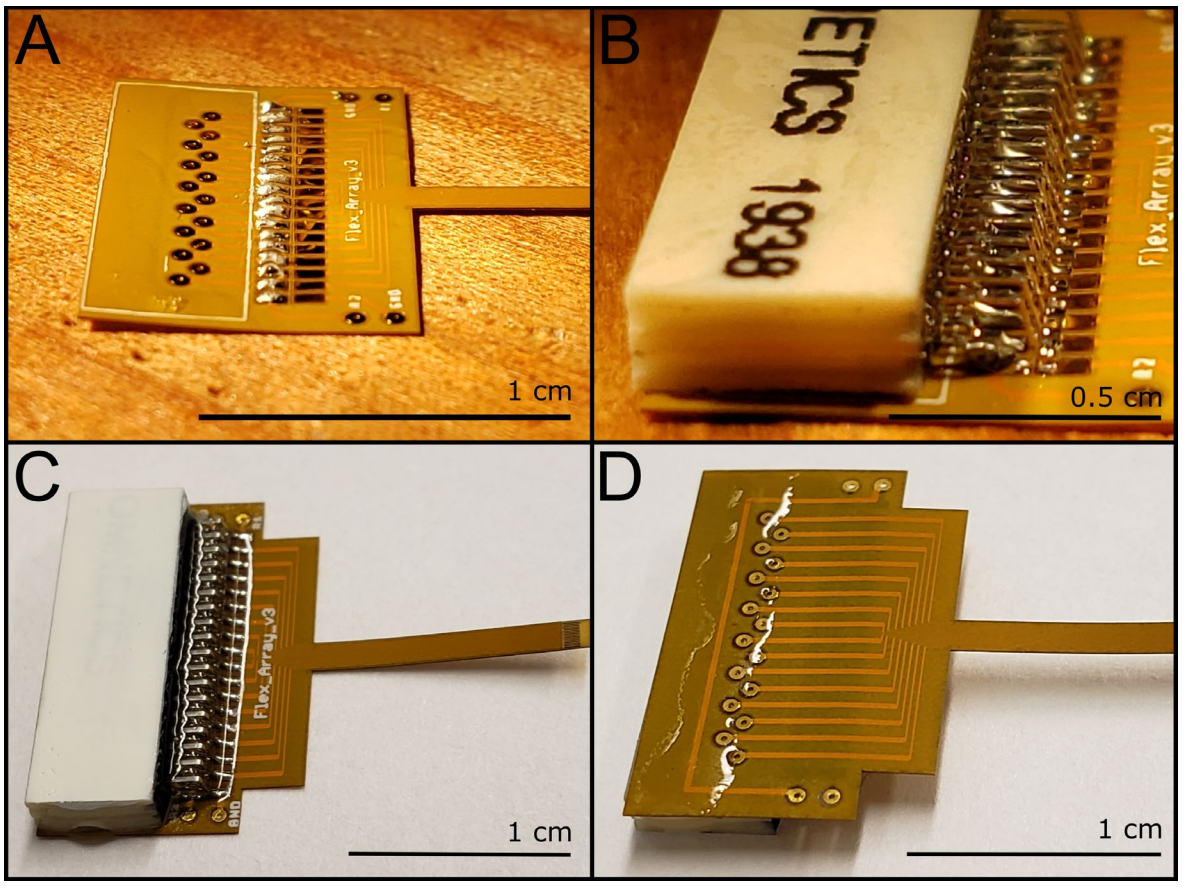

Figure 16: Soldering and insulation steps for the Flex Array. (A) Laying the solder for the bottom connector pins. (B) Back pins secured in place with the front pins ready for soldering. (C) Delayed set epoxy insulated Flex Array;

note that the delayed-set epoxy does not cover the reference and ground vias on either side. (D) Backside of the Flex Array with a band of delayed set epoxy across the pad vias (not the ground and reference vias) and wrapped around the side of the board toward the edge of the connector. Scale bar = 0.5 cm (B) and 1 cm (A, C, D).

4.3.4 Fiber Placement and UV epoxy

The prepared PCB was placed onto putty under the stereoscope (in the video, the putty is placed on a wooden block for ease of movement). Pulled glass capillaries (TW120-3, World Precision Instruments, Sarasota, FL) were made using a glass puller and filament (P-97 and FB315B, Sutter Instrument Co., Novato, CA) under the following settings: Heat= 900, Pull= 70, Velocity= 35, Time= 200, Pressure= 900 (numbers are unitless and specific to this device). Pulled capillary tips were cut to easily fit between the traces of the board (Figure 17 A). Silver epoxy (H20E, Epoxy Technology, Billerica, MA) was mixed in a dish according to manufacturer specifications. The glass capillary tip was dipped into silver epoxy and applied between pairs of adjacent traces (Figure 17 B) resulting in 8 pairs of connected traces. Traces are shorted together in this way to ease the manual demand of epoxy and fiber laying, however, one fiber per trace is possible for a practiced user (supplemental).

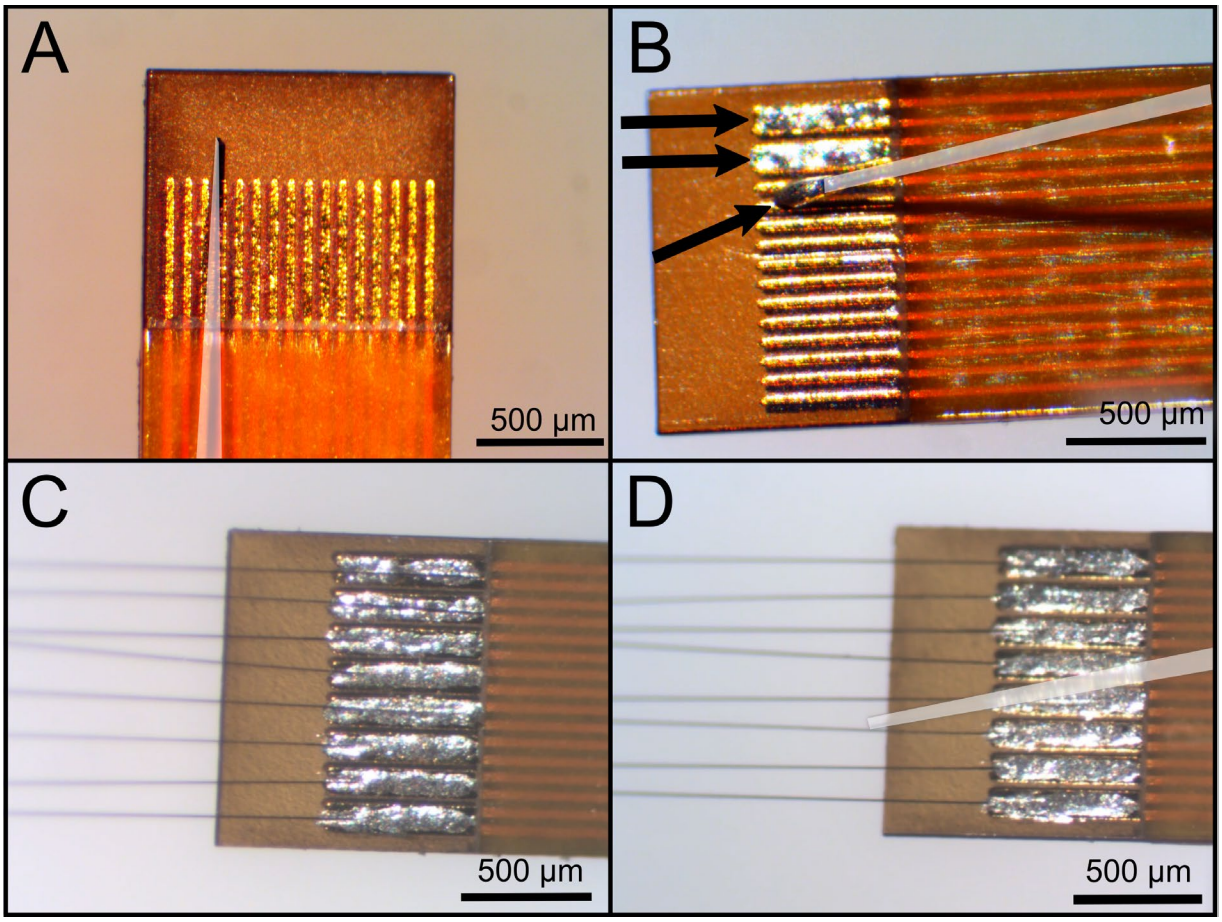

Figure 17: Applying silver epoxy and aligning carbon fibers between the traces of the Flex Array. Capillaries have been highlighted with a white overlay. (A) The end of the capillary fits between the traces to get (B) clean silver epoxy (denoted with arrows at the end of the capillary and within the traces) deposition without spillover outside of the trace pairs. (C) Carbon fibers are placed into the epoxy and then (D) straightened with a clean capillary. Scale bars = 500 µm.

Fibers were initially cut to 2-4 mm in length with a straight razor and separated into single fibers. This was accomplished by gently pulling a laminated piece of paper over the top of the carbon fiber bundle. The laminated paper helps to transfer static into the fibers causing them to separate on their own. A pair of Teflon coated tweezers (11626-11, Fine Science Tools, Foster City, CA) was used to pick up a single carbon fiber segment. Fibers were placed in the silver epoxy mounds (Figure 17 C). A clean capillary was used to adjust the fibers, so they were perpendicular to the end of the board, parallel to the length of the board, and buried beneath the epoxy (Figure 17 D). Carbon fibers were kept clean of silver epoxy past the edge of the board.

Arrays were placed on a wooden block without putty, with the carbon fiber portion stick over the edge, and then put into an oven for 20 minutes at 140 °C to cure the epoxy. The wooden block allows for easy transport of the device in and out of the oven, while also holding no static charge that could deform the carbon fibers' placement. The technique was repeated on the backside of the array resulting in a 16-fiber array. After curing, traces were visually inspected to ensure the connections had no shorts between fibers. Any epoxy shorts or spills were removed with a clean pulled glass capillary. A practiced user can achieve placement angles that are within 0.35 degrees for all fibers perpendicular to the edge of the board [104].

Next, the traces were insulated with a small amount of UV epoxy (OG-143, Epoxy Technology, Billerica, MA) placed on the end of the board using a clean pulled glass capillary (Figure 18 A). The amount of UV epoxy was enough to cover all traces and encapsulate all silver epoxy as this epoxy is meant to insulate the traces and fibers both from each other and from fluid interferences introduced in experiments. The probe was cured under a UV light (SpotCure-B6, Kinetic Instruments Inc, Bethel, CT) for a minimum of 2 minutes (Figure 18 B). The epoxy was checked by lightly tapping the sur-face with a clean pulled glass capillary to make sure it was fully cured (hard) before repeating on the other side; if not fully cured (sticky, soft), it was placed under the UV light for an additional 2 minutes. Once cured, fibers were cut to 1 mm lengths using stainless steel microsurgical scissors (15002-08, Fine Science Tools, Foster City, CA). When properly insulated, the board will have a small hard bubble on either side (Figure 18 B inset).

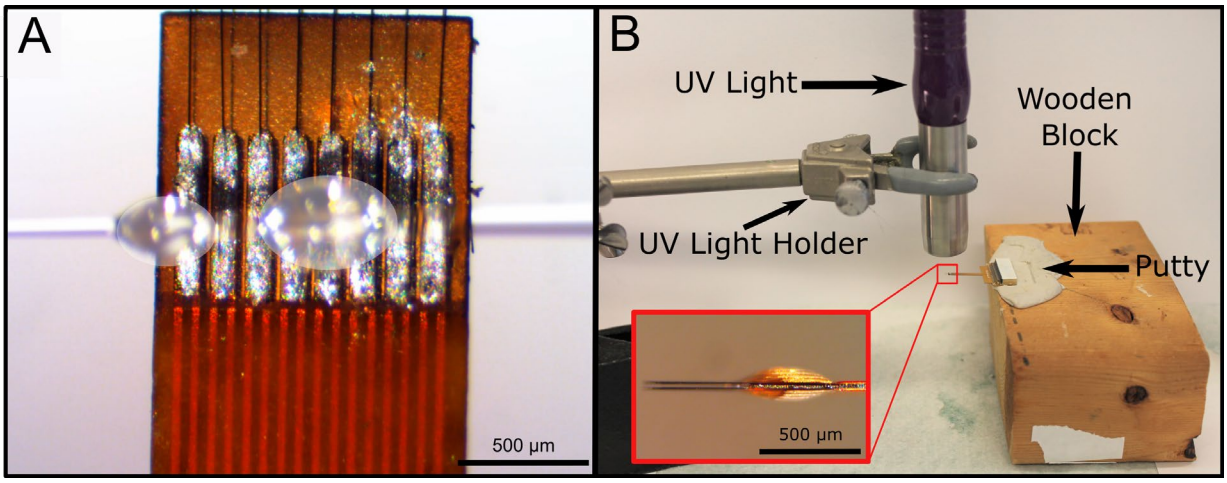

Figure 18: Insulation with UV Epoxy Application (A) UV epoxy is applied using a clean capillary and two drops of UV epoxy (marked with white overlays). UV epoxy is applied in droplets of 0.25-0.75 mm diameters until the UV epoxy forms a smooth bubble over the top of the traces. (B) UV epoxy is cured under UV light. The Flex Array is placed in putty on a wooden block for ease of movement and alignment underneath the UV light. The UV light is held with a holder ~1 cm above the end of the Flex Array. Inset (B) shows the side profile of a properly UV epoxy-insulated Flex Array. The UV epoxy bubble on either side of the board is roughly 50 µm in height. Scale bars = 500 µm (A and inset B).

4.3.5 Checking Electrical Connections

A 1 kHz impedance scan was taken to confirm the fibers were electrically connected to the Omnetics connector and no shorts existed between fibers. Fibers were submerged 1 mm in 1x PBS (BP3994, Fisher, Waltham, MA) with an Ag|AgCl reference electrode (RE-5B, BASi, West Lafayette, MA) and a stainless-steel rod as the counter electrode (Figure 19). A PGSTAT12 Autolab (EcoChemie, Utrecht, Netherlands) and NOVA software provided by the vendor were used to take the measurements. Results were analyzed using custom MATLAB scripts (MathWorks, Natick, MA). Measurements were taken at multiple steps during the build process to verify connections. Typical impedance ranges varied depending on the build step (Table 3). Once there was confidence in each build step, the number of impedance scans were reduced. Currently, they are performed only prior to Parylene C insulation and then as prescribed by the tip treatment procedure.

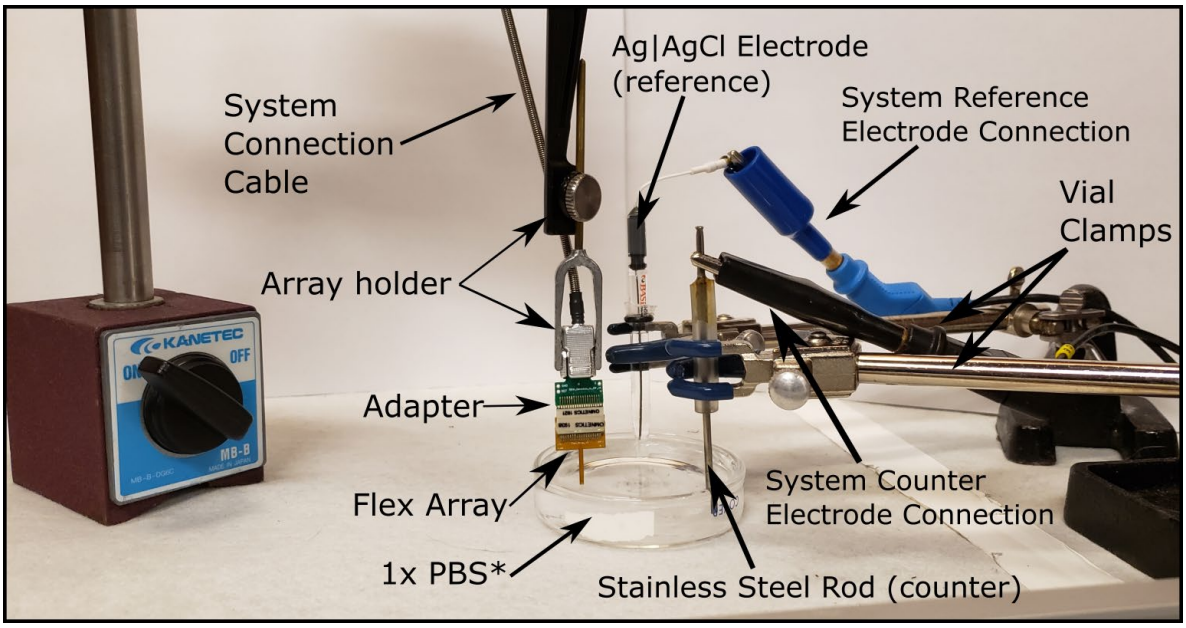

Figure 19: Setup for impedance measurements. All parts are labeled, and system connectors and adapters are system-dependent. PBS is starred as the solution is swapped for PEDOT:pTS later on in the build; however, the setup is identical otherwise. Abbreviations: PBS = phosphate-buffered saline; PEDOT:pTS = poly(3,4-ethylenedioxythiophene):ptoluenesulfonate.

BUILD STEP	EXPECTED 1KHZ IMPEDANCE (kΩ)
Bare Fiber	150-300
Bare Fiber with UV Insulation	400-500
Parylene C Insulated Fibers	>50,000
Nd:YAG Laser Cut	<15,000
Blowtorched	300-400
UV Laser Cut*	300-500
PEDOT:pTS Coated	<110

Table 3: Typical range of impedances after each build stage (n = 272). *n = 16. PEDOT:pTS-treated probes above 110 kΩ may still record signals; however, all treated electrodes typically fall under this value. Abbreviations: PEDOT:pTS =poly(3,4-ethylenedioxythiophene):p-toluenesulfonate; Neodymium-doped yttrium aluminum garnet.

4.3.6 Parylene C Insulation

The Flex Array's backend connector was masked using the mating connector (A79025-001) to prevent the internal pins of the Omnetics connector from being coated during the

insulation process. A batch of arrays (8-12) were placed into a box with a raised, adhesive platform such that the connector end of the probe was resting on the platform and the majority of the board was overhanging the edge of the raised plat-form (Figure 20). We used inverted Fisher Tape super glued to a piece of foam as the raised platform.

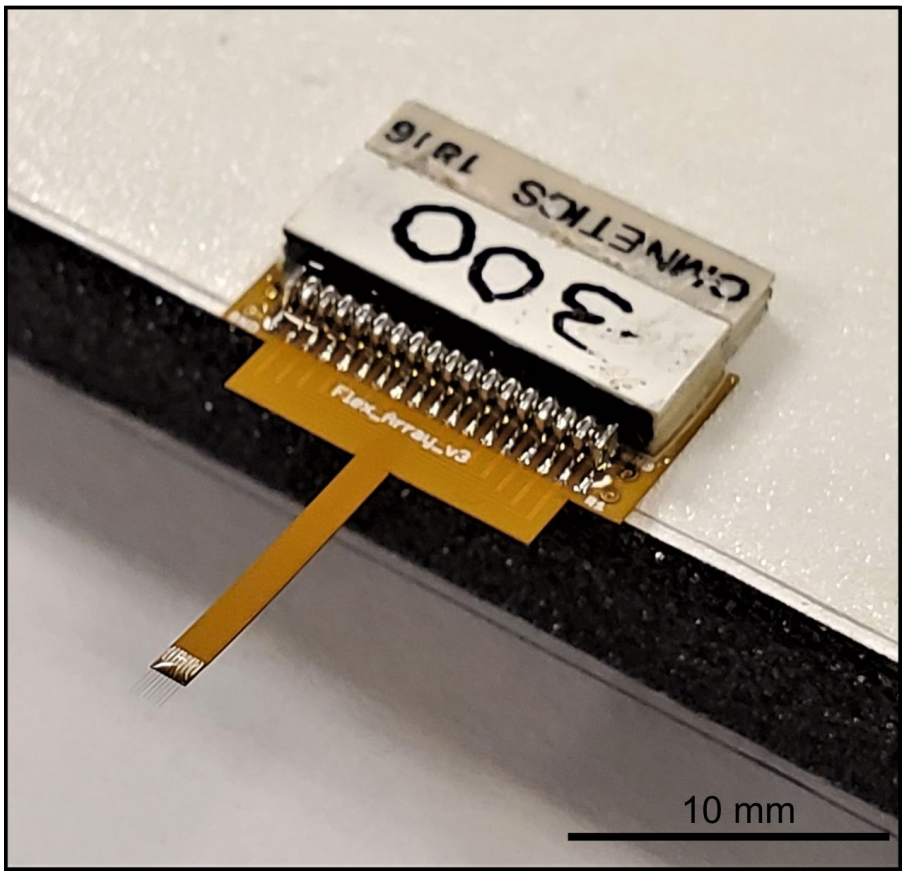

Figure 20: Flex Array prepared for Parylene C coating. The Flex Array is secured to a raised foam platform with tape, adhesive side up during the coating process. Scale bar =10 mm.

Arrays were coated with a conformal layer of Parylene C (thickness = 800 nm) using the Parylene C Deposition System 2035 (Specialty Coatings Systems, Indianapolis, IN) located within the Lurie Nanofabrication Facility at the University of Michigan, following deposition rate guidelines of the machine. Many cleanrooms at research universities will have this deposition capability, which is easy for an individual to learn. A batch of 5 probes were sent to

Specialty Coating Systems (Indianapolis, IN) to determine the viability of outsourcing this step to remove the only fabrication step that requires a cleanroom.

After Parylene C insulation, the backend masking was removed and the arrays were placed into a new box. A new box is required as the tape in the box that went through Parylene C deposition will be coated as well and unable to hold the arrays in place. The arrays were stored in a cool, dry, and dark place and considered shelf stable. An inventory of arrays was built up and used when needed for experiments.

4.3.7 Tip Preparation Methods

One of three methods was used to re-expose carbon at the tip of the fiber: neodymium-doped yttrium aluminum garnet (Nd:YAG) laser cut, blowtorch, or ultraviolet (UV) laser. The fibers must be cut by one of these three methods as scissor cutting alone is not sufficient to reliably re-expose the tip of the carbon fiber [140]. Fibers under 500 μm "self-insert" (require no additional or specialized insertion techniques) into the cortex [104], but for nerve or muscle a final length of ≤ 300 μm with sharpened tips was required [65].

4.3.8 Nd:YAG Laser Cut

Fibers were first cut to 550 μm with surgical scissors. A 532 nm Nd:YAG pulsed laser (LCS-1, New Wave Research, Fremont, CA: 5 mJ/pulse, 5ns duration, 900 mW) was used to further expose the carbon in conjunction with a Karl Suss probe station (LC3, SUSS MicroTec, Garching, Germany) for fiber alignment as shown previously [140]. The fibers were aligned inside of a 22 x 50 μm cutting window and the tips were cut off with 2-3 pulses resulting in a final length of 500 μm. The Parylene C ablated only slightly back (<10 μm) from the tip after each cut [140].

4.3.9 Blowtorch

While Nd:YAG laser cut fibers reliably re-expose fiber tips, access to such a laser can be limiting. It also only provides blunt cylindrical electrode tips that have some difficulty inserting into muscle and nerve. Thus, a modified approach to previous sharpening methodology [131], [177] was taken using a butane blowtorch (Microtorch MT-51B, Master Appliance, Racine, WI). Fibers were cut to 300 μm using surgical scissors. Using previously developed methods for nerve electrodes [174] an array was sub-merged in a dish of deionized water with the connector secured to the base of the dish with putty. The board was visually leveled and the water level was adjusted using a pipette and a pen camera (MS100, Teslong, Shenzhen, China) to ensure that the fibers were touching the surface of the water. A 3-5 mm flame from the blowtorch was run over the top of the fibers in a back-and-forth motion to sharpen the fibers (supple-mental for video). The array was removed from the putty and inspected under a stereoscope for pointed tips. The process was repeated until points were able to be observed under a stereoscope.

4.3.10 UV Laser Cut

A UV laser can also be used to both cut and sharpen carbon fibers similarly to the blowtorch method. While the UV laser is currently unable to be used with Flex Arrays due to the board's small pitch size between fibers and rows of fibers, it does show promise with the larger pitch of the ZIF and Wide Board designs. This method is being developed to give a pathway to laser cutting with an easily obtainable UV laser to re-move the access barrier that the Nd:YAG laser may provide. Thus, carbon fibers (2 mm length) were mounted on a ZIF and Parylene C insulated. A 1500 mW UV laser head (WER, Shanghai City, China) was affixed to three orthogonally configured motorized stages and then its focal point was moved across the fiber plane to cut the fibers to 500 μm [178].

4.3.11 PEDOT:pTS Coating

For all tip cutting methods, an additional conductive layer must be added to the exposed carbon site to further reduce its impedance. In previous work, poly(3,4-ethylenedioxythiophene):sodium p-toulenesulfonate (PEDOT:pTS) has been used. A 50 mL solution of 0.01 M 3,4-ethylenedioxythiophene (483028, Sigma-Aldrich, St. Louis, MO) and 0.1 M sodium p-toluenesulfonate (152536, Sigma-Aldrich, St. Louis, MO) was stirred overnight, then refrigerated, and replaced every 30 days. This solution was stored in a light resistant container as it is light sensitive.

Probe impedances were taken in 1x PBS solution with the same parameters used previously; "broken" (missing fiber) and "bad" (impedances > 1MΩ) channels were noted and not included in the PEDOT:pTS coating. Fibers with a good connection (typically 14-16 of the fibers) were electroplated with the PEDOT:pTS solution by applying 600 pA per fiber for 600 s using a PGSTAT12 Autolab. After electroplating, a final impedance measurement was taken and fibers with an impedance over 110 kΩ were designated "bad" in the probe's documentation.

4.3.12 Finalizing the Probe

The final step for finishing the probe was to solder ground and reference wires (Teflon Coated Silver Wire #AGT05100, World Precision Instruments, Sarasota, FL) to the probes. As the ground and reference vias were coated in Parylene C, they were scraped clean with tweezers on the top and bottom of the board. Two 5 cm silver wires were de-insulated on either end (1 cm and ~2 mm). The 2 mm exposed portion of the wires were placed into the ground and reference vias and soldered into place. The excess wire was cut away from the backside solder joint (Figure 21 A and B). Probes were placed in a storage box with the reference and ground wires secured away from the electrode tips (Figure 21 C).

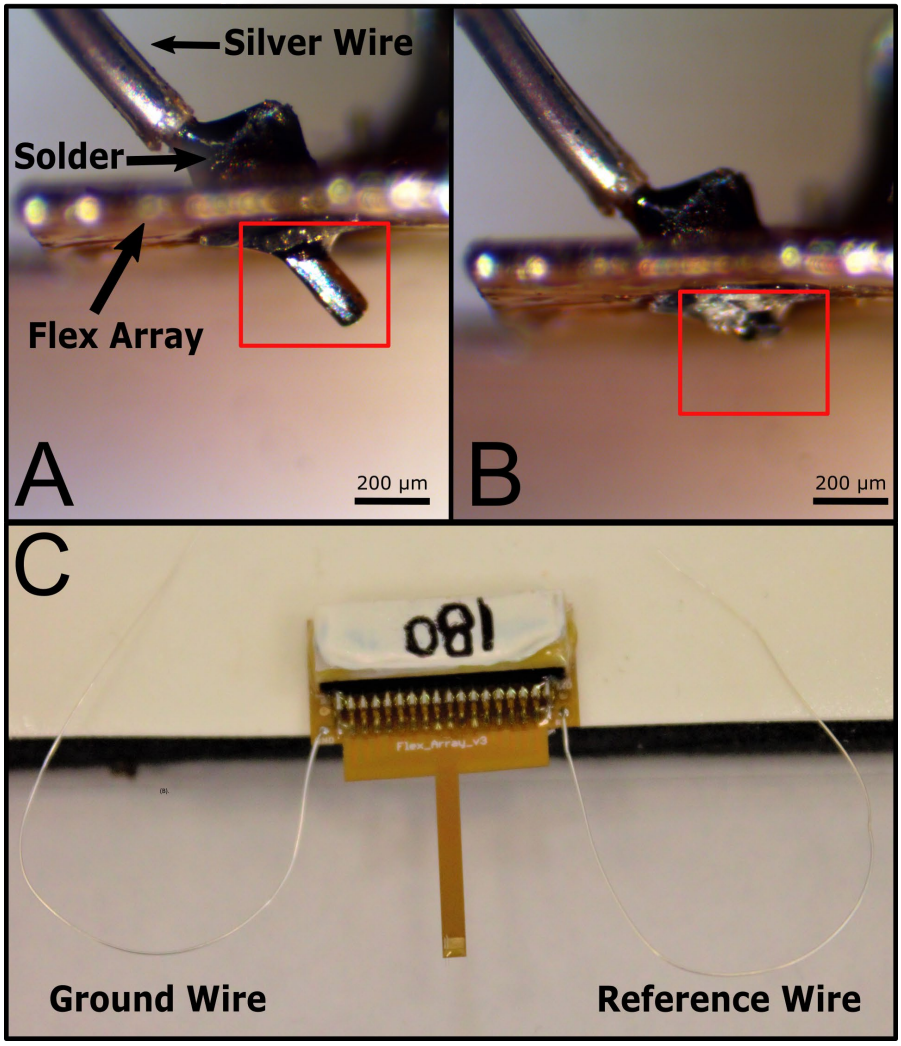

Figure 21: Ground and reference wires attached to the finalized Flex Array. Solder was applied to each side of the via on either side of the board (A) to create a secure bond. ePhys vias are labeled on the board as GND and Ref and paired on opposite sides of the board from one another. There are two additional vias also labeled GND and Ref2. Both GND vias are shorted together. Ref2 is meant to be used in electrochemical experiments. Excess wire in (A) is denoted with a red box and is removed (B) from the backside of the probe (red box shows where wire used to be) to help with noise reduction and handling the probe. (C) Final Flex Array stored for future use. Note that the paired GND and Ref vias on this board make it designated for ePhys recordings. Scale bars = 200 µm (A, B). Abbreviations: ePhys = electrophysiology; GND = ground; Ref = reference.

4.3.13 Surgery Protocol

All animal procedures were approved by the University of Michigan Institutional Animal Care and Use Committee.

Surgical procedures for acute recordings followed Patel et al 2015 [104]. To summarize, an adult male Long Evans rat weighing approximately 300 g was anesthetized using a combination of ketamine (90 mg/kg) and xylazine (10 mg/kg). A bone screw (19010-00, Fine Science Tools, Foster City, CA) was used as the common reference and ground at the posterior edge of the skull. A 2.5 mm by 2.5 mm craniotomy was made over the right hemisphere's motor cortex. After dura resection, a ZIF array with 4 UV laser treated fibers was inserted to a depth of 1.2 mm. All ePhys data was collected using a ZC16 headstage, RA16PA pre-amplifier, and RX5 Pentusa base station (Tucker-Davis Technologies, Alachua, FL). The pre-amplifier high-pass filtered at 2.2 Hz, anti-alias filtered at 7.5 kHz, and sampled at 25 kHz. The recording session was 10 minutes long.

4.3.14 Spike Sorting

Offline Sorter (OFS, Plexon, Dallas, TX) software was used to spike sort the data following the methods outlined in [109]. Channels were high-pass filtered (250 Hz corner, 4th order Butterworth) and waveforms were detected at -3.5*RMS threshold. Cluster centers were identified in principle component states using a K-means sorting method. Obvious noise clusters were eliminated from the data set. A Gaussian model was used to cluster the remaining clusters. Spikes with similar characteristics were combined and averaged over the cluster. Carbon fiber electrodes with discernible units were deemed viable. A minimum of 10 waveforms were required for a unit to be included in the data.

4.3.15 SEM Imaging

An FEI Nova 200 Nanolab Focused Ion Beam Workstation and Scanning Electron Microscope (FEI, Hillsboro, OR) was used for SEM imaging of Nd:YAG laser and blowtorch

prepared fibers. Prior to imaging, samples were gold sputter coated with an SPI-Module Sputter Coater (SPI Supplies, West Chester, PA). Images of UV laser pre-pared fibers were obtained with the JEOL InTouchScope Scanning Electrode Micro-scope (JSM-IT500HR, JEOL, Tokyo, Japan).

4.4 Results

4.4.1 Tip validation: SEM images

Previous work [174] showed that scissor cutting resulted in unreliable impedances as Parylene C folded across the recording site. Scissor cutting is used here only to cut fibers to a desired length before processing with an additional finish cutting method. SEM images of the tips were used to determine the exposed carbon length and tip geometry (Figure 22).

Scissor and Nd:YAG laser-cut fibers were previously reviewed [103], [174]. Scissor-cut fibers (Figure 22 A) have inconsistent tip geometries, with Parylene C folding over the end when cut [174]. The Nd:YAG laser-cut fibers remain consistent in recording site area, shape, and impedance (Figure 22 B). Blowtorched fibers [174] lead to the highest electrode size and shape variability but also resulted in a sharpened tip, allowing for insertion into tough tissue. On an average, 140 µm of carbon was re-exposed, with a smooth transition area between the carbon and Parylene C insulation (Figure 22 C). UV laser-cut fibers were similar to blowtorched fibers, showing 120 µm of carbon exposed from the tip (Figure 22 D). Impedances indicated that either the UV laser or blowtorch tip cutting methods are suitable for ePhys and are viable solutions for laboratories without access to a Nd:YAG laser.

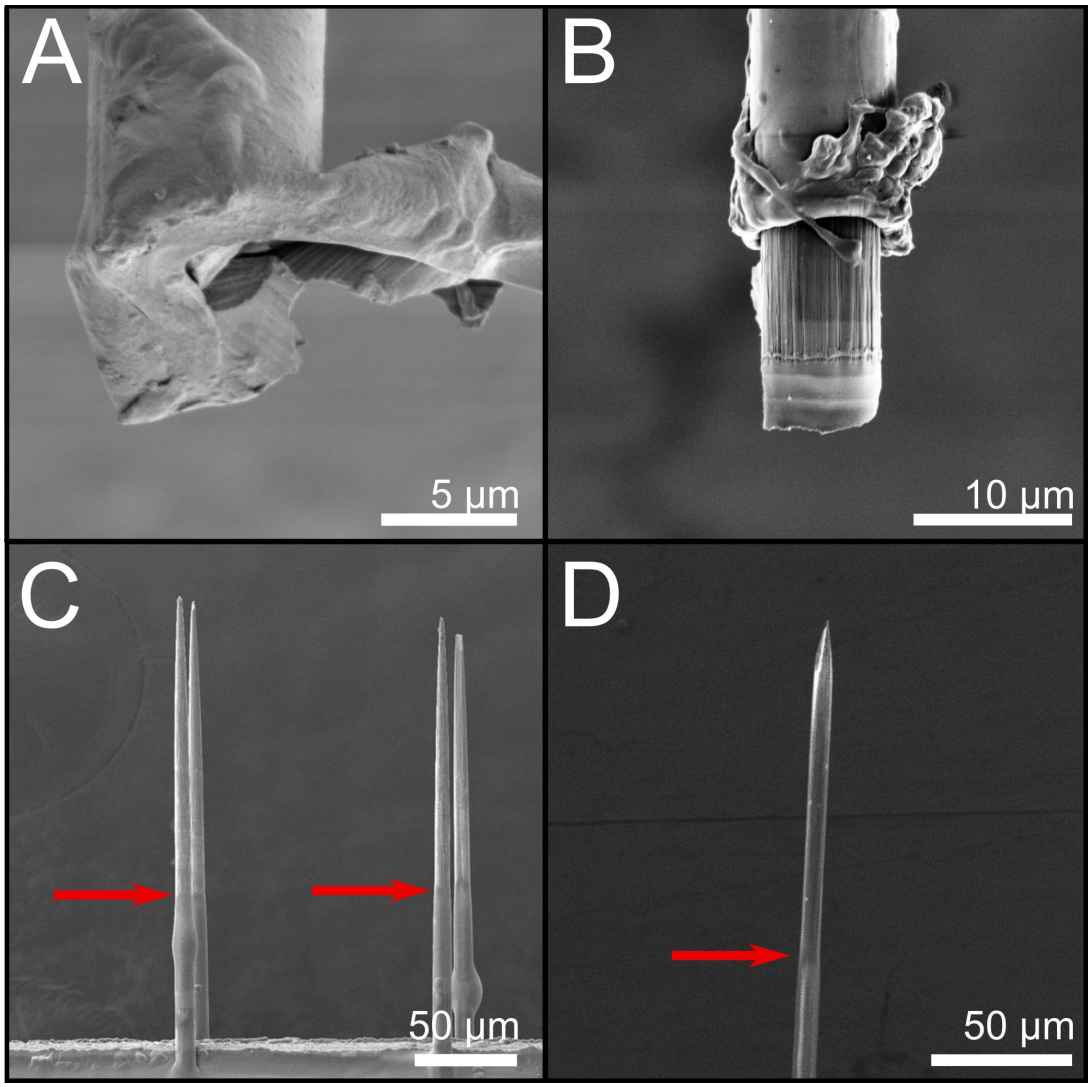

Figure 22: SEM images of fibers with different tip-cutting techniques. (A) Scissor-cut fiber with very little exposed carbon. (B) Nd:YAG laser cut. (C) Blowtorched fiber with ~140 mm of carbon exposed from the tip. (D) UV laser-cut fibers with ~120 mm of carbon exposed from the tip. Red arrows indicate the transition area between Parylene C and bare carbon fiber. Scale bars = 5 µm (A), 10 µm (B), 50 µm (C, D). Abbreviations: SEM = scanning electron microscopic; Nd:YAG = Neodymiumdoped yttrium aluminum garnet.

4.4.2 Tip validation: electrical recording

Figure 23 shows the resulting impedances from each preparation method using Flex Arrays. The resultant values are within an appropriate range for ePhys recording. Nd:YAG laser-cut fibers resulted in the smallest surface area but the highest impedances, even with the PEDOT:pTS coating (bare carbon: 4138 ± 110 kΩ; with PEDOT:pTS: 27 ± 1.15 kΩ; n = 262). This is followed by the inverse relationship in blowtorched (bare carbon: 308 ± 7 kΩ; with

PEDOT:pTS: 16 ± 0.81 kΩ; n = 262) and UV laser-cut (bare carbon: 468 ± 85.7 kΩ; with PEDOT:pTS: 27 ± 2.83 kΩ; n = 7) fibers that have a large surface area and low impedances. However, in all cases, the PEDOT:pTS-coated fibers do fall under the 110 kΩ threshold that was set previously to indicate a good, low impedance electrode.

Acute ePhys recordings were taken from a Long Evans rat acutely implanted with a ZIF array with UV laser-cut and PEDOT:pTS-treated fibers to demonstrate the viability of this method. ePhys has previously been tested and proven with scissor-cut [20] and Nd:YAG- [103] and blowtorch-treated fibers [65], [109] and so was not revalidated in this text. Acute recordings from four UV laser treatment fibers (2 mm in length) that were simultaneously implanted in rat motor cortex (n = 1) are presented in Figure 24Figure 23. Three units were found across all fibers, suggesting that the treatment of the fibers with the inexpensive UV laser is similar to other cutting methods that enable the carbon fiber to record neural units, as would be expected by the SEMs and impedances. While carbon fiber arrays are easily built and modified to suit the user's needs, it should be noted that additional validation is necessary for some builds (Table 3), while others are less suitable for certain end tasks.

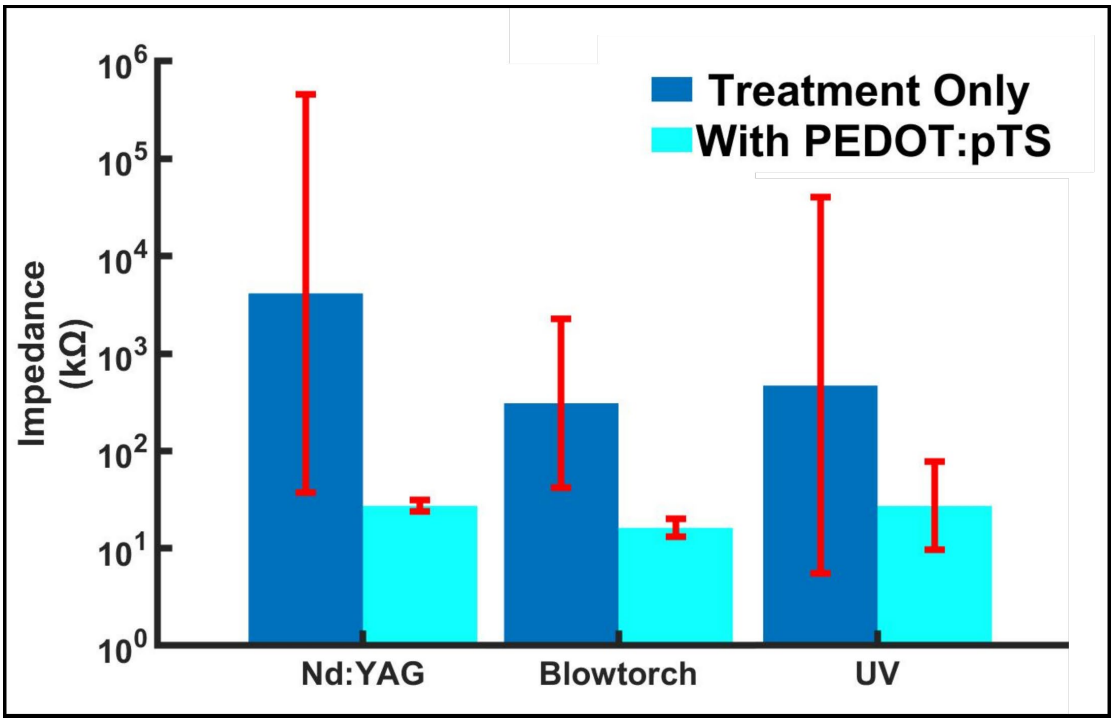

Figure 23: Impedance differences between only applying the treatment (bare carbon exposed) and with the addition of PEDOT:pTS. In all cases, the addition of PEDOT:pTS decreases the impedance by an order of magnitude. Sample size: Nd:YAG = 262, Blowtorch = 262, UV = 7. UV sample size difference is due to the novelty of the preparation method; however, it shows a similar range to blowtorch, as expected. Impedance data are expressed as mean ± standard error. Abbreviations: PEDOT:pTS = poly(3,4-ethylenedioxythiophene):p-toluenesulfonate; Neodymium-doped yttrium aluminum garnet.

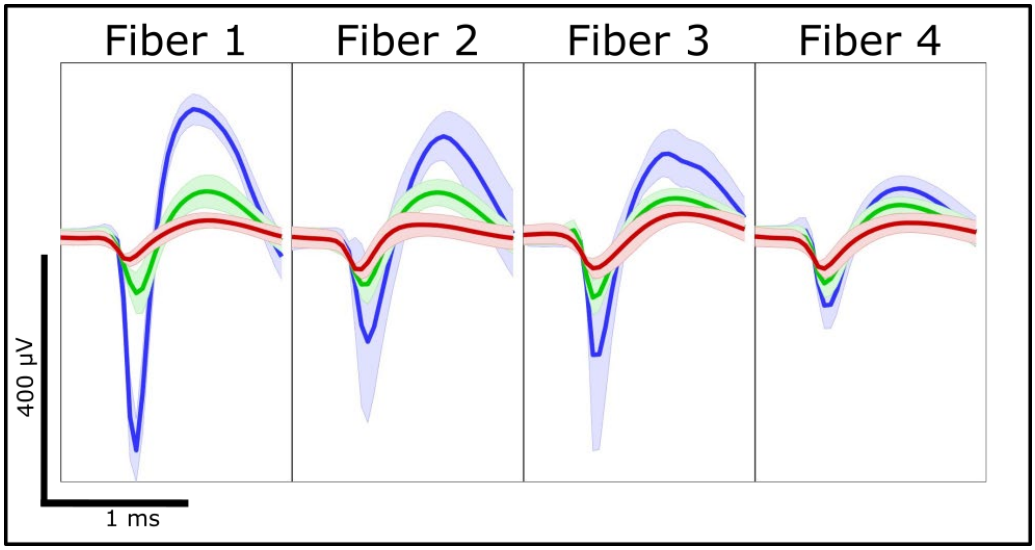

Figure 24: Acute electrophysiological spiking data from four UV laser-cut electrodes.

4.4.3 Commercial Parylene C

Commercially coated arrays were determined to have a Parylene C thickness of 710 nm by the vendor, well within the target range of insulation. The arrays were prepared for ePhys recordings using the blowtorch tip preparation. Impedances were taken after preparation of the tips and compared to existing data. A blowtorched and PEDOT:pTS-coated probe had an average of 14.5 ± 1.3 kΩ impedance across 16 fibers. SEM images were taken of the tip and shank to compare Parylene C deposition (Figure 25 A,B, respectively). These results show that the use of a commercial vendor did not change the expected impedance values, suggesting that this will be an equally viable substitution to deposition in the university cleanroom.

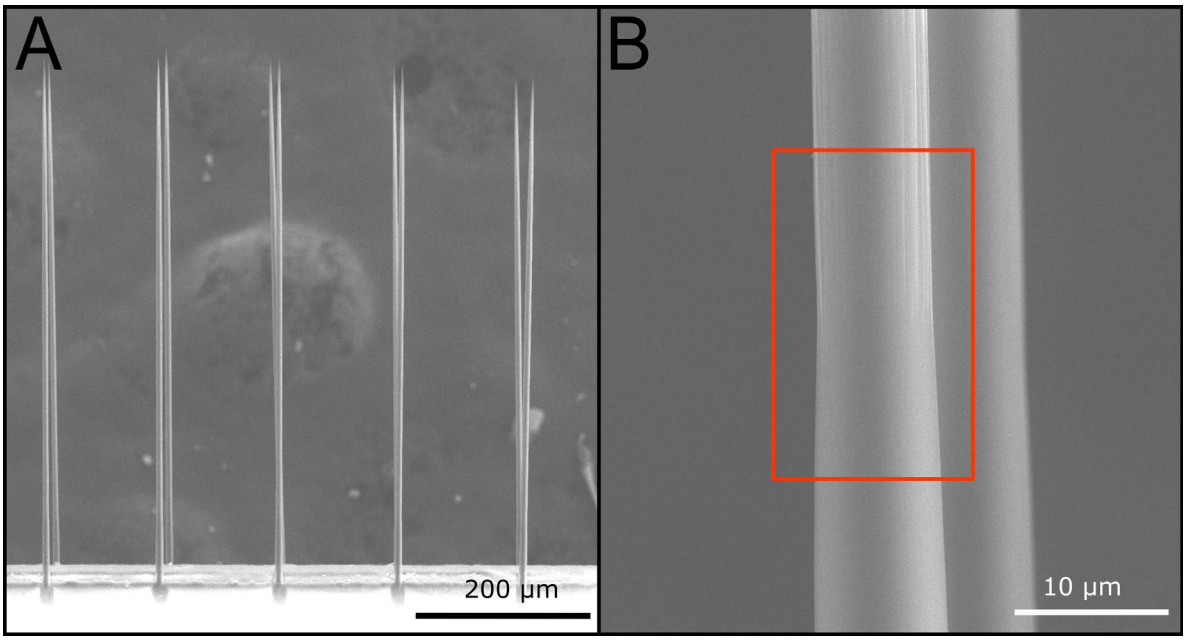

Figure 25: Commercial Parylene C-coated arrays. (A) The sharpened array shows uniform sharpening across all fibers indicating that there are no drawbacks to commercial coating. (B) After blowtorching, the transition (red box) between bare carbon fiber and Parylene C shows no discernable difference between arrays coated in a cleanroom facility. Scale bars = 200 µm (A) and 10 µm (B).

4.4.4 Device cost analysis

Provided all tools and bulk materials (e.g., epoxies, solder) are accessible to the researcher, a Parylene C user fee of $41, and a batch of 8 probes, the total materials cost is $1168 ($146 per probe). Personnel effort (Table 4) is ~25 h for the batch. If using a substituted

fabrication step, the cost of the probes will vary based on commercial Parylene C coating cost ($500–800 quoted). The time for the build steps (Table 4) is grouped together for all instances of a repeated tasks for simplicity. Build times for designs with a larger pitch (Wide Board and ZIF) are dramatically reduced as the manually intensive steps (e.g., carbon fiber placement) are easier and faster to complete.

ACTIVITY	TIME FOR 8 DEVICES (HRS)
All Soldering	5
Insulating Omnetics	1
Populating Carbon Fibers	10
Insulating Traces with UV Epoxy	0.5
Parylene C Deposition	1.5
Nd:YAG Laser Cutting	1
Blowtorching	1
UV LASER CUTTING	1.5
All Impedance Testing	4.5
PEDOT:pTS Deposition	1.5
Recipe Used	Total Hours
Nd:YAG Laser Cut	25
Blowtorch	25
UV Laser Cut	25.5

Table 4: Time required for each step of a fabrication process. Soldering of the connector and ground and reference wires have been combined here to simplify the activity list. Abbreviations: PEDOT:pTS = poly(3,4-ethylenedioxythiophene):ptoluenesulfonate; Neodymium-doped yttrium aluminum garnet.

4.5 Discussion

4.5.1 Material substitutions

While all materials used are summarized in the Table of Materials, very few of the materials are required to come from specific vendors. The Flex Array board must come from the listed vendor as they are the only company that can print the flexible board. The Flex Array connector must also be ordered from the vendor listed as it is a proprietary connector. Parylene C is highly recommended as the insulation material for the fibers as it provides a conformal coating

at room temperature in a reliable manner that can then withstand the in vivo environment. The polyimide board and epoxies on the board cannot tolerate high temperatures required for other insulation techniques. All other materials can be purchased from other vendors or be swapped out for alternatives at the users' discretion. This build is meant to be flexible and customizable to fit the end user's experiment. However, it should be noted that any changes from the materials or vendors listed must be validated by the end user.

4.5.2 Troubleshooting build issues

Silver epoxy deposition tends to fail for several reasons: the width of the capillary is too wide to fit between traces, the width of the capillary is too thin to pick up and deposit epoxy, or an excess of epoxy is on the capillary. The first two problems can be solved by cutting a new capillary of a more appropriate size; the latter by dipping the capillary into the epoxy with a lighter hand or removing a portion of the epoxy blob by gently dabbing the capillary onto a spare nitrile glove.

Deciding how to prepare the electrode is often a difficult decision for many users. However, determining what is needed for the experiment will help illuminate the decision. For acute surgeries, blunt tips can be used if the site size of the electrode is important; however, they will only insert into softer tissue (brain) and only at sub-500 μm target depths.

Going into deeper brain structures is possible using a glass cannula [104]; however, this can cause scarring and associated unreliability in ePhys recordings. Fibers must be less than 300 μm when sharpened to be able to penetrate harder tissues (nerve) as the shorter length provides a

stiffer backbone for insertion [65], [109]. Sharpened fibers have also recently been observed to penetrate to 1 mm depths in the brain [109].

While the arrays discussed in this paper are an excellent starting point for many labs, newer probes using carbon fibers have also been developed to chronically target deeper areas in brain [104], [108], [130]. In nerve, electrodes of low invasiveness and high selectivity are an ongoing research topic [109], [151], [160]. Jiman et al. [65] were able to detect multiunit activity within the nerve with minimal invasiveness and increased selectivity using a carbon fiber silicone array [109], which mirrors the design of the Flex Array presented here.

4.5.3 Parylene C accessibility

Parylene C is a method of conformal coating at room temperature that has been used as a biocompatible insulator in many implanted devices. The technique requires a specialized tool in a cleanroom and takes about an hour to learn. A cursory survey of institutions that have previously requested carbon fiber arrays from our group was conducted to determine Parylene C deposition accessibility. We found that out of 17 institutes, 41% had access to Parylene C-coating systems on their campus. For universities without access to a Parylene C-coating system, commercial coating services are a viable alternative as demonstrated here. Alternatively, outsourcing to a nearby university cleanroom may also be of interest to laboratories with no direct access to a Parylene C deposition system. To reduce the cost per device, we advise sending out larger batches of arrays as commercial systems are often able to accommodate larger samples.

4.5.4 Optimizing tip preparations

Additional tip preparations need to be investigated for these fibers as the current tip preparations require the end user to choose between penetrating ability and a small recording site. While the Nd:YAG laser-cut fibers provide a small site size [174], the ability to penetrate stiffer tissue (muscle, nerve) is almost non-existent, and access to a laser setup capable of this cutting technique can be difficult and expensive. While blowtorching allows for a quick and economical way to get sharpened tips that can penetrate many tissues [65], the tip geometry is large and may be inconsistent from fiber to fiber [174]. UV laser cutting also provides low impedances and large surface areas but with the added benefit of more consistent exposure. The UV laser is more accessible than the Nd:YAG laser; however, laboratories would need to engineer a way to align the laser with fibers and would not be able to use the Flex Array due to the pitch of the fibers being smaller than the laser's focal point diameter. Previous work showed the fabrication of small, sharpened fibers via etching [138], [139]. This approach could result in a small, reliable electrode geometry and would preserve the sharpened tip necessary for penetrating nerve and muscle.

Our current tip coating, PEDOT:pTS, may also need to be replaced as it tends to degrade overtime, which is an undesirable trait for a chronic probe [103], [140], [179]. A lack of PEDOT:pTS longevity leads to higher impedances and therefore lower signal quality, in part due to increased background noise. To increase longevity in these fiber tips, investigation into the feasibility of platinum-iridium coatings is being conducted. Platinum-iridium would allow for a greater surface area [68], [140] concentrated on the tip of the electrode, keeping a low impedance [28], [68], [180] and allow for longer, chronic stability [68], [180]. Other coatings, such as PEDOT/graphene oxide [181] and gold [67], have been utilized to lower carbon fiber electrode impedances, although these coatings are typically used for chemical-sensing probes rather than

for ePhys recordings. Due to the inherent properties of carbon fibers [182], the carbon fiber array presented here can be converted from a probe optimized for ePhys to a chemical-sensing device with a simple change of tip preparation [104], [183].

Chapter 5 Emerging Capabilities

5.1 Introduction

While the research presented previously has been a part of larger projects and publications, other efforts have been made to investigate carbon fiber capabilities further. Summarized below are several of the efforts I have made toward other research projects that have not yet been completed.

5.2 Parametric Etching

While the chemical etching presented in this thesis was successful in making a small electrode tip, the parameters of the etch can be modified to tune the tip geometry to its specific purpose, such as having a larger surface area for stimulation that can't be achieved through current methods. Etching parameters laid out in Chapter 2 were modified in both the voltage amplitude applied and the length of time the tips were exposed. Arrays were constructed with 8 carbon fibers, Parylene C coated, and etched. SEM images and measurements were taken to measure the geometry. Preliminary data (Table 5) shows that modifying these parameters does impact the final geometry of the electrode, however, further analysis is needed. Additionally, the current protocol allows the acid solution to cool during the etch; keeping the acid heated during the etch to a consistent temperature may help to reduce variability seen in etching and improve the tenability of the etch.

	Time (s)		
Voltage (V)	1	1.5	3
4.24	19.0 ± 2.6		41.0 ± 2.1
3.54	79.4 ± 14.8	154.2 ±19.5	
2	201.6 ± 27.7		167.7 ± 9.1

Table 5: Surface areas of exposed carbon on SPFe under different parameters.

5.3 Muscle Recoding

Single-fiber SPFe were prepared by attaching a carbon fiber to the end of an exposed wire. The fiber was encapsulated in silicone, cut to a desired length, and then the tip was etched to 10 µm height. The fiber was inserted into the leg muscle of rat and the innervating nerve was electrically stimulated to produce a contraction in the muscle. The SPFe survived insertion, the contraction of muscle, and recorded compound multi-action potentials. The SPFe survival was confirmed with a 1 kHz impedance measurement. Figure 26 shows an example set of waveforms recorded on a single fiber electrode.

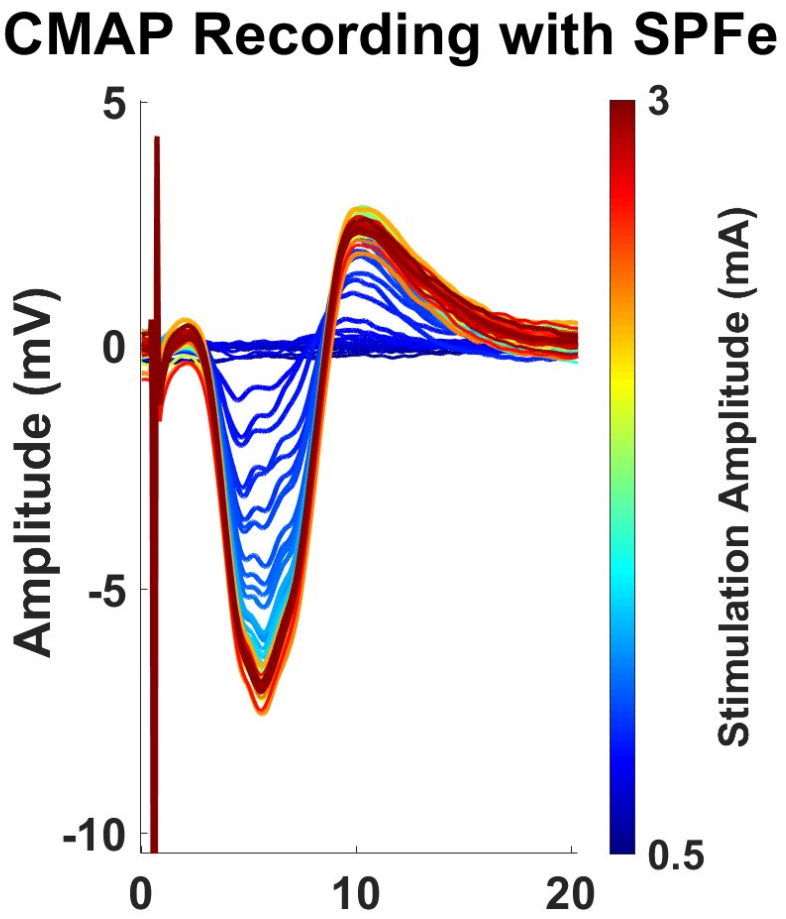

Figure 26: Multiple CMAP Recording from SPFe in muscle. Each line represents a trial and its color is associated with the stimulation amplitude.

Chapter 6
Discussion

6.1 Conclusion

In this thesis, I have shown small pointed carbon fiber electrodes to be useful in neural research across multiple animals and multiple modalities. First, I fabricated carbon fiber electrode recording sites using an acid etch to cellular scale (10 μm in height). I showed that despite their size, they were able to be inserted and still remain viable as electrodes that can record ePhys signals or stimulate selectively. Second, I have produced a model of carbon fibers with varying diameters and exposure mirroring those found in literature and modeled the recorded response in a simplified nerve to show the predicted benefit of these small pointed fiber electrodes. Finally, I have created an open-source tool kit for neuroscience labs to make carbon fiber arrays accessible. Providing this technology in an open-source manner allows researchers to quickly fabricate and modify carbon fiber arrays at the bench for their particular experimental design. This work has been an effort to make the carbon fiber electrode more accessible to neuroscience research with the ultimate goal to expand the scope of science experiments possible.

6.2 The Usefulness of Carbon Fibers

This thesis has been a love letter to carbon fibers and carbon based electrodes. However, it has not yet discussed in full the breadth of possible uses for carbon fibers in neural interfacing and neuroscience research. Here I will discuss possible models for carbon fibers neural arrays. In

this thesis, the SPFe have shown the ability to penetrate into multiple tissues from nerve to retina, retaining the ability to record and stimulate. This opens many possibilities for other animal tissue models that have been notably inaccessible.

6.2.1 Lower-Order Vertebrate Models

One model that has been difficult to access is mouse spinal cord [184]. Mice are a small animal and their spinal cords are typically only in 2-3 mm diameter [185], [186] with axon diameters ranging from 0.8 – 1.8 μm [186]. Many electrodes are not able to access the spinal cord selectively or at all due purely to the size mismatch between axons and electrode size – recall that the smallest are around 100 μm^2 [5], [57] and this does not include the added substrate material supporting the electrode needed to penetrate the spinal cord. Carbon fibers offer a possible avenue into both accessing and interfacing with this small model – especially with the SPFe which can be modified further to have an exposed height of ~1 μm (SA ≈ 10 μm^2) [138], [139]. SPFe have been shown to penetrate tough nerve tissue [65], [109] and could be a way to penetrate spinal cord. Additionally, as the carbon fiber would be supporting itself in the insertion, the total implant footprint would be determined by the size of the carbon fiber and any insulation.

Another small vertebrate model that carbon fibers could be useful for are birds [187], [188]. Understanding how birds learn song allow researchers to study how neurons encode and store these vocal patterns [188]. This offers insights into how humans are able to encode these types of signals to produce speech music as well [187]. This type of research is important for people that need a computer interface to communicate as the neural networks storing language information can be decoded into speech directly from the brain [36], [189]. However, songbirds, like mice, are small and delicate. Currently small electrodes like patch clamp [188] and wire

electrodes [187] are used to access these small anatomies. A carbon fibers could allow for improved recording capability as their small diameter could create more densely packed electrodes while still remaining selective in cell recording.

6.2.2 Small Cell Models

Small cells are challenging to interface with in a meaningful way. Small neurons in the higher layers of brain are often monitored using ECoG sensors – especially in epilepsy monitoring [21]. However, ECoG signals give a general sense of brain activity and make estimates as to when a seizure is impending. Even today, doctors and researchers have a difficult time with statistical validation of the predictions made through BCI [190], [191]. These ECoG sensors do not have the spatiotemporal sensitivity needed to track individual neurons in the upper layers of the brain. However, SPFe may offer an avenue into recording more selectively in conjunction with an ECoG array to offer better, more sensitive prediction models. A better prediction model is key for these technologies to be adopted in clinical treatment.

Additionally, retinal implants have suffered immensely from a lack of access to the cell bodies they need to stimulate as previous implants have relied on indirect stimulation of the targeted cells [144], [192]. Penetrating, three-dimensional electrodes have been proposed as a way to directly simulate the targeted cells [193]. Carbon fibers have been shown in this thesis to stimulate single cells in retina. This level of selectivity and the ability to penetrate the retina provide a strong avenue for carbon fiber retinal prosthesis that could improve the resolution of eyesight and thus improve vision restoration attempts.

6.2.3 Higher-Order Vertebrate Models

Preliminary data from Steve Kemp's lab **(**Figure 26**)** shows potential for muscle recording using SPFe. Current Regenerative Peripheral Nerve Interfaces (RPNIs) [194] use wire electrodes to record muscle signal to provide a patient control of a robotic arm. It was found that these RPNIs helped to restore not only motor control, but also allowed patients to feel the object (whether it was hard or soft, heavy or light) which provided better feedback to the patient for handling objects [195], [196]. A carbon fiber electrode could be used in an RPNI to help increase the ability for a user to feel what the robotic hand sensors feel by implanting them into the cutaneous cells that are responsible for this touch feedback.

Non-human primate motor control research currently relies heavily on silicon implants such as the Utah array to record signals in motor cortex that are then decoded into motion. However, as discussed, silicon is not necessarily the best option for implant as they can be rejected, lose function, or just have very low recording yield after implant [81], [88]. Carbon fibers may offer a more selective and less invasive method to record from the motor cortex. Additionally, with increased selectivity of spiking neurons, this may provide insights to help improve motor control BCI by isolating individual finger movement [197] which is currently very difficult to decode.

Provided carbon fibers work in non-human primates, there is a strong case to move these arrays into human subjects as well. A carbon fiber device in the brain may allow for better decoding in human and allow for quicker integration between human and robotic arm. Better and quicker integration allows a user to more quickly adapt to and learn how to use a robotic arm. Additionally, if the carbon fiber array is able to allow for more selective decoding, this will allow users to integrate the arm into their identity improving long-term use and care for the prosthetic.

6.2.4 Invertebrate Models

In Chapter 2, we briefly discussed the use of octopus and sea slug in neuroscience research using the SPFe. Due to their successes in these areas, the SPFe could be useful in recording from other invertebrates as well. Insect models, like damselfly predation studies, could benefit from SPFe as they are better scaled to their model size [198]. This could open up many avenues for understanding how bees learn and communicate [199] and form societies [200] – which can help to understand how humans do the same things.

6.2.5 Neuroscience Labs

SPFes are an excellent addition to a neuroscience lab. Carbon fibers are easy and cheap to obtain and a lab can build an array using open-source PCBs and commercial Parylene C coating to create their own specialized arrays for use in research without the need for a MEMS engineer and pricey prototyping. We have previously discussed the applications of carbon fibers in regard to ePhys recording, however, another method of investigation, fast-scan cyclic voltammetry (FSCV) is possible using carbon fibers [135], [181], [183]. To recap the versatility of the open-source carbon fiber array in chapter 4 for ePhys investigation, carbon fibers arrays allow researchers to work on multiple investigation levels from cells in a dish to *in vivo* recording. Researchers can modify the lengths of the carbon fibers on an array allowing them to track different signals at different depths in a given tissue. This can be especially helpful in brain where some parts, like hippocampus, can be easily missed by arrays because they are so thin. Adding a stepped layout to the fiber lengths can allow for researchers to implant and then confirm with histology later which fibers were in the correct position for recording.

FSCV is used to track chemicals and neurotransmitters in the brain [135], [181]. Essentially, FSCV is a way to monitor chemicals entering and exiting a part of the brain by recording and characterizing the redox peaks occurring at the electrode site [201]. For example,

addition studies might track dopamine levels after giving an animal a dose of an addictive substance, such as nicotine or alcohol, to find ways to inhibit the addiction behavior [202]. Parkinson's research may use it to track the progression of the disease to discover the mechanisms that cause it – and those that can be implemented to stop its progression [203]. Carbon fibers are a good choice for this application because the tip geometry can be modified to attach to several different transmitters [204] and again, are cheap and easy to come by. While the SPFe presented in this thesis may not be ideal for this application due to their small surface area, other etching parameters may allow for a tunable electrode that is more suited to this task.

6.2.6 Carbon Fiber Models

The work done with the carbon fiber model in this paper is useful in its simplicity. The carbon fiber models are based on parameters given in previous papers and data sheets. These models were used in ePhys demonstrations, but could be coupled with the indentation data in chapter 5, and its future paper, to construct insertion models to predict optimal pitches for insertion into tissues. These models could further be used to look at recording and stimulation overlap and all that good stuff. Considering the lack of electrical data for small axons [44], these small carbon fibers could offer insight into the biophysics occurring in these tissues to provide better quantitative data for mathematical models rather than having to "extrapolate" these numbers based on trends [44]. Better understanding of these small axons could open doors for understanding how reverse recruitment occurs in stimulation. The SPFe recording ability *in vivo* opens doors for validation and creation of more sensitive and accurate models for small, currently inaccessible cells and axons.

6.3 Carbon Fibers of the Future

In ten years, I believe that carbon fibers in humans will be possible in clinical trials. In brain, with either a diamond or silicon backend, CF arrays would easily be able to be more densely packed than current commercial penetrating arrays. Eye prosthesis will be advanced with both implants in visual cortex and in the retinal. I hope that in 10 years we are able to decode octopus movements and understand how our extremely distant cousins work so well while being so different. I want to decode the thoughts of an octopus.

Ultimately, I look forward to a world where neural arrays are entirely organic. As I started my research career in a carbon lab, I am well aware of the many ways it can be manipulated to act as an insulator, conductor, semi-conductor, capacitor, resistor, and so much more. One day people will have implants that are less invasive, more effective, and made of the same stuff that they are They will have a life where metal detectors don't ring out because of an implant, MRIs are safe to have, and the device lasts the lifetime of the person using it. I believe in bioelectronic medicine, and I believe that carbon provides us a way to unlock the potential of brain machine interfaces.

Appendix

Supplemental Information for Aim 3

Build Differences

Wide Board

Soldering: Wide Board connectors use a DIP connector which utilizes pins that slot into vias on the board. A DIP connector was placed on the back side of the board with the pins of the connector protruding through the vias into the connector, holding them in place for soldering. Flux was applied to the pins and soldered in place. Flux was cleaned with IPA and cotton applicators.

Fiber Population and Insulation: PCBs were roughened around the traces at the end of the board to allow for better adhesion of the insulating epoxy in a later step. Silver epoxy was applied directly to the traces with the wooden tip of a cotton applicator and a carbon fiber was placed on each trace. Carbon fibers are typically cut to be much longer (1cm) for these devices as they are used primarily in soak testing [103], [140]. This additional length allows more flexibility within the carbon fibers, so additional care is required when handling the fibers. Epoxy was cured using manufacturer recommended parameters. Traces were insulated with 353ND-T epoxy and cured following manufacturer recommended settings,

Tip Cutting: Due to the typically longer length of fibers on these boards, implementing an air dam to reduce currents around the fibers is necessary to keep them still for the Nd:YAG laser. Blowtorching is not a viable solution as the fibers tend to float around and bend rather than

extend to the surface of the water. Due to the movement of the motorized stage and difficulty of including an air dam, the UV laser cutting method was not tested.

ZIF

Soldering: The ZIF PCB utilizes a Hirose connector designed to interface with Tucker-Davis Technologies ZIF headstages. Flux was applied to the soldering pads on one side of the PCB and the connector was secured onto the board by first soldering the opposite corners of the Hirose connector before soldering the rest of the connector's pins. This was then repeated on the other side of the board. Flux was cleaned off the board with IPA. A plastic shroud was then placed around the end of the board and pressed into the board until the ends of the shrouds 'clicked' into place around the connector. At this point, a drop of super glue was applied to one side of the shroud to secure the shroud to the board, being careful not to get any glue on the soldering pads.

Fiber Population and Insulation: Silver epoxy was applied to each trace with a pulled capillary to form a small mound along the length of the trace. Carbon fibers were then placed into the epoxy keeping the fibers straight by aligning with the trace. Epoxy was cured at 140ºC for 20 minutes then deposition was repeated on the opposite side of the board.

Insulating epoxy (353ND-T, Epoxy Technology, Billerica, MA) was prepared according to vendor specifications and applied to the traces of the boards using a glass capillary. Boards were cured at 120ºC for 20 minutes. This process was repeated on the opposite side of the board.

32 Channel Flex Array

Instead of shorting pairs of traces on the Flex Array together, one carbon fiber can be attached to one individual trace to provide 32 channels of individual recording data. This method takes months of practice to build up the dexterity needed for this precise technique. Testing on

implants and recording with these devices have been limited in our lab due to unforeseen lab closures.

Fiber Population: Carbon fibers were picked up with tweezers and the tips of the fiber were dipped into a different silver epoxy (HPS-030LV, NovaCentrix, Austin, TX). The epoxy was distributed along the trace until enough was deposited for the carbon fiber to be placed on the trace and buried in the epoxy. This was repeated for the remaining traces. Fibers were aligned with a clean pulled glass capillary and then cured at 140ºC for 20 minutes. Fibers were placed on the backside of the board similarly and then insulated with UV epoxy following the standard procedure.

Bibliography

[1] R. Ham and L. Cotton, *Limb Amputation*. Boston, MA: Springer US, 1991. doi: 10.1007/978-1-4899-3152-8.

[2] A. Kawala-Sterniuk *et al.*, "Summary of over Fifty Years with Brain-Computer Interfaces—A Review," *Brain Sci.*, vol. 11, no. 1, Art. no. 1, Jan. 2021, doi: 10.3390/brainsci11010043.

[3] L. F. Nicolas-Alonso and J. Gomez-Gil, "Brain Computer Interfaces, a Review," *Sensors*, vol. 12, no. 2, Art. no. 2, Feb. 2012, doi: 10.3390/s120201211.

[4] R. Chen, A. Canales, and P. Anikeeva, "Neural recording and modulation technologies," *Nat. Rev. Mater.*, vol. 2, no. 2, Art. no. 2, Jan. 2017, doi: 10.1038/natrevmats.2016.93.

[5] A. C. Patil and N. V. Thakor, "Implantable neurotechnologies: a review of micro- and nanoelectrodes for neural recording," *Med. Biol. Eng. Comput.*, vol. 54, no. 1, pp. 23–44, Jan. 2016, doi: 10.1007/s11517-015-1430-4.

[6] "Spinal Cord Injury (SCI) 2016 Facts and Figures at a Glance," *J. Spinal Cord Med.*, vol. 39, no. 4, pp. 493–494, Jul. 2016, doi: 10.1080/10790268.2016.1210925.

[7] W. Ding *et al.*, "Spinal Cord Injury: The Global Incidence, Prevalence, and Disability From the Global Burden of Disease Study 2019," *Spine*, vol. 47, no. 21, pp. 1532–1540, Nov. 2022, doi: 10.1097/BRS.0000000000004417.

[8] Z. Khazaeipour, S.-M. Taheri-Otaghsara, and M. Naghdi, "Depression Following Spinal Cord Injury: Its Relationship to Demographic and Socioeconomic Indicators," *Top. Spinal Cord Inj. Rehabil.*, vol. 21, no. 2, pp. 149–155, 2015, doi: 10.1310/sci2102-149.

[9] R. Masri and A. Keller, "CHRONIC PAIN FOLLOWING SPINAL CORD INJURY," *Adv. Exp. Med. Biol.*, vol. 760, pp. 74–88, 2012.

[10] S. Harkema, C. Angeli, and Y. Gerasimenko, "Historical development and contemporary use of neuromodulation in human spinal cord injury," *Curr. Opin. Neurol.*, vol. 35, no. 4, p. 536, Aug. 2022, doi: 10.1097/WCO.0000000000001080.

[11] C. Im and J.-M. Seo, "A review of electrodes for the electrical brain signal recording," *Biomed. Eng. Lett.*, vol. 6, no. 3, pp. 104–112, Aug. 2016, doi: 10.1007/s13534-016-0235-1.

[12] N. X., K. T.B., L. N., M. S., S. T., and D. P., "A critical review of interfaces with the peripheral nervous system for the control of neuroprostheses and hybrid bionic systems," *J. Peripher. Nerv. Syst.*, vol. 10, no. 3, pp. 229–258, 2005.

[13] M. Zhang, Z. Tang, X. Liu, and J. Van der Spiegel, "Electronic neural interfaces," *Nat. Electron.*, vol. 3, no. 4, Art. no. 4, Apr. 2020, doi: 10.1038/s41928-020-0390-3.

[14] M. A. Moffitt and C. C. McIntyre, "Model-based analysis of cortical recording with silicon microelectrodes," *Clin. Neurophysiol.*, vol. 116, no. 9, pp. 2240–2250, Sep. 2005, doi: 10.1016/j.clinph.2005.05.018.

[15] C. E. Larson and E. Meng, "A review for the peripheral nerve interface designer," *J. Neurosci. Methods*, vol. 332, Feb. 2020, doi: 10.1016/j.jneumeth.2019.108523.

[16] L. Yanovitch, D. Raz-Prag, and Y. Hanein, “A new high-resolution three-dimensional retinal implant: System design and preliminary human results,” *bioRxiv*, p. 2022.09.14.507901, Sep. 2022, doi: 10.1101/2022.09.14.507901.
[17] M. E. M. Stamp, W. Tong, K. Ganesan, S. Prawer, M. R. Ibbotson, and D. J. Garrett, “3D Diamond Electrode Array for High-Acuity Stimulation in Neural Tissue,” *ACS Appl. Bio Mater.*, vol. 3, no. 3, pp. 1544–1552, Mar. 2020, doi: 10.1021/acsabm.9b01165.
[18] T. K. Lohmann *et al.*, “The very large electrode array for retinal stimulation (VLARS)—A concept study,” *J. Neural Eng.*, vol. 16, no. 6, p. 066031, Nov. 2019, doi: 10.1088/1741-2552/AB4113.
[19] F. E. Abd El-Samie, T. N. Alotaiby, M. I. Khalid, S. A. Alshebeili, and S. A. Aldosari, “A Review of EEG and MEG Epileptic Spike Detection Algorithms,” *IEEE Access*, 2018, doi: 10.1109/ACCESS.2018.2875487.
[20] D. J. DiLorenzo, “Neurovista: Concept to first-in-man: The war story behind launching a venture to treat epilepsy.,” *Surg. Neurol. Int.*, vol. 10, p. 175, 2019, doi: 10.25259/SNI_422_2019.
[21] G. P. Thomas and B. C. Jobst, “Critical review of the responsive neurostimulator system for epilepsy,” *Med. Devices Evid. Res.*, vol. 8, pp. 405–411, Oct. 2015, doi: 10.2147/MDER.S62853.
[22] I. Moreno-Duarte, L. R. Morse, M. Alam, M. Bikson, R. Zafonte, and F. Fregni, “Targeted therapies using electrical and magnetic neural stimulation for the treatment of chronic pain in spinal cord injury,” *NeuroImage*, vol. 85, pp. 1003–1013, Jan. 2014, doi: 10.1016/j.neuroimage.2013.05.097.
[23] S. G. J. Boccard, E. A. C. Pereira, and T. Z. Aziz, “Deep brain stimulation for chronic pain,” *J. Clin. Neurosci.*, vol. 22, no. 10, pp. 1537–1543, Oct. 2015, doi: 10.1016/j.jocn.2015.04.005.
[24] H. Knotkova *et al.*, “Neuromodulation for chronic pain,” *The Lancet*, vol. 397, no. 10289, pp. 2111–2124, May 2021, doi: 10.1016/S0140-6736(21)00794-7.
[25] O. M. Bradfield, “Hearing Parents’ Voices: Parental Refusal of Cochlear Implants and the Zone of Parental Discretion,” *J. Bioethical Inq.*, vol. 19, no. 1, pp. 143–150, Mar. 2022, doi: 10.1007/s11673-021-10154-8.
[26] F. D. U. Bucheli, “Bioethical thinking of cochlear implant in the treatment of deafness,” *Wearable Technol.*, vol. 1, no. 2, Art. no. 2, Oct. 2023, doi: 10.54517/wt.v1i2.1670.
[27] H. Lane and B. Bahan, “Article Commentary: Ethics of cochlear implantation in young children: A review and reply from a Deaf-World Perspective,” vol. 119, no. 4, 1998, doi: 10.1016/S0194-5998(98)70070-1.
[28] C. D. Lee, E. M. Hudak, J. J. Whalen, A. Petrossians, and J. D. Weiland, “Low-Impedance, High Surface Area Pt-Ir Electrodeposited on Cochlear Implant Electrodes,” *J. Electrochem. Soc.*, vol. 165, no. 12, pp. G3015–G3017, 2018, doi: 10.1149/2.0031812jes.
[29] S. P. Godar and R. Y. Litovsky, “Experience with bilateral cochlear implants improves sound localization acuity in children,” in *Otology and Neurotology*, Oct. 2010, pp. 1287–1292. doi: 10.1097/MAO.0b013e3181e75784.
[30] J. L. Collinger *et al.*, “Collaborative Approach in the Development of High-Performance Brain–Computer Interfaces for a Neuroprosthetic Arm: Translation from Animal Models to Human Control,” *Clin. Transl. Sci.*, vol. 7, no. 1, pp. 52–59, 2014, doi: 10.1111/cts.12086.
[31] C. E. Bouton, “Chapter 22 - Merging brain-computer interface and functional electrical stimulation technologies for movement restoration,” in *Handbook of Clinical Neurology*, vol.

168, N. F. Ramsey and J. del R. Millán, Eds., in Brain-Computer Interfaces, vol. 168. , Elsevier, 2020, pp. 303–309. doi: 10.1016/B978-0-444-63934-9.00022-6.
[32] "Stephen Hawking: Biography, Scientist, Relativity, ALS," Biography. Accessed: Jan. 24, 2024. [Online]. Available: https://www.biography.com/scientists/stephen-hawking
[33] B. J. Carr *et al.*, "Stephen William Hawking CH CBE. 8 January 1942—14 March 2018," *Biogr. Mem. Fellows R. Soc.*, vol. 66, pp. 267–308, Apr. 2019, doi: 10.1098/rsbm.2019.0001.
[34] "Stephen Hawking's Voice, Made By A Man Who Lost His Own," BeyondWords. Accessed: Jan. 24, 2024. [Online]. Available: https://beyondwords.io/blog/stephen-hawkings-voice/
[35] D. Klatt, "The klattalk text-to-speech conversion system," in *ICASSP '82. IEEE International Conference on Acoustics, Speech, and Signal Processing*, May 1982, pp. 1589–1592. doi: 10.1109/ICASSP.1982.1171431.
[36] F. R. Willett *et al.*, "A high-performance speech neuroprosthesis," *Nature*, vol. 620, no. 7976, Art. no. 7976, Aug. 2023, doi: 10.1038/s41586-023-06377-x.
[37] S. B. Borgheai *et al.*, "Enhancing Communication for People in Late-Stage ALS Using an fNIRS-Based BCI System," *IEEE Trans. Neural Syst. Rehabil. Eng.*, vol. 28, no. 5, pp. 1198–1207, May 2020, doi: 10.1109/TNSRE.2020.2980772.
[38] A. B. Theibert, "Organization & Cells of the Nervous System," in *Essentials of Modern Neuroscience*, F. R. Amthor, A. B. Theibert, D. G. Standaert, and E. D. Roberson, Eds., New York, NY: McGraw Hill, 2020. Accessed: Jan. 22, 2024. [Online]. Available: neurology.mhmedical.com/content.aspx?aid=1174242128
[39] S. F. Cogan, "Neural Stimulation and Recording Electrodes," *Annu Rev Biomed Eng*, vol. 10, no. 1, pp. 275–309, 2008, doi: 10.1146/annurev.bioeng.10.061807.160518.
[40] R. Plonsey and R. C. Barr, *Bioelectricity: a quantitative approach*, 3rd ed. New York, NY: Springer, 2007.
[41] R. A. Normann and E. Fernandez, "Clinical applications of penetrating neural interfaces and Utah Electrode Array technologies," *J. Neural Eng.*, vol. 13, no. 6, p. 061003, Oct. 2016, doi: 10.1088/1741-2560/13/6/061003.
[42] B. Genç *et al.*, "Apical dendrite degeneration, a novel cellular pathology for Betz cells in ALS," *Sci. Rep.*, vol. 7, p. 41765, Feb. 2017, doi: 10.1038/srep41765.
[43] A. Saliani, B. Perraud, T. Duval, N. Stikov, S. Rossignol, and J. Cohen-Adad, "Axon and Myelin Morphology in Animal and Human Spinal Cord," *Front. Neuroanat.*, vol. 11, 2017, Accessed: Jan. 17, 2024. [Online]. Available: https://www.frontiersin.org/articles/10.3389/fnana.2017.00129
[44] N. A. Pelot, C. E. Behrend, and W. M. Grill, "Modeling the response of small myelinated axons in a compound nerve to kilohertz frequency signals," *J. Neural Eng.*, vol. 14, no. 4, 2017, doi: 10.1088/1741-2552/aa6a5f.
[45] M. Mierzejewski, H. Steins, P. Kshirsagar, and P. D. Jones, "The noise and impedance of microelectrodes," *J. Neural Eng.*, vol. 17, no. 5, p. 052001, Oct. 2020, doi: 10.1088/1741-2552/abb3b4.
[46] W. M. Tsang and M. Je, "Flexible electrode for implantable neural devices," in *Neural Computation, Neural Devices, and Neural Prosthesis*, Springer New York, 2014, pp. 121–156. doi: 10.1007/978-1-4614-8151-5_6.
[47] S. M. Wellman *et al.*, "A Materials Roadmap to Functional Neural Interface Design," *Adv. Funct. Mater.*, vol. 28, no. 12, Mar. 2018, doi: 10.1002/adfm.201701269.

[48] C. Boehler, S. Carli, L. Fadiga, T. Stieglitz, and M. Asplund, “Tutorial: guidelines for standardized performance tests for electrodes intended for neural interfaces and bioelectronics,” *Nat. Protoc. 2020 1511*, vol. 15, no. 11, pp. 3557–3578, Oct. 2020, doi: 10.1038/s41596-020-0389-2.
[49] J. P. Neto *et al.*, “Does impedance matter when recording spikes with polytrodes?,” *Front Neurosci*, vol. 12, pp. 1–9, 2018, doi: 10.3389/fnins.2018.00715.
[50] R. Ding, N. C. Miller, K. M. Woeppel, X. T. Cui, and T. D. B. Jacobs, “Surface Area and Local Curvature: Why Roughness Improves the Bioactivity of Neural Implants,” *Langmuir*, vol. 38, no. 24, pp. 7512–7521, Jun. 2022, doi: 10.1021/acs.langmuir.2c00473.
[51] C. Bodart *et al.*, “Electropolymerized Poly(3,4-ethylenedioxythiophene) (PEDOT) Coatings for Implantable Deep-Brain-Stimulating Microelectrodes,” *ACS Appl. Mater. Interfaces*, vol. 11, no. 19, pp. 17226–17233, May 2019, doi: 10.1021/acsami.9b03088.
[52] G. Dijk, H. J. Ruigrok, and R. P. O’Connor, “Influence of PEDOT:PSS Coating Thickness on the Performance of Stimulation Electrodes,” *Adv. Mater. Interfaces*, vol. 7, no. 16, p. 2000675, Aug. 2020, doi: 10.1002/ADMI.202000675.
[53] R. A. Green, N. H. Lovell, G. G. Wallace, and L. A. Poole-warren, “Biomaterials Conducting polymers for neural interfaces : Challenges in developing an effective long-term implant q,” vol. 29, pp. 3393–3399, 2008, doi: 10.1016/j.biomaterials.2008.04.047.
[54] E. della Valle *et al.*, “Electrodeposited Platinum Iridium Enables Microstimulation With Carbon Fiber Electrodes,” *Front. Nanotechnol.*, vol. 3, Dec. 2021, doi: 10.3389/fnano.2021.782883.
[55] T. Chung, J. Q. Wang, J. Wang, B. Cao, Y. Li, and S. W. Pang, “Electrode modifications to lower electrode impedance and improve neural signal recording sensitivity,” *J Neural Eng*, vol. 12, no. 5, 2015, doi: 10.1088/1741-2560/12/5/056018.
[56] S. Paik, Y. Park, and D. D. Cho, “Roughened polysilicon for low impedance microelectrodes in neural probes,” vol. 13, pp. 373–379, 2003.
[57] K. Scholten and E. Meng, “Materials for microfabricated implantable devices: a review,” *Lab. Chip*, vol. 15, no. 22, pp. 4256–4272, 2015, doi: 10.1039/C5LC00809C.
[58] L. Karumbaiah *et al.*, “Relationship between intracortical electrode design and chronic recording function,” *Biomaterials*, vol. 34, no. 33, pp. 8061–8074, Nov. 2013, doi: 10.1016/j.biomaterials.2013.07.016.
[59] E. Axpe, G. Orive, K. Franze, and E. A. Appel, “Towards brain-tissue-like biomaterials,” *Nat. Commun.*, vol. 11, no. 1, Art. no. 1, Jul. 2020, doi: 10.1038/s41467-020-17245-x.
[60] R. Biran, D. C. Martin, and P. A. Tresco, “The brain tissue response to implanted silicon microelectrode arrays is increased when the device is tethered to the skull,” *J Biomed Mater Res - Part A*, vol. 82, no. 1, pp. 169–178, 2007, doi: 10.1002/jbm.a.31138.
[61] E. Patrick, V. Sankar, W. Rowe, S.-F. Yen, J. C. Sanchez, and T. Nishida, “Flexible polymer substrate and tungsten microelectrode array for an implantable neural recording system,” in *2008 30th Annual International Conference of the IEEE Engineering in Medicine and Biology Society*, Aug. 2008, pp. 3158–3161. doi: 10.1109/IEMBS.2008.4649874.
[62] E. M. Maynard, C. T. Nordhausen, and R. A. Normann, “The Utah Intracortical Electrode Array : a recording structure for potential brain-computer interfaces,” vol. 102, pp. 228–239, 1997.

[63] T. Szikszay, T. Hall, and H. von Piekartz, “In vivo effects of limb movement on nerve stretch, strain, and tension: A systematic review,” *J. Back Musculoskelet. Rehabil.*, vol. 30, no. 6, pp. 1171–1186, Nov. 2017, doi: 10.3233/BMR-169720.
[64] I. Tasaki, *Physiology and electrochemistry of nerve fibers*. in Biophysics and bioengineering series, no. v. 3. New York: Academic Press, 1982.
[65] A. A. Jiman *et al.*, “Multi-channel intraneural vagus nerve recordings with a novel high-density carbon fiber microelectrode array,” Nature Research, Dec. 2020. doi: 10.1038/s41598-020-72512-7.
[66] J. T. Marmerstein, G. A. McCallum, and D. M. Durand, “Decoding Vagus-Nerve Activity with Carbon Nanotube Sensors in Freely Moving Rodents,” *Biosensors*, vol. 12, no. 2, Art. no. 2, Feb. 2022, doi: 10.3390/bios12020114.
[67] S. Mohanaraj *et al.*, “Gold nanoparticle modified carbon fiber microelectrodes for enhanced neurochemical detection,” *J. Vis. Exp.*, vol. 2019, no. 147, 2019, doi: 10.3791/59552.
[68] A. Petrossians *et al.*, “Electrodeposition and Characterization of Thin-Film Platinum-Iridium Alloys for Biological Interfaces,” *J Electrochem Soc*, vol. 158, no. 5, pp. D269–D276, 2011, doi: 10.1149/1.3578048.
[69] K. D. Wise, D. J. Anderson, J. F. Hetke, D. R. Kipke, and K. Najafi, “Wireless implantable microsystems: High-density electronic interfaces to the nervous system,” in *Proceedings of the IEEE*, Jan. 2004, pp. 76–97. doi: 10.1109/JPROC.2003.820544.
[70] K. L. Drake and K. D. Wise, “Performance of Planar Multisite Microprobes in Recording Extracellular Single-Unit Intracortical Activity,” vol. 35, no. 9, 1988.
[71] Y. Yao, M. N. Gulari, B. Casey, J. A. Wiler, and K. D. Wise, “Silicon microelectrodes with flexible integrated cables for neural implant applications,” *Proc 3rd Int IEEE EMBS Conf Neural Eng*, pp. 398–401, 2007, doi: 10.1109/CNE.2007.369693.
[72] J. J. Jun *et al.*, “Fully integrated silicon probes for high-density recording of neural activity,” *Nature*, vol. 551, no. 7679, pp. 232–236, Nov. 2017, doi: 10.1038/nature24636.
[73] R. J. Vetter *et al.*, “Chronic neural recording using silicon-substrate microelectrode arrays implanted in cerebral cortex,” *IEEE Trans. Biomed. Eng.*, vol. 51, no. 6, pp. 896–904, Jun. 2004, doi: 10.1109/TBME.2004.826680.
[74] H. A. C. Wark *et al.*, “A new high-density (25 electrodes/mm2) penetrating microelectrode array for recording and stimulating sub-millimeter neuroanatomical structures,” *J Neural Eng*, vol. 10, no. 4, 2013, doi: 10.1088/1741-2560/10/4/045003.
[75] D. R. Kipke, R. J. Vetter, J. C. Williams, and J. F. Hetke, “Silicon-Substrate Intracortical Microelectrode Arrays for Long-Term Recording of Neuronal Spike Activity in Cerebral Cortex,” *IEEE Trans. Neural Syst. Rehabil. Eng.*, vol. 11, no. 2, pp. 151–155, Jun. 2003, doi: 10.1109/TNSRE.2003.814443.
[76] A. Bragin, J. Hetke, C. L. Wilson, D. J. Anderson, J. Engel, and G. Buzsáki, “Multiple site silicon-based probes for chronic recordings in freely moving rats: Implantation, recording and histological verification,” *J. Neurosci. Methods*, vol. 98, no. 1, pp. 77–82, 2000, doi: 10.1016/S0165-0270(00)00193-X.
[77] P. R. Patel *et al.*, “Utah array characterization and histological analysis of a multi-year implant in non-human primate motor and sensory cortices,” *J. Neural Eng.*, Dec. 2022, doi: 10.1088/1741-2552/ACAB86.

[78] M. P. Ward, P. Rajdev, C. Ellison, and P. P. Irazoqui, “Toward a comparison of microelectrodes for acute and chronic recordings,” *Brain Res*, vol. 1282, pp. 183–200, Jul. 2009, doi: 10.1016/j.brainres.2009.05.052.
[79] M. B. Christensen, S. M. Pearce, N. M. Ledbetter, D. J. Warren, G. A. Clark, and P. A. Tresco, “The foreign body response to the Utah Slant Electrode Array in the cat sciatic nerve,” *Acta Biomater.*, vol. 10, no. 11, pp. 4650–4660, 2014, doi: 10.1016/j.actbio.2014.07.010.
[80] R. Biran, D. C. Martin, and P. A. Tresco, “Neuronal cell loss accompanies the brain tissue response to chronically implanted silicon microelectrode arrays,” vol. 195, no. 1, pp. 115–126, Sep. 2005, doi: 10.1016/j.expneurol.2005.04.020.
[81] J. C. Barrese *et al.*, “Failure mode analysis of silicon-based intracortical microelectrode arrays in non-human primates,” *J Neural Eng*, vol. 066014, no. 6, 2013, doi: 10.1088/1741-2560/10/6/066014.
[82] B. Thielen and E. Meng, “A comparison of insertion methods for surgical placement of penetrating neural interfaces,” *J. Neural Eng.*, vol. 18, no. 4, p. 041003, Apr. 2021, doi: 10.1088/1741-2552/abf6f2.
[83] R. Fiáth *et al.*, “Slow insertion of silicon probes improves the quality of acute neuronal recordings,” *Sci. Rep.*, vol. 9, no. 1, Art. no. 1, Jan. 2019, doi: 10.1038/s41598-018-36816-z.
[84] A. Lecomte, E. Descamps, and C. Bergaud, “A review on mechanical considerations for chronically-implanted neural probes,” *J. Neural Eng.*, vol. 15, no. 3, 2018, doi: 10.1088/1741-2552/aa8b4f.
[85] Z. Zhang, J. Nong, and Y. Zhong, “Antibacterial, anti-inflammatory and neuroprotective layer-by-layer coatings for neural implants,” *J. Neural Eng.*, vol. 12, no. 4, p. 046015, Jun. 2015, doi: 10.1088/1741-2560/12/4/046015.
[86] A. Golabchi, B. Wu, B. Cao, C. J. Bettinger, and X. T. Cui, “Zwitterionic polymer/polydopamine coating reduce acute inflammatory tissue responses to neural implants,” *Biomaterials*, vol. 225, p. 119519, Dec. 2019, doi: 10.1016/j.biomaterials.2019.119519.
[87] M. B. Christensen and P. A. Tresco, “The foreign body response and morphometric changes associated with mesh-style peripheral nerve cuffs,” *Acta Biomater.*, vol. 67, pp. 79–86, Feb. 2018, doi: 10.1016/j.actbio.2017.11.059.
[88] T. D. Y. Kozai *et al.*, “Mechanical failure modes of chronically implanted planar silicon-based neural probes for laminar recording,” *Biomaterials*, vol. 37, pp. 25–39, Jan. 2015, doi: 10.1016/j.biomaterials.2014.10.040.
[89] R. Caldwell, M. G. Street, R. Sharma, P. Takmakov, B. Baker, and L. Rieth, “Characterization of Parylene-C degradation mechanisms : In vitro reactive accelerated aging model compared to multiyear in vivo implantation,” *Biomaterials*, vol. 232, no. January 2019, p. 119731, 2020, doi: 10.1016/j.biomaterials.2019.119731.
[90] K. Scholten, H. Xu, D. Song, and E. Meng, “A Shared Resource for Building Polymer-Based Microelectrode Arrays as Neural Interfaces,” in *2023 11th International IEEE/EMBS Conference on Neural Engineering (NER)*, Apr. 2023, pp. 1–4. doi: 10.1109/NER52421.2023.10123883.
[91] A. M. Cobo *et al.*, “Parylene-Based Cuff Electrode With Integrated Microfluidics for Peripheral Nerve Recording, Stimulation, and Drug Delivery,” 2018, doi: 10.1109/JMEMS.2018.2881908.

[92] S. A. Hara *et al.*, “Long-term stability of intracortical recordings using perforated and arrayed Parylene sheath electrodes,” *J. Neural Eng.*, vol. 13, no. 6, pp. 1–17, Nov. 2016, doi: 10.1088/1741-2560/13/6/066020.
[93] H. Yu, W. Xiong, H. Zhang, W. Wang, and Z. Li, “A Parylene Self-Locking Cuff Electrode for Peripheral Nerve Stimulation and Recording,” *J. MICROELECTROMECHANICAL Syst.*, vol. 23, no. 5, 2014, doi: 10.1109/JMEMS.2014.2333733.
[94] T. Boretius *et al.*, “A transverse intrafascicular multichannel electrode (TIME) to interface with the peripheral nerve,” *Biosens Bioelectron*, vol. 26, no. 1, pp. 62–69, 2010, doi: 10.1016/j.bios.2010.05.010.
[95] J. Badia, T. Boretius, A. Pascual-Font, E. Udina, T. Stieglitz, and X. Navarro, “Biocompatibility of chronically implanted transverse intrafascicular multichannel electrode (TIME) in the rat sciatic nerve,” *IEEE Trans. Biomed. Eng.*, vol. 58, no. 8, pp. 2324–2332, 2011, doi: 10.1109/TBME.2011.2153850.
[96] J. Badia, T. Boretius, D. Andreu, C. Azevedo-Coste, T. Stieglitz, and X. Navarro, “Comparative analysis of transverse intrafascicular multichannel, longitudinal intrafascicular and multipolar cuff electrodes for the selective stimulation of nerve fascicles,” *J. Neural Eng.*, vol. 8, no. 3, 2011, doi: 10.1088/1741-2560/8/3/036023.
[97] C. Hassler, T. Boretius, and T. Stieglitz, “Polymers for neural implants,” *J. Polym. Sci. Part B Polym. Phys.*, vol. 49, no. 1, pp. 18–33, 2011, doi: 10.1002/polb.22169.
[98] L. Luan *et al.*, “Ultraflexible nanoelectronic probes form reliable, glial scar-free neural integration,” no. February, pp. 1–10, 2017, doi: 10.1126/sciadv.1601966.
[99] X. Wei *et al.*, “Nanofabricated Ultraflexible Electrode Arrays for High-Density Intracortical Recording,” *Adv. Sci.*, vol. 5, no. 6, Jun. 2018, doi: 10.1002/ADVS.201700625.
[100] A. J. Shoffstall and J. R. Capadona, “Bioinspired materials and systems for neural interfacing,” *Curr. Opin. Biomed. Eng.*, vol. 6, pp. 110–119, Jun. 2018, doi: 10.1016/J.COBME.2018.05.002.
[101] X. Yang *et al.*, “Bioinspired neuron-like electronics,” vol. 18, no. 5, pp. 510–517, May 2019, doi: 10.1038/s41563-019-0292-9.
[102] S. P. Marshall, W.-C. Lin, P. R. Patel, A. J. Shih, and C. A. Chestek, “Effects of geometry and material on the insertion oi very small neural electrode,” in *2016 38th Annual International Conference of the IEEE Engineering in Medicine and Biology Society (EMBC)*, Orlando, FL, USA: IEEE, Aug. 2016, pp. 2784–2788. doi: 10.1109/EMBC.2016.7591308.
[103] P. R. Patel *et al.*, “Chronic in vivo stability assessment of carbon fiber microelectrode arrays,” *J. Neural Eng.*, vol. 13, no. 6, p. 66002, 2016, doi: 10.1088/1741-2560/13/6/066002.
[104] P. R. Patel *et al.*, “High density carbon fiber arrays for chronic electrophysiology, fast scan cyclic voltammetry, and correlative anatomy,” *J. Neural Eng.*, vol. 17, no. 5, p. 056029, Oct. 2020, doi: 10.1088/1741-2552/abb1f6.
[105] G. A. McCallum *et al.*, “Chronic interfacing with the autonomic nervous system using carbon nanotube (CNT) yarn electrodes,” *Sci. Rep.*, vol. 7, no. 1, pp. 1–14, Dec. 2017, doi: 10.1038/s41598-017-10639-w.
[106] P. R. Patel *et al.*, “Insertion of linear 8.4 μ m diameter 16 channel carbon fiber electrode arrays for single unit recordings,” *J Neural Eng*, vol. 12, no. 4, p. 46009, 2015, doi: 10.1088/1741-2560/12/4/046009.
[107] Y. Huan *et al.*, “Carbon fiber electrodes for intracellular recording and stimulation,” *J. Neural Eng.*, vol. 18, no. 6, Dec. 2021, doi: 10.1088/1741-2552/ac3dd7.

[108] G. Guitchounts and D. Cox, "64-Channel Carbon Fiber Electrode Arrays for Chronic Electrophysiology," *Sci. Rep.*, vol. 10, no. 1, 2020, doi: 10.1038/s41598-020-60873-y.
[109] E. J. Welle *et al.*, "Sharpened and mechanically robust carbon fiber electrode arrays for neural interfacing," *IEEE Trans Neural Syst Rehabil Eng*, vol. Accepted., pp. 1–18, 2021.
[110] A. M. Lozano *et al.*, "Deep brain stimulation: current challenges and future directions," *Nat. Rev. Neurol. 2019 153*, vol. 15, no. 3, pp. 148–160, Jan. 2019, doi: 10.1038/s41582-018-0128-2.
[111] J. R. Hetling and M. S. Baig-Silva, "Neural prostheses for vision: Designing a functional interface with retinal neurons," *Neurol. Res.*, vol. 26, no. 1, pp. 21–34, Jan. 2004, doi: 10.1179/016164104773026499.
[112] M. A. Lebedev and M. A. L. Nicolelis, "Brain-Machine Interfaces: From Basic Science to Neuroprostheses and Neurorehabilitation," *Physiol Rev*, vol. 97, no. 2, pp. 767–837, 2017, doi: 10.1152/physrev.00027.2016.
[113] A. Sharma *et al.*, "Long term in vitro functional stability and recording longevity of fully integrated wireless neural interfaces based on the Utah Slant Electrode Array," vol. 045004, 2011, doi: 10.1088/1741-2560/8/4/045004.
[114] C. A. Chestek *et al.*, "Long-term stability of neural prosthetic control signals from silicon cortical arrays in rhesus macaque motor cortex," *J. Neural Eng.*, vol. 045005, no. 4, Aug. 2011, doi: 10.1088/1741-2560/8/4/045005.
[115] X. Xie *et al.*, "Long-term reliability of Al 2 O 3 and Parylene C bilayer encapsulated Utah electrode array based neural interfaces for chronic implantation," vol. 026016, doi: 10.1088/1741-2560/11/2/026016.
[116] A. V. Ulyanova *et al.*, "Multichannel silicon probes for awake hippocampal recordings in large animals," *Front. Neurosci.*, vol. 13, no. APR, p. 397, Apr. 2019, doi: 10.3389/FNINS.2019.00397/BIBTEX.
[117] S. J. Wilks, S. M. Richardson-burns, J. L. Hendricks, D. C. Martin, and K. J. Otto, "Poly (3 , 4-ethylenedioxythiophene) as a micro-neural interface material for electrostimulation," vol. 2, no. June, pp. 1–8, 2009, doi: 10.3389/neuro.16.007.
[118] J. P. Seymour, D. R. K. Ã, and D. R. Kipke, "Neural probe design for reduced tissue encapsulation in CNS," *Biomaterials*, vol. 28, no. 25, pp. 3594–3607, Sep. 2007, doi: 10.1016/j.biomaterials.2007.03.024.
[119] J. L. Skousen, S. M. E. Merriam, O. Srivannavit, G. Perlin, K. D. Wise, and P. A. Tresco, "Reducing surface area while maintaining implant penetrating profile lowers the brain foreign body response to chronically implanted planar silicon microelectrode arrays," in *Progress in Brain Research*, vol. 194, Elsevier B.V., 2011, pp. 167–180. doi: 10.1016/B978-0-444-53815-4.00009-1.
[120] Z. Zhao, X. Li, F. He, X. Wei, S. Lin, and C. Xie, "Parallel , minimally-invasive implantation of ultra-flexible neural electrode arrays," *J Neural Eng*, 2019, doi: 10.1088/1741-2552/ab05b6.
[121] F. Deku, Y. Cohen, A. Joshi-Imre, A. Kanneganti, T. Gardner, and S. Cogan, "Amorphous silicon carbide ultramicroelectrode arrays for neural stimulation and recording," *J Neural Eng*, pp. 0–20, 2018, doi: https://doi.org/10.1088/1361-6528/aa8b39.
[122] A. Obaid, Y.-W. Wu, M. Hanna, W. Nix, J. Ding, and N. Melosh, "Ultra-sensitive measurement of brain penetration with microscale probes for brain machine interface considerations", doi: 10.1101/454520.

[123] A. Weltman, J. Yoo, and E. Meng, “Flexible, penetrating brain probes enabled by advances in polymer microfabrication,” *Micromachines*, vol. 7, no. 10, 2016, doi: 10.3390/mi7100180.
[124] A. Obaid *et al.*, “Massively parallel microwire arrays integrated with CMOS chips for neural recording,” *Sci. Adv.*, vol. 6, no. 12, 2020, doi: 10.1126/SCIADV.AAY2789/SUPPL_FILE/AAY2789_SM.PDF.
[125] S. Vasudevan, K. Patel, and C. Welle, “Rodent model for assessing the long term safety and performance of peripheral nerve recording electrodes,” *J Neural Eng*, vol. 14, no. 1, 2017, doi: 10.1088/1741-2552/14/1/016008.
[126] H. Yang, M. T. Rahman, D. Du, R. Panat, and Y. Lin, “3-D printed adjustable microelectrode arrays for electrochemical sensing and biosensing,” *Sens. Actuators B Chem*, vol. 230, pp. 600–606, 2016, doi: 10.1016/j.snb.2016.02.113.
[127] M. Sadeq Saleh *et al.*, “CMU Array: A 3D Nano-Printed, Customizable Ultra-High-Density Microelectrode Array Platform”, doi: 10.1101/742346.
[128] M. Kollo *et al.*, “CHIME: CMOS-Hosted in vivo Microelectrodes for Massively Scalable Neuronal Recordings,” *Front. Neurosci.*, vol. 14, p. 834, Aug. 2020, doi: 10.3389/FNINS.2020.00834/BIBTEX.
[129] A. Prasad *et al.*, “Comprehensive characterization and failure modes of tungsten microwire,” vol. 056015, 2012, doi: 10.1088/1741-2560/9/5/056015.
[130] T. L. Massey, S. R. Santacruz, J. F. Hou, K. S. J. Pister, J. M. Carmena, and M. M. Maharbiz, “A high-density carbon fiber neural recording array technology,” *J Neural Eng*, vol. 16, no. 016024, 2019.
[131] W. F. Gillis *et al.*, “Carbon fiber on polyimide ultra-microelectrodes,” *J. Neural Eng.*, vol. 15, no. 1, Feb. 2018, doi: 10.1088/1741-2552/aa8c88.
[132] Y. Lee, C. Kong, J. W. Chang, and S. B. Jun, “Carbon-Fiber Based Microelectrode Array Embedded with a Biodegradable Silk Support for In Vivo Neural Recording,” vol. 34, no. 4, pp. 1–15, 2019.
[133] R. S. Zoll, C. B. Schindler, T. L. Massey, D. S. Drew, M. M. Maharbiz, and K. S. J. Pister, “MEMS-Actuated Carbon Fiber Microelectrode for Neural Recording,” pp. 1–6, 2018.
[134] F. Zhu *et al.*, “Flexural characterization of carbon nanotube (CNT) yarn neural Electrodes,” *Mater. Res. Express*, vol. 6, no. 4, 2019, doi: 10.1088/2053-1591/aafbf7.
[135] A. C. Schmidt *et al.*, “Carbon Nanotube Yarn Electrodes for Enhanced Detection of Neurotransmitter Dynamics in Live Brain Tissue,” no. 9, pp. 7864–7873, 2013.
[136] J. M. Richie *et al.*, “Benchtop Carbon Fiber Microelectrode Array Fabrication Toolkit,” *bioRxiv*, p. 2021.03.22.436422, Mar. 2021, doi: 10.1101/2021.03.22.436422.
[137] K. T. Kawagoe, J. A. Jankowski, and R. Mark Wightman, “Etched Carbon-Fiber Electrodes as Amperometric Detectors of Catecholamine Secretion from Isolated Biological Cells,” *Anal. Chem.*, vol. 63, no. 15, pp. 1589–1594, 1991, doi: 10.1021/ac00015a017.
[138] H. Khani and D. O. Wipf, “Fabrication of Tip-Protected Polymer-Coated Carbon-Fiber Ultramicroelectrodes and pH Ultramicroelectrodes,” *J. Electrochem. Soc.*, vol. 166, no. 8, pp. B673–B679, 2019, doi: 10.1149/2.0941908jes.
[139] E. E. D. M. El-Giar and D. O. Wipf, “Preparation of tip-protected poly(oxyphenylene) coated carbon-fiber ultramicroelectrodes,” *Electroanalysis*, vol. 18[1] E. E, no. 23, pp. 2281–2289, 2006, doi: 10.1002/elan.200603637.

[140] E. J. Welle *et al.*, "Ultra-small carbon fiber electrode recording site optimization and improved in vivo chronic recording yield," *J. Neural Eng.*, vol. 17, no. 2, 2020, doi: 10.1088/1741-2552/ab8343.
[141] J. Lim *et al.*, "A Light-Tolerant Wireless Neural Recording IC for Motor Prediction with Near-Infrared-Based Power and Data Telemetry," *IEEE J. Solid-State Circuits*, vol. 57, no. 4, pp. 1061–1074, Apr. 2022, doi: 10.1109/JSSC.2022.3141688.
[142] T. S. Skoglund, R. Pascher, and C. H. Berthold, "The existence of a layer IV in the rat motor cortex.," *Cereb. Cortex*, vol. 7, no. 2, pp. 178–180, Mar. 1997, doi: 10.1093/cercor/7.2.178.
[143] H. Pockberger, "Electrophysiological and morphological properties of rat motor cortex neurons in vivo," *Brain Res.*, vol. 539, no. 2, pp. 181–190, Jan. 1991, doi: 10.1016/0006-8993(91)91619-C.
[144] Y.-C. Chang, D. H. Ghaffari, R. H. Chow, and J. D. Weiland, "Stimulation strategies for selective activation of retinal ganglion cell soma and threshold reduction," *J. Neural Eng.*, vol. 16, no. 2, p. 026017, Apr. 2019, doi: 10.1088/1741-2552/aaf92b.
[145] D. H. Ghaffari *et al.*, "Intraretinal stimulation with high density carbon fiber microelectrodes," *2023 11th Int. IEEEEMBS Conf. Neural Eng. NER*, pp. 1–4, Apr. 2023, doi: 10.1109/NER52421.2023.10123735.
[146] T. Vanburen, C. Cywiak, P. Telgkamp, C. L. Mallett, and G. Pelled, "Establishing an Octopus Ecosystem for Biomedical and Bioengineering Research," *J. Vis. Exp. JoVE*, vol. 2021, no. 175, Sep. 2021, doi: 10.3791/62705.
[147] K. A. Ludwig, R. M. Miriani, N. B. Langhals, M. D. Joseph, D. J. Anderson, and D. R. Kipke, "Using a common average reference to improve cortical neuron recordings from microelectrode arrays," *J Neurophysiol*, vol. 101, no. 3, pp. 1679–1689, 2009, doi: 10.1152/jn.90989.2008.
[148] E. Della Valle, E. J. Welle, C. A. Chestek, and J. D. Weiland, "Compositional and morphological properties of platinum-iridium electrodeposited on carbon fiber microelectrodes," *J. Neural Eng.*, vol. 18, no. 5, p. 054001, Sep. 2021, doi: 10.1088/1741-2552/AC20BB.
[149] M. Zhou, B. K. Young, E. della Valle, B. Koo, J. Kim, and J. D. Weiland, "Full-field, conformal epiretinal electrode array using hydrogel and polymer hybrid technology," *Sci. Rep.*, vol. 13, no. 1, Art. no. 1, Apr. 2023, doi: 10.1038/s41598-023-32976-9.
[150] T. M. Bruns, R. A. Gaunt, and D. J. Weber, "Multielectrode array recordings of bladder and perineal primary afferent activity from the sacral dorsal root ganglia," *J. Neural Eng.*, vol. 8, no. 5, Oct. 2011, doi: 10.1088/1741-2560/8/5/056010.
[151] H. Kim *et al.*, "Cuff and sieve electrode (CASE): The combination of neural electrodes for bi-directional peripheral nerve interfacing," *J. Neurosci. Methods*, vol. 336, no. January, Apr. 2020, doi: 10.1016/j.jneumeth.2020.108602.
[152] N. A. Brill *et al.*, "Evaluation of high-density, multi-contact nerve cuffs for activation of grasp muscles in monkeys," *J Neural Eng*, vol. 15, no. 3, p. 36003, 2018, doi: 10.1088/1741-2552/aa8735.
[153] D. J. Tyler and D. M. Durand, "Functionally selective peripheral nerve stimulation with a flat interface nerve electrode," *IEEE Trans Neural Syst Rehabil Eng*, vol. 10, no. 4, pp. 294–303, 2002, doi: 10.1109/TNSRE.2002.806840.

[154] P. B. Yoo and D. M. Durand, “Selective recording of the canine hypoglossal nerve using a multicontact flat interface nerve electrode,” *IEEE Trans. Biomed. Eng.*, vol. 52, no. 8, pp. 1461–1469, Aug. 2005, doi: 10.1109/TBME.2005.851482.
[155] A. Branner and R. A. Normann, “A multielectrode array for intrafascicular recording and stimulation in sciatic nerve of cats,” *Brain Res. Bull.*, vol. 51, no. 4, pp. 293–306, 2000, doi: 10.1016/S0361-9230(99)00231-2.
[156] D. J. Bakkum *et al.*, “The Axon Initial Segment is the Dominant Contributor to the Neuron’s Extracellular Electrical Potential Landscape,” *Adv. Biosyst.*, vol. 3, no. 2, p. 1800308, Feb. 2019, doi: 10.1002/adbi.201800308.
[157] M. W. Barnett and P. M. Larkman, “The action potential,” *Pract. Neurol.*, vol. 7, no. 3, pp. 192–197, Jun. 2007.
[158] C. C. McIntyre, A. G. Richardson, and W. M. Grill, “Modeling the Excitability of Mammalian Nerve Fibers: Influence of Afterpotentials on the Recovery Cycle,” *J. Neurophysiol.*, vol. 87, no. 2, pp. 995–1006, Feb. 2002, doi: 10.1152/jn.00353.2001.
[159] P. H. Veltink, B. K. Van Veen, J. J. Struijk, J. Holsheimer, and H. B. K. Boom, “A Modeling Study of Nerve Fascicle Stimulation,” *IEEE Trans. Biomed. Eng.*, vol. 36, no. 7, pp. 683–692, 1989, doi: 10.1109/10.32100.
[160] S. Romeni, G. Valle, A. Mazzoni, and S. Micera, “Tutorial: a computational framework for the design and optimization of peripheral neural interfaces,” *Nat. Protoc.*, vol. 15, no. 10, pp. 3129–3153, Oct. 2020, doi: 10.1038/s41596-020-0377-6.
[161] Cytec Thornel, “Cytec Thornel ® T-300 1K Carbon Fiber , Polyacrylonitrile (PAN) Precursor Contact Songhan Plastic Technology Co ., Ltd .,” p. 51131842, 2015.
[162] S. F. Lempka *et al.*, “Optimization of Microelectrode Design for Cortical Recording Based on Thermal Noise Considerations,” pp. 3361–3364, 2006.
[163] K. M. Szostak, L. Grand, and T. G. Constandinou, “Neural interfaces for intracortical recording: Requirements, fabrication methods, and characteristics,” *Front. Neurosci.*, vol. 11, no. DEC, Dec. 2017, doi: 10.3389/fnins.2017.00665.
[164] J. P. Cunningham, P. Nuyujukian, V. Gilja, C. A. Chestek, S. I. Ryu, and K. V. Shenoy, “A closed-loop human simulator for investigating the role of feedback control in brain-machine interfaces,” *J. Neurophysiol.*, vol. 105, no. 4, pp. 1932–1949, 2011, doi: 10.1152/jn.00503.2010.
[165] K. Yoshida, M. J. Bertram, T. G. Hunter Cox, and R. R. Riso, “Peripheral nerve recording electrodes and techniques,” in *Neuroprosthetics: Theory and Practice: Second Edition*, 2017, pp. 377–466. doi: 10.1142/9789813207158_0014.
[166] Y. M. Dweiri, M. A. Stone, D. J. Tyler, G. A. McCallum, and D. M. Durand, “Fabrication of High Contact-Density, Flat-Interface Nerve Electrodes for Recording and Stimulation Applications,” *J Vis Exp*, no. 116, pp. 1–11, 2016, doi: 10.3791/54388.
[167] A. L. Ciancio *et al.*, “Control of prosthetic hands via the peripheral nervous system,” *Front Neurosci*, vol. 10, no. APR, pp. 1–17, 2016, doi: 10.3389/fnins.2016.00116.
[168] Ardiem Medical, “Neural Cuff.” Accessed: Mar. 05, 2021. [Online]. Available: http://www.ardiemmedical.com/neural-cuff/
[169] M. for L. Science, “Nerve Cuff Electrode.” p. 1, 2021. [Online]. Available: https://www.microleadsneuro.com/research-products/?jumpto=nerve-cuff
[170] J. T. Mortimer, W. F. Agnew, K. Horch, P. Citron, G. Creasey, and C. Kantor, “Perspectives on New Electrode Technology for Stimulating Peripheral Nerves with

Implantable Motor Prostheses," *IEEE Trans. Rehabil. Eng.*, vol. 3, no. 2, 1995, doi: 10.1109/86.392373.
[171] W. M. Grill, S. E. Norman, and R. V. Bellamkonda, "Implanted Neural Interfaces : Biochallenges and Engineered Solutions," *Annu Rev Biomed Eng*, vol. 11, pp. 1–25, 2009, doi: 10.1146/annurev-bioeng-061008-124927.
[172] T. D. Yoshida Kozai *et al.*, "Ultrasmall implantable composite microelectrodes with bioactive surfaces for chronic neural interfaces," *Nat. Mater.*, vol. 11, no. 12, pp. 1065–1073, Dec. 2012, doi: 10.1038/nmat3468.
[173] N. Saito *et al.*, "Application of carbon fibers to biomaterials: A new era of nano-level control of carbon fibers after 30-years of development," *Chem Soc Rev*, vol. 40, no. 7, pp. 3824–3834, 2011, doi: 10.1039/c0cs00120a.
[174] E. J. Welle *et al.*, "Fabrication and characterization of a carbon fiber peripheral nerve electrode appropriate for chronic recording," 2019.
[175] T. L. Massey *et al.*, "Open-source automated system for assembling a high-density microwire neural recording array," *2016 Int. Conf. Manip. Autom. Robot. Small Scales MARSS 2016*, 2016, doi: 10.1109/MARSS.2016.7561750.
[176] H. N. Schwerdt *et al.*, "Subcellular probes for neurochemical recording from multiple brain sites," *Lab Chip*, 2017, doi: 10.1039/C6LC01398H.
[177] G. Guitchounts, J. E. Markowitz, W. A. Liberti, and T. J. Gardner, "A carbon-fiber electrode array for long-term neural recording," *J. Neural Eng.*, vol. 046016, no. 4, Aug. 2013, doi: 10.1088/1741-2560/10/4/046016.
[178] T. Dong, L. Chen, and A. Shih, "Laser Sharpening of Carbon Fiber Microelectrode Arrays for Brain Recording," *J. Micro Nano-Manuf.*, vol. 8, no. 4, Dec. 2021, doi: 10.1115/1.4049780.
[179] S. Venkatraman *et al.*, "In vitro and in vivo evaluation of PEDOT microelectrodes for neural stimulation and recording," *IEEE Trans. Neural Syst. Rehabil. Eng.*, vol. 19, no. 3, pp. 307–316, 2011, doi: 10.1109/TNSRE.2011.2109399.
[180] I. R. Cassar *et al.*, "Electrodeposited platinum-iridium coating improves in vivo recording performance of chronically implanted microelectrode arrays," *Biomaterials*, vol. 205, no. November 2018, pp. 120–132, 2019, doi: 10.1016/j.biomaterials.2019.03.017.
[181] I. M. Taylor *et al.*, "Enhanced dopamine detection sensitivity by PEDOT/graphene oxide coating on in vivo carbon fiber electrodes," *Biosens. Bioelectron.*, vol. 89, pp. 0–1, 2017, doi: 10.1016/j.bios.2016.05.084.
[182] B. Pusch, Jens, Wohlmann, J. Pusch, and B. Wohlmann, "Chapter 2 - Carbon Fibers," in *Inorganic and Composite Fibers*, B. Mahltig and Y. Kyosev, Eds., in The Textile Institute Book Series. , Woodhead Publishing, 2018, pp. 31–51. [Online]. Available: http://www.sciencedirect.com/science/article/pii/B9780081022283000025
[183] D. Budai, I. Hernádi, B. Mészáros, Z. K. Bali, and K. Gulya, "Electrochemical responses of carbon fiber microelectrodes to dopamine in vitro and in vivo," *Acta Biol. Szeged.*, vol. 54, no. 2, pp. 155–160, 2010.
[184] C. F. Meehan, K. A. Mayr, M. Manuel, S. T. Nakanishi, and P. J. Whelan, "Decerebrate mouse model for studies of the spinal cord circuits," *Nat. Protoc.*, vol. 12, no. 4, Art. no. 4, Apr. 2017, doi: 10.1038/nprot.2017.001.
[185] U. F. O. Themes, "Spinal Cord – MR of Rodent Models," Radiology Key. Accessed: Jan. 30, 2024. [Online]. Available: https://radiologykey.com/spinal-cord-mr-of-rodent-models/

[186] H. H. Ong and F. W. Wehrli, “Quantifying axon diameter and intra-cellular volume fraction in excised mouse spinal cord with q-space imaging,” *NeuroImage*, vol. 51, no. 4, pp. 1360–1366, Jul. 2010, doi: 10.1016/j.neuroimage.2010.03.063.
[187] “A neural circuit for vocal production responds to viscerosensory input in the songbird.” Accessed: Jan. 30, 2024. [Online]. Available: https://journals.physiology.org/doi/epdf/10.1152/jn.00400.2023
[188] J. Singh Alvarado *et al.*, “Neural dynamics underlying birdsong practice and performance,” *Nature*, vol. 599, no. 7886, Art. no. 7886, Nov. 2021, doi: 10.1038/s41586-021-04004-1.
[189] E. C. Leuthardt *et al.*, “Using the electrocorticographic speech network to control a brain – computer interface in humans,” vol. 036004, 2011, doi: 10.1088/1741-2560/8/3/036004.
[190] E. Bou Assi, D. K. Nguyen, S. Rihana, and M. Sawan, “Towards accurate prediction of epileptic seizures: A review,” *Biomed. Signal Process. Control*, vol. 34, pp. 144–157, Apr. 2017, doi: 10.1016/j.bspc.2017.02.001.
[191] A. Yadollahpour and M. Jalilifar, “Seizure Prediction Methods: A Review of the Current Predicting Techniques,” *Biomed. Pharmacol. J.*, vol. 7, no. 1, pp. 153–162, May 2015.
[192] B. P. Christie, K. R. Ashmont, P. A. House, and B. Greger, “Approaches to a cortical vision prosthesis: Implications of electrode size and placement,” *J. Neural Eng.*, vol. 13, no. 2, Feb. 2016, doi: 10.1088/1741-2560/13/2/025003.
[193] T. Flores, X. Lei, T. Huang, H. Lorach, R. Dalal, and D. Palanker, “Optimization of pillar electrodes in subretinal prosthesis for enhanced proximity to target neurons,” 2018.
[194] P. P. Vu *et al.*, “Closed-Loop Continuous Hand Control via Chronic Recording of Regenerative Peripheral Nerve Interfaces,” *IEEE Trans. Neural Syst. Rehabil. Eng.*, vol. 26, no. 2, pp. 515–526, Feb. 2018, doi: 10.1109/TNSRE.2017.2772961.
[195] P. P. Vu *et al.*, “Restoration of Proprioceptive and Cutaneous Sensation Using Regenerative Peripheral Nerve Interfaces in Humans with Upper Limb Amputations,” *Plast. Reconstr. Surg.*, vol. 149, no. 6, p. 1149e, Jun. 2022, doi: 10.1097/PRS.0000000000009153.
[196] M. A. Gonzalez *et al.*, “Electrical Stimulation of Regenerative Peripheral Nerve Interfaces (RPNIs) Induces Referred Sensations in People With Upper Limb Loss,” *IEEE Trans. Neural Syst. Rehabil. Eng.*, vol. 32, pp. 339–349, 2024, doi: 10.1109/TNSRE.2023.3345164.
[197] S. R. Nason *et al.*, “Real-time linear prediction of simultaneous and independent movements of two finger groups using an intracortical brain-machine interface,” *Neuron*, vol. 109, no. 19, pp. 3164-3177.e8, Oct. 2021, doi: 10.1016/j.neuron.2021.08.009.
[198] J. A. Supple *et al.*, “Binocular Encoding in the Damselfly Pre-motor Target Tracking System,” *Curr. Biol.*, vol. 30, no. 4, pp. 645-656.e4, Feb. 2020, doi: 10.1016/J.CUB.2019.12.031.
[199] M. F. Brill, M. Reuter, W. Rössler, and M. F. Strube-Bloss, “Simultaneous Long-term Recordings at Two Neuronal Processing Stages in Behaving Honeybees,” *JoVE J. Vis. Exp.*, no. 89, p. e51750, Jul. 2014, doi: 10.3791/51750.
[200] J. Carcaud, M. Otte, B. Grünewald, A. Haase, J. C. Sandoz, and M. Beye, “Multisite imaging of neural activity using a genetically encoded calcium sensor in the honey bee,” *PLOS Biol.*, vol. 21, no. 1, p. e3001984, Jan. 2023, doi: 10.1371/JOURNAL.PBIO.3001984.
[201] N. Elgrishi, K. J. Rountree, B. D. McCarthy, E. S. Rountree, T. T. Eisenhart, and J. L. Dempsey, “A Practical Beginner’s Guide to Cyclic Voltammetry,” *J. Chem. Educ.*, vol. 95, no. 2, pp. 197–206, Feb. 2018, doi: 10.1021/acs.jchemed.7b00361.

[202] S. A. Kodirov, “Addictive neurons,” *Ther. Targets Neurol. Dis.*, vol. 4, p. e1498, 2017.
[203] D. P. Covey and P. A. Garris, “Using fast-scan cyclic voltammetry to evaluate striatal dopamine release elicited by subthalamic nucleus stimulation,” in *2009 Annual International Conference of the IEEE Engineering in Medicine and Biology Society*, Sep. 2009, pp. 3306–3309. doi: 10.1109/IEMBS.2009.5333768.
[204] H. Rafi and A. G. Zestos, “Review—Recent Advances in FSCV Detection of Neurochemicals via Waveform and Carbon Microelectrode Modification,” *J. Electrochem. Soc.*, vol. 168, no. 5, p. 057520, May 2021, doi: 10.1149/1945-7111/ac0064.